REPORT DOCUMENTATION PAGE

Form Approved
OMB No. 0704-0188

1. AGENCY USE ONLY *(Leave blank)*	2. REPORT DATE	3. REPORT TYPE AND DATES COVERED
		THESIS

4. TITLE AND SUBTITLE
MEASUREMENTS OF THE HEAT TRANSFER COEFICIENT DISTRIBUTION ON FLAT AND RIBBED SURFACES WITH INTERRUPTED HEATING USING THERMOCHROMIC LIQUID CRYSTALS

5. FUNDING NUMBERS

6. AUTHOR(S)
CAPT WOLF JASON D

7. PERFORMING ORGANIZATION NAME(S) AND ADDRESS(ES)
UNIVERSITY OF CALIFORNIA AT DAVIS

8. PERFORMING ORGANIZATION REPORT NUMBER

9. SPONSORING/MONITORING AGENCY NAME(S) AND ADDRESS(ES)
THE DEPARTMENT OF THE AIR FORCE
AFIT/CIA, BLDG 125
2950 P STREET
WPAFB OH 45433

10. SPONSORING/MONITORING AGENCY REPORT NUMBER

FY99-42

11. SUPPLEMENTARY NOTES

12a. DISTRIBUTION AVAILABILITY STATEMENT
Unlimited distribution
In Accordance With AFI 35-205/AFIT Sup 1

12b. DISTRIBUTION CODE

13. ABSTRACT *(Maximum 200 words)*

19990120 022

14. SUBJECT TERMS

15. NUMBER OF PAGES
113

16. PRICE CODE

17. SECURITY CLASSIFICATION OF REPORT	18. SECURITY CLASSIFICATION OF THIS PAGE	19. SECURITY CLASSIFICATION OF ABSTRACT	20. LIMITATION OF ABSTRACT

Measurements of the Heat Transfer Coefficient Distribution
On Flat and Ribbed Surfaces with Interrupted Heating
Using Thermochromic Liquid Crystals

By

Jason D. Wolf

B.S. (United States Air Force Academy) 1992

THESIS

Submitted in partial satisfaction of the requirements for the degree of

MASTER OF SCIENCE

in

Mechanical Engineering

in the

OFFICE OF GRADUATE STUDIES

of the

UNIVERSITY OF CALIFORNIA

DAVIS

Approved:
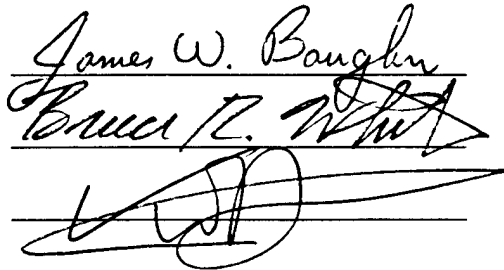
Committee in Charge

1998

i

Acknowledgments

I would like to thank several people who have made this past year's work so rewarding. Without their help this project would have been more difficult, would have taken longer, and would not have added joy to my life. Professor James Baughn is a special agent of the heat transfer world. His guidance kept me on schedule and on the right track. I have learned more than I can say working with him. Doctoral student Michael Anderson is one of the best teachers I know. His help with image processing and liquid crystals proved invaluable. James Mayhew (USAF Ret.) is an invaluable member of any team. His expertise with gold film and wind tunnel testing improved my results. They both unselfishly devoted their time and energy to this endeavor. Undergraduate Christopher Gordon was my experimentation right-hand man. His help in liquid crystal calibration and data collection saved me weeks of work.

I would like to thank two shops here at Davis: Electronics General Services, for providing for the longevity and accuracy of the test equipment, and the Student Engineering Shop, where Mike Akahori and Dave Hook provided help in model fabrication and design.

I am grateful to Professor Case Van Dam and Professor Bruce White, who have given quality inputs and have devoted their valuable time to the review and correction of this thesis.

Finally, I want to thank my biggest supporter and light of my life, Kari. Her love gives me the strength to take on some of life's biggest challenges – and succeed!

Abstract

Measurements of the heat transfer coefficient distribution on flat and ribbed surfaces with interrupted heating are presented. One application of this type of thermal boundary condition is the cooling of surface mounted modules in electronic packaging. Heating occurs at the modules, with no heating between the modules. The heat transfer measurements in the present study are made using the heated-coating method with a thermochromic liquid crystal (TLC). The "coating" is vacuum-deposited gold on a plastic sheet, which is mounted on a Styrofoam surface. The gold film is electrically heated to produce the surface heat flux. The surface temperature is measured by capturing color images of the TLC, using the hue technique. These surface temperature plots are transformed into heat transfer coefficient distributions on the surface of the models.

Interrupted heating on the flat surface is obtained by heating strips perpendicular to the freestream flow, with insulated spaces between the strips. The ribbed surface is heated on the top of the ribs only, with insulated unheated cavities in-between.

The results show that, as expected, the local heat transfer coefficient is higher on the heated strips of the flat surface interrupted heating case, than would be present at the same locations with a uniform heat flux. The interruption of the thermal boundary layer at each unheated section allows it to "reset", thereby causing the higher heat transfer on the following heated section. The ribbed model shows a slight increase in heat transfer on the ribs above that of the flat plate interrupted heating model. The cavities appear to introduce mixing that causes this change. The increase in h due to the ribs is small, however, when compared to the effect of the interrupted heating.

Table of Contents

List of Symbols

English letter symbols

A	Area of surface (m^2)
b_x	68% bias limit in x
°C	Degrees Celsius
CCD	Charge Coupled Device
CF	Coverage Factor
DB	Decibels
f	Correction factor for resistance per square
h	Convective heat transfer coefficient ($W/m^2 \cdot K$)
HP	Horsepower
HSV	Hue, Saturation, Value color space
I	Current (amps)
k	Thermal conductivity ($W/m \cdot K$)
K	Kelvin
N	Number of data points
NaN	Not-a-Number (Matlab uses)
Pr	Prandtl number
q_{cond}	Heat loss due to conduction
q_e	Surface heat flux due to electrical heating (W/m^2)
q_l	Radiative heat flux due to incident lighting (W/m^2)
Q	Power (W)
R'	Resistance per square (Ω/square)
Re	Reynolds number
RGB	Red, Green, Blue color space
R30C10W	Liquid crystal having a red start temperature of 30°C, with a bandwidth of 10°C
SEE	Standard Error of Estimate

S_x	68% precision limit in x, or standard deviation in x
T_∞	Freestream air temperature
T_{LC}	Surface temperature (of liquid crystal)
w	Width of surface (m)
x	Characteristic length used for Nu, Re calculations

Greek letter symbols

ε	Emissivity of surface
σ	Stefan-Boltzmann constant (5.67×10^{-8} W/m$^2\cdot$K^4), standard deviation. in Equations (5) and (6)
ξ	Unheated starting length (m)

Subscripts

∞	Freestream air property
LC	Liquid crystal
cond	Conduction
conv	Convection
e	Electrical
l	Incident lighting
rad	Thermal radiation

List of Figures

List of Tables

I Introduction and Background

There have been many studies of the heat transfer coefficient distribution on flat and ribbed surfaces. In most (if not all) of these studies the surfaces were at a uniform temperature or had a uniform surface heat flux, perhaps due to electrical heating. In these cases, a thermal boundary layer builds, resulting in a decrease in the heat transfer coefficient along the surfaces. In the present study, a non-uniform or interrupted heating is used on the surfaces. This causes an interruption in the thermal boundary layer, significantly changing the heat transfer. One application of this condition is in electronic component packaging, where transistors, microchips, and other modules are mounted on a printed circuit board (i.e., surface mounted modules). In these cases the heating is usually limited to the components, with the board acting like an insulated surface.

There are several recent attempts to model flow and heat transfer with this type of interrupted heating. For example, Ang and Yap (1998) numerically simulated the ribbed wall flow condition for laminar flow in a channel. They considered various inter-module spacing, channel heights, and heights of implanted barriers used to augment heat transfer. They found that the heat transfer rate (and Nusselt number) increased significantly near the leading edge of each module as inter-module spacing is increased. They also found that reduction in the channel height at a fixed flow rate results in higher heat transfer rates, as well as increased pressure drop across the modules. In another study, Hacker and Eaton (1997) investigated the effect of an arbitrarily varying thermal boundary condition on the convective heat transfer in a backward-facing step flow. Their results show that, in the separated flow, the effects of localized heating are felt only a short distance upstream and downstream, and the local heat transfer is less sensitive to thermal boundary conditions than in the laminar case.

In the present study, heat transfer coefficient distributions were investigated for three cases. First, a turbulent boundary layer over a flat plate with uniform heating is studied. The turbulent boundary layer is achieved by tripping the flow 0.1 m upstream of the model.

The second case involves a turbulent boundary layer over a flat plate with interrupted heating. The heating takes place on sections (i.e. strips) mounted perpendicular to the flow, with unheated strips between the heated ones. Three separate widths of heated and unheated strips are studied. They are:

- Spacing #1) 38 mm heated / 25 mm unheated
- Spacing #2) 25 mm heated / 38 mm unheated
- Spacing #3) 16 mm heated / 47 mm unheated.

For the third case, measurements are made of heat transfer from a ribbed model with a turbulent boundary layer. The model is heated on the top surface of the ribs only, with unheated insulated cavities between the ribs. The rib width and inter-rib spacing were of the same size as one of the flat plate interrupted heating models (spacing #1).

All three cases are studied at three flow velocities: 10 m/s, 14.2 m/s, and 20 m/s. It is hoped that testing these three models provides an interrupted heating database for future experimental data and numerical code comparisons.

A. Turbulent Boundary Layer over a Flat Plate with Uniform Heating

The heat transfer due to laminar and turbulent boundary layers over a flat plate has been investigated in great detail. Although more complicated than the laminar flow case, a turbulent boundary layer has been fully characterized by the early work of Reynolds, and later by many others. Kays and Crawford (1980) summarize results for both laminar and turbulent boundary layers. In both cases, the nature of the thermal boundary conditions is important in characterizing the flow. Maintaining a laminar flow over models in a wind tunnel is difficult. The boundary layer trips easily and not uniformly. Therefore, it was decided to purposefully trip the boundary layer upstream of the models in the present study, to obtain a constant turbulent boundary layer in the region of interest. The heat transfer solution for a uniform temperature thermal boundary condition in a turbulent boundary layer is given by the following equation (Incropera, Dewitt 1990):

$$Nu_x = 0.0296 \cdot Re_x^{4/5} \cdot Pr^{1/3} \qquad \text{for } 0.6 < Pr < 60 \qquad (1)$$

The uniform heat flux boundary condition yields the following analytical solution, which is approximately 4% greater than the uniform temperature solution:

$$Nu_x = 0.0308 \cdot Re_x^{4/5} \cdot Pr^{1/3} \tag{2}$$

In the present study, we supply a uniform heat flux to the surface via an electrically energized gold film, so Equation (2) above is appropriate. However, this solution applies for a uniform heat flux that starts at the same location as the velocity boundary layer. Because the boundary layer is tripped 10 cm upstream of the leading edge of the plate, we have the special case known as an unheated starting length, where $T_s = T_\infty$. Figure 1, below, illustrates the difference in the velocity and thermal boundary layers for this condition.
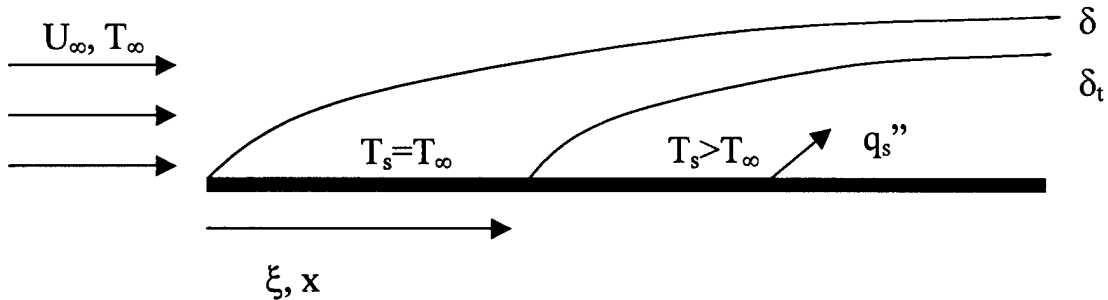
Figure 1 Unheated Starting Length

This situation requires use of the following formula (Incropera, Dewitt 1990):

$$Nu_x = \frac{Nu_x \big|_{\xi=0}}{[1 - (\xi/x)^{9/10}]^{1/9}} \tag{3a}$$

where $Nu_x \big|_{\xi=0}$ is found by Equation (2)

Determining the unheated starting length, ξ, in Equation (3a) is not as clear as it may seem. Since ξ is

measured from the start of the turbulent boundary layer to the start of the constant heat flux boundary

condition, it is important to know where the turbulent boundary layer begins. In this study, a 3 mm

diameter brass dowel is placed 10 cm upstream of the leading edge of the heated plate, thus, we know that

ξ is on the order of 10 cm. By convention, the location of the start of the turbulent boundary layer must be

further upstream than the trip, as the boundary layer can not have zero thickness at the location of the trip.

Heat transfer coefficient is calculated using the Nusselt number results from Equations (2) and (3a), and the

following equation:

$$Nu_x = \frac{h \cdot x}{k}$$
(3b)

where   x is shown in Figure 1
k is thermal conductivity of air (W/m·K)

B. Turbulent Boundary Layer over a Flat Plate with Interrupted Heating

In the second case, the thermal boundary layer is allowed to grow for a distance, x, then begins to "reset"

by the absence of any surface heat flux: i.e., an interrupted heating condition. The flat plate model above is

modified so that heating occurs only on strips perpendicular to the flow direction, with an unheated strip

immediately after each heated strip. In effect, the flow encounters a series of unheated starting length

problems, with the thermal boundary layer growing again at the start of each heated section. In this case,

the freestream air temperature (as it reaches the leading edge of each heated strip) is warmer for each

successive strip due to upstream heating that has already occurred, until a steady, periodic condition is

reached. The author is not aware of a theory that provides a solution for the interrupted heating case.

Results are presented for three different lengths of flat plate interrupted heating in an attempt to

characterize the thermal boundary layer growth and heat transfer coefficient profiles for this special

situation.

C. Turbulent Boundary Layer over a Ribbed Surface with Interrupted Heating

Heat transfer from ribbed surfaces has been studied often. Most, if not all of the studies, however, have heating from the ribs as well as the cavities. Here, we investigate the case where the heating occurs on the top surface of the ribs only, with unheated insulated cavities in-between. The rib tops are aligned with the tunnel wall, so the first heated strip encounters the freestream air in much the same way as the flat plate model (see Figures 2-4). The ribs are 38 mm wide and have bordering channels that are 19 mm deep and 25 mm wide. These channels promote circulation and mixing in the velocity boundary layer. Therefore, it is expected that the ribs would do a more effective job of resetting the thermal boundary layer, causing higher heat transfer when compared to the heat transfer on successive interrupted heating sections of the flat plate model.

The ribbed flow condition has practical relevance to electronic cooling issues, as the geometry and thermal boundary conditions are similar to surface-mounted modules (chip arrays) on a printed circuit board. Recently, there is a trend toward higher densities of modules in electronic packaging. Researchers are working toward better thermal management, thereby increasing reliability and performance levels of the components. Bar-Cohen & Witzman (1993) noted that a relatively small 10°C -20°C increase in chip temperatures could lead to a 50% drop in component reliability levels. Others have performed experimental work to characterize the two-dimensional flow field, namely Sparrow et al. (1982), Kang et al. (1990), and Wirtz and Chen (1992). The latter group performed experiments in the laminar-transitional regime for air flowing over a two-dimensional array of rectangular ribs in a rectangular duct. The Reynolds number range, based on the approximate hydraulic diameter (2H) was 2000 < Re < 7500. They found that the heat transfer increased with increasing Re, due to an increase in the effective shear stress along the ribbed wall.

Numerical work has also been done in this field. In addition to the work of Ang and Yap (1998) discussed earlier, Agonafer and Moffat (1985) used a commercial finite-control-volume code, PHOENICS, to simulate fluid flow and heat transfer characteristics of electronics modules. Their heat transfer coefficient results agreed with experimental data in the fully developed region to within 8%.

II Experimental Method and Apparatus

A. Model Design and Fabrication

Diagrams of the flat plate with uniform heating, as well as the flat plate and ribbed models with interrupted heating are shown on the following pages. For the flat plate with uniform heating, the entire 0.42 m length is covered with gold film and is electrically heated. For the interrupted heating models, the heating takes place only on the gold film regions specified.

Several different materials were considered for the flat and ribbed models used in these experiments. Dow blue Styrofoam was chosen because of its ease of machining to exact specifications, insulating properties, and gold film mounting characteristics. Rough-cut machining of the Styrofoam pieces was performed in the UC Davis Student Machine Shop, using a rotary table saw. Rough edges were sanded by hand using fine grain sandpaper, as were the upper surfaces upon which the gold film was mounted.

Both models are constructed of two pieces of Styrofoam: a 1.5 in (38 mm) thick piece to span the entire width and height of the rear wind tunnel test section frame, and a ¾ in (19 mm) piece used to construct the flat plate or ribbed sections, as appropriate. For an average surface temperature of 40°C, at the upper limit of our liquid crystal temperature range, it was determined that a rear section thickness of 38 mm would limit back-side conduction losses to less than 2%, which was deemed acceptable. The 19 mm section was chosen for the top side of the model because this thickness ensured a smooth match between the inside wind tunnel wall and the model surfaces to minimize leading-edge disturbances.

After sanding, the upper model surfaces were sprayed with 3M Super-77 Spray Adhesive and allowed to dry for approximately 2 minutes. The gold film, which had been cut to exacting specifications, was then carefully positioned on each glued surface. An artist's rubber roller was used to smoothly apply the gold film to the Styrofoam surface and eliminate air pockets.

V=10, 14.2, 20 m/s

12"/0.30 m
tunnel width

24"/0.61m Opening Length

16.5"/0.42 m Gold Film

19 mm   Blue Styrofoam

38 mm   Blue Styrofoam
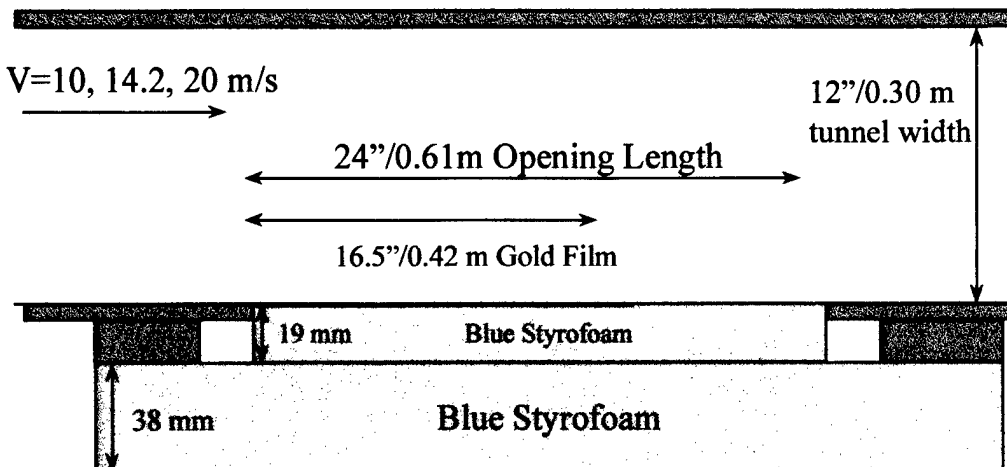
Figure 2 Flat Plate Uniform Heating Model, Top View

V=10, 14.2, 20 m/s

12"/0.30 m
tunnel width

24"/0.61 m Opening Length

38 mm gold film sections, 25 mm spacing

19 mm   Blue Styrofoam

38 mm   Blue Styrofoam
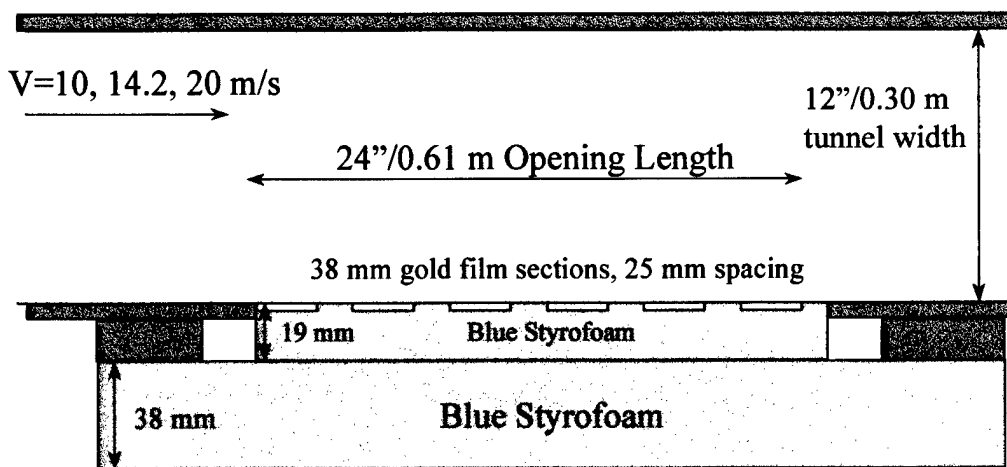
Figure 3 Flat Plate Interrupted Heating Model, Top View

V=10, 14.2, 20 m/s

12"/0.30 m
tunnel width

7 heated ribs, total length 0.42 m

38 mm

25 mm

Gold Film on upper surfaces

19 mm

38 mm

Blue Styrofoam
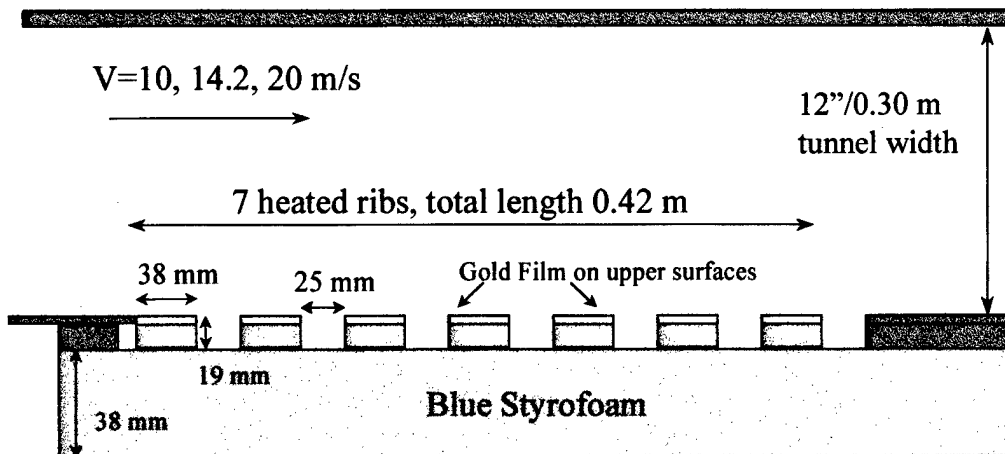
Figure 4 Ribbed Interrupted Heating Model, Top View

To provide the heat flux to the surface, copper tape (0.038mm thick, 6.35mm wide) is connected to the edges of the gold film surface. An HP 6286A DC power supply is connected to the copper tape with large diameter, 14 gauge and 16 gauge, low resistance wire. The wire is soldered to the copper tape, and both the flat plate interrupted heating sections as well as the ribbed model heated sections are wired in parallel. To ensure better electrical contact between the copper tape and gold film, the juncture is painted with GC Electronics silver print and allowed to dry overnight. Flat black (tempera) paint is then applied to the silver print to prevent excessive light reflection from the model lighting into the camera.

A background coat of Hallcrest BB-G1 black paint is sprayed onto the gold film, and allowed to dry overnight. A microencapsulated Thermochromic Liquid Crystal (TLC) is then applied on top of the black paint.

B. Wind Tunnel

Aerolab built the wind tunnel used in this series of tests. It is an open circuit tunnel with a test section that is 12 inches square and 24 inches long. The test section has an aluminum floor, with hinged sides and a removable top made of Plexiglas. The 10 HP motor in this wind tunnel is capable of producing a maximum air velocity of 65 m/s. The tests were conducted at speeds of 10 m/s, 14.2 m/s, and 20 m/s. Although the wind tunnel is equipped to measure test section airspeed via onboard pressure ports, the author chose to install a Pitot-static probe and measure the velocity directly, using an inclined manometer.

Several modifications were made to the tunnel to permit more accurate velocity and temperature measurements, to support the precision required in this experiment. These modifications included replacing the Plexiglas top with a wooden replica through which a Pitot-static tube was inserted for accurate velocity measurement. Also, the force balance was removed, and the tunnel floor sealed with black duct tape to prevent light reflection and air leaks through the perforated surface. The top of the tunnel received the same covering as the bottom, to ensure symmetrical light reflection from both surfaces. The front Plexiglas door was held closed by the lighting apparatus, and the back Plexiglas door removed to enable installation of the Styrofoam models, which are discussed in the next section. A single screw hole at the vertical midpoint of the tunnel wall was opened up to permit installation of a thermistor probe into the freestream airflow. This probe was located approximately 0.5 m downstream of the test section, and extended about 0.15 m into the freestream flow. This location ensured stable and accurate freestream air temperature measurements for the duration of the testing. The top-down diagram on the following page shows the placement of the thermistor and Pitot-static probes in the wind tunnel, as well as lighting and camera positions in relation to the test model.
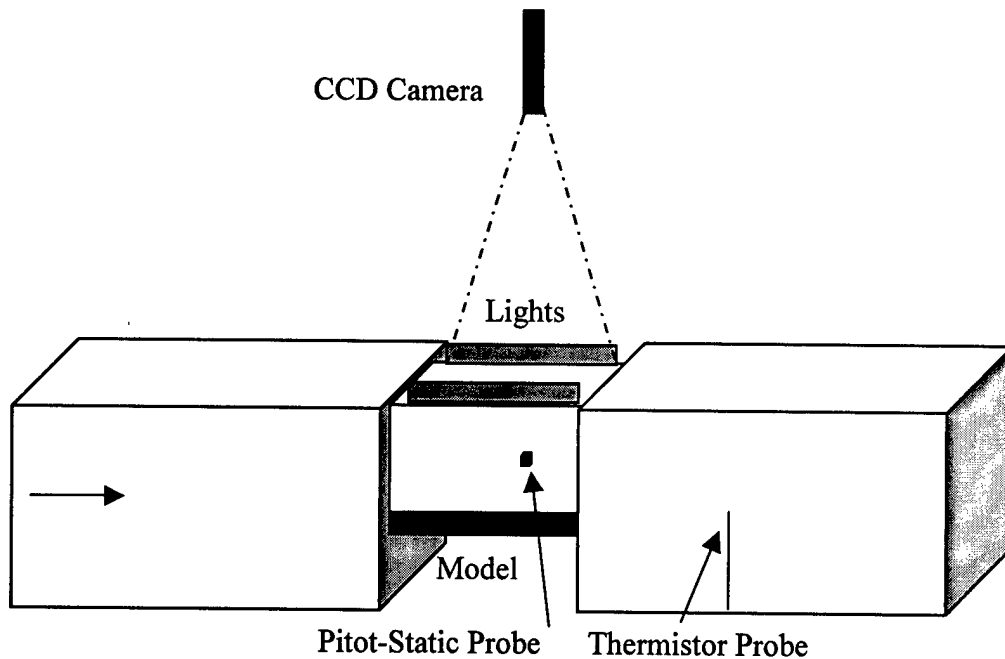
Figure 5 Experimental Setup

C. Data Reduction Equation

For these tests the local heat transfer coefficient is calculated using a surface energy balance on the models:

$$q_{conv} = h(T_{LC} - T_{t\infty}) = q_e + q_l - q_{rad} - q_{cond} \tag{4a}$$

Neglecting the conduction losses through the styrofoam, expanding the radiation term and solving for the convective heat transfer coefficient yields:

$$h = \frac{q_e + q_l - \varepsilon \cdot \sigma \cdot (T_{LC}{}^4 - T_\infty{}^4)}{(T_{LC} - T_\infty)} \tag{4b}$$

where q_e = heat flux from electrical power in (W/m^2)
   q_l = heat flux from the incident lighting (W/m^2)
   ε = emissivity of model surface
   σ = Stefan-Boltzman constant

T_{LC} = temperature of the liquid crystal surface
T_∞ = temperature of the freestream air

Note that the freestream temperature in Equation (4a) is a total temperature. Since we are working with

flow at low Mach number, it is assumed that the temperature sensed by the thermistor is approximately

equal to the total temperature. Therefore, Equation (4b) contains the term T_∞.

D. Gold Film (Heat Flux Term)

To produce the surface electrical heating (q_e in Equation (4)), it is necessary to supply a known power to

the surface of the models in a uniform manner. Cortaulds gold film is used for this purpose. The gold film

is a 0.007" (7 mil) thick sheet of flexible Mylar backing, with a very fine layer of vacuum-deposited gold

on the upper surface. The resistance of the gold film is specified in terms of a resistance per square (R').

This is a common way to express the resistance of surface coatings, and is simply equal to the resistance of

any size square sample. The actual resistance of an arbitrary rectangular piece is proportional to its length

and inversely proportional to its width. The resistance of the gold film on the flat plate model, as well as

the resistance of the film on the ribbed model sections, was measured. The resistance per square was found

to be 2.42 Ω at 24°C. Since the resistance per square is commonly expressed in terms of its value at 40°C

(R40), we must scale this value to account for the difference in temperature. Baughn et al. (1985) found

the temperature coefficient of the gold coating to be 0.0011 per °C. The resistance of our coating at 40°C

is: R40 = 2.42Ω • (1+0.0011 • (1/°C) • (40°C -24°C)) = 2.46 Ω, which agrees well with previous tests of

samples using this particular gold film (Butler, 1995). When current is passed through the gold film via

electrodes attached to the edges, the material behaves in a predictable manner, exhibiting surface heating

proportional to the power applied to the film.

E. Surface Temperature Measurement using TLC's (T_{LC} term)

The models' heated surfaces were coated with Thermochromic Liquid Crystals, which change hue with temperature. Hallcrest BM/R30C10W/C17-10 TLC's were used, with a red start temperature of 30°C. This liquid crystal had a bandwidth of 10°C. Liquid crystal selection is outlined in Appendix A. Images are captured, and hue data converted to temperature using 6th order temperature/hue calibration curves. Details of the liquid crystal calibration procedures are contained in Appendix B, along with calibration curves for the seven specific plate areas used.

F. Data Collection

Two primary concerns effected the development of the experimental plan. First, we had to ensure the models reached steady state with the environment. That is, to ensure that the power input was being balanced by the convective heat transfer from the surface, and the liquid crystal hue was not changing over time. The figure below shows mean plate hue over time for a representative flat plate run at a high power setting. Hue increases for times less than 10 minutes, after which point the hue fluctuates about a constant value and the test conditions have reached steady state. Therefore, each test condition was stabilized for a minimum of 10 minutes before an image was acquired.
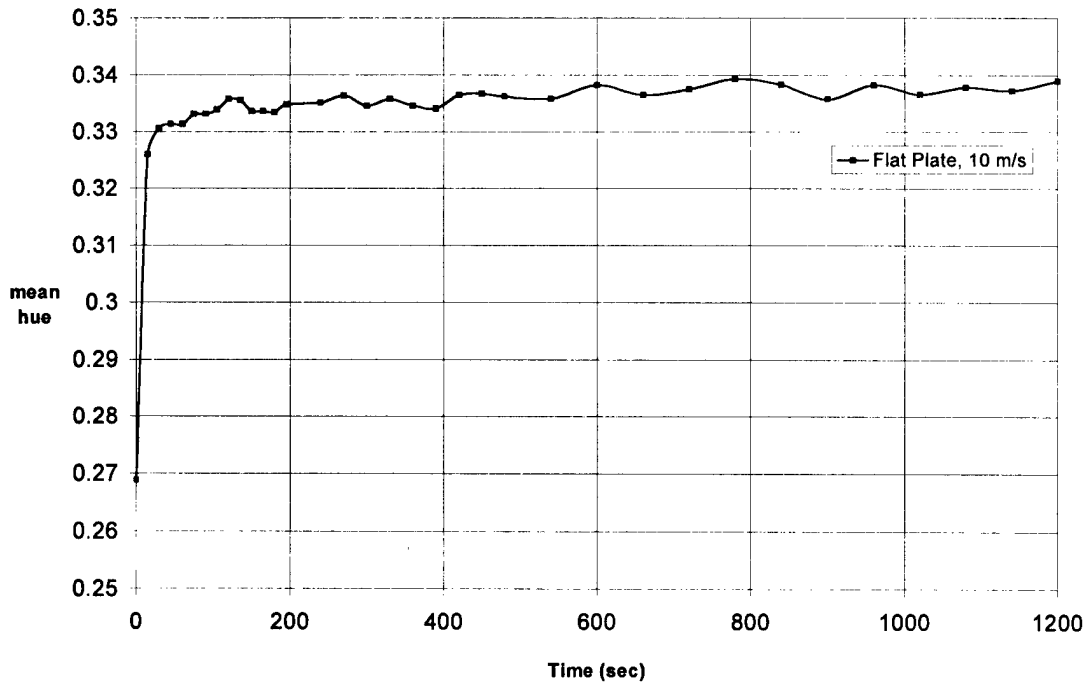
Figure 6 Mean Hue Change over Time

Second, the test plan had to ensure that hysteresis in the liquid crystal would be avoided. Prior to its use in this series of tests, the R30C10W liquid crystal was tested for calibration curve performance and hysteresis occurrence. It was found that this particular liquid crystal has a bandwidth very close to the advertised 10°C, and that hysteresis on cooling could be avoided by keeping the temperature below 52.5°C. Because the upstream portion of our model experiences higher heat transfer than the downstream portion, the temperature of the downstream sections can be much higher than those toward the leading edge. Consequently, runs progressed from low power (and low temperature) to high power. Care was taken to ensure the trailing edge did not exceed the upper limit of the color play, or about 40°C, thereby avoiding hysteresis effects.

For each model tested, three or more images were captured at different power settings, at each of three freestream velocities, for a minimum of nine images per model. The wind tunnel was allowed to stabilize

after selecting each new test speed. Power, freestream velocity, and freestream temperature were monitored during the course of each run.

Images were captured using a 3-chip Sony XC003 CCD camera. This is connected to a Matrox Meteor RGB framegrabber card installed in a Micron 166 MHz PC with 128 MB of RAM. Each image is captured as a 3-D matrix of red, green, and blue values. The image size is 480×640 pixels, thus the matrix is 480x640x3 (approximately 0.9 MB). Settings used for the camera are listed below.

Table 1 Digital Camera Menu Settings

Setting	Value	Setting	Value
Gain	+0 DB	H. Phase	00
Color Temperature	5600 K	Gamma	OFF
White Balance	MANUAL	DTL	OFF
Red/Blue Gain	-027/+042	G. Sync	ON
Shutter	OFF	Genlock	NORMAL
Frame/Field	FRM	D-SUB	VBS

A Macbeth Color Checker color rendition chart was used to adjust the balance of the color rendition system used in these experiments. Since the reflected light is a function of the incident light's spectral characteristics, it may be necessary to modify the camera settings whenever the light source is changed. To perform this adjustment, several of the Color Checker's gray squares were captured using the default settings on the RGB camera. Then, the red and blue gains were adjusted (green cannot be separately adjusted) so the average red and blue components for each square were equal to the respective green component for each square (any true gray has equal amounts of R, G, & B). These settings, Red –27, Blue +42, were used throughout all test runs. The same lights and UV filters were used for all measurements. Sufficient lighting was present to preclude the need for an overall gain setting. Instead, the camera iris was reduced to produce peak R, G, or B values under the 255 maximum for this 8 bit measurement. This iris setting remained constant for all runs as well. ·

III Data Reduction - Image Processing

Image processing is performed using MATLAB 5.1 and its Image Processing Toolbox. An image is captured for the entire flat plate or ribbed model with the RGB 3-chip camera. This image is a 3-D matrix of R, G, and B components, each of which are 480×640 pixels. The R, G, B image is converted to Hue, Saturation, and Value using a Matlab routine. The hue component is processed into temperature using a Temperature/Hue calibration curve. In order to account for the effect of changes in lighting angle across the plate, seven different calibration curves mentioned previously were used. Each curve corresponds to one of the heated ribs and its neighboring unheated section. In the span-wise direction, each image section is 57 pixels high (approximately 4 cm). Thus, our new image is 57x640 pixels, and is the same area used in both the calibration runs and the model image processing.

Matlab m-files were written to process the images, and contain 17 separate steps used to read the images, analyze the data, and output to a file. These image processing steps are detailed below, and are highlighted in the six page m-file code that comprises Appendix H.

Step 1. Read in images (each at a different power setting) for a given tunnel airspeed.

Step 2. Crop image from 480x640 to 57x640, corresponding to 3.8 cm x 42 cm.

Step 3. Convert cropped image from R, G, B to Hue, Saturation, Value colorspace using Matlab code.

Step 4. Considering one column at a time, calculate the mean hue and standard deviation in hue.

Step 5. Apply Chauvenet's Criterion to the column data and recalculate mean hue and standard deviation in hue. (For a more complete description of Chauvenet's Criterion, see Appendix E or ref. 12)

Step 6. If hue falls outside of calibration range (0.20 to 0.63), make it a NaN.

Step 7. Define the areas of interest – where the leading edge is, where the ribs and spaces lie on the plate.

Step 8. Load in the 6th order polynomial calibration curves and SEE data for each of the 7 areas.

Step 9. Convert hue to temperature using the calibration data specific to each area.

Step 10. Calculate the 68% uncertainty in temperature.

Step 11. Input power setting, q_e, and freestream air temperature, T_∞, for the specified runs.

Step 12. Input uncertainty analysis data – bias and precision limits for each of the elemental source in h.

Step 13. Calculate h profile from temperature profile.

Step 14. Calculate sensitivity coefficients in h for uncertainty analysis.

Step 15. Compare h values at each column position, for different power settings. Choose the h that has the lowest associated uncertainty.

Step 16. Calculate relative uncertainty in h and save to output matrix.

Step 17. Output results (h profile and uncertainty for each data point) to a file for use in MS Excel.

Calculating the uncertainty in h is an integral part of the data reduction. For details of the uncertainty analysis, the reader is directed to Appendix E.

IV Results and Discussion

A. Flat Plate

One of the captured RGB images from the flat plate (uniform heating) model is shown in Figure 7, below.

The leading edge (red color) is at the lowest TLC temperature (near 30°C), the green region (middle) is at

higher temperatures, and the blue (trailing edge) is at the highest temperature (near 40°C). It is clear that

the left-to-right flow is cooling the plate more at the leading edge and less toward the trailing edge. The

plate shows good spanwise temperature uniformity and a temperature gradient in the streamwise direction.

Red   Green   Blue
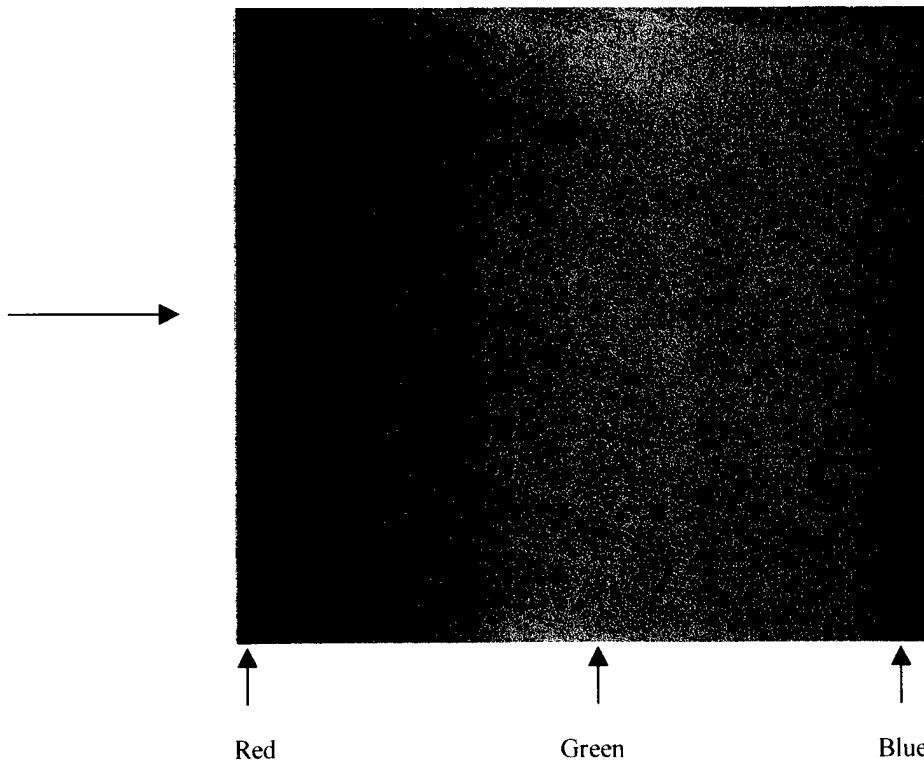
Figure 7 Flat Plate RGB Image

The performance at three different velocities was studied: 10 m/s, 14.2 m/s, and 20 m/s. An unheated

starting length was present due to the boundary layer trip installed 10 cm upstream of the flat plate heated

model. This caused a turbulent boundary layer to form, allowing comparison to turbulent theory instead of

working with the difficult-to-control transitional case. The effective unheated starting length was

estimated, since the precise starting point of the turbulent boundary layer was unknown. We would expect

the unheated starting length to be greater than the distance between the trip and the model, as the turbulent velocity boundary layer can not have zero thickness at the location of the trip. An estimated unheated starting length of 0.2 m matched experimental results closely, and is used in the theoretical curves shown in Figure 8, as well as in the flat plate data reduction found in Appendix I.

The heat transfer results for the flat plate runs at 10 m/s, 14.2 m/s, and 20 m/s are shown in Figure 8. They are compared to flat plate theory for a turbulent boundary layer, with a uniform heat flux thermal boundary condition. Each point on the curves represents the mean temperature value of a column of pixels, which is converted to heat transfer coefficients (as described in Section III). Each column is 0.68 mm wide; so the entire plate length of 0.42 m is represented by a smooth curve of 620 column values. For clarity, only every 8th point is shown on the flat plate graph.
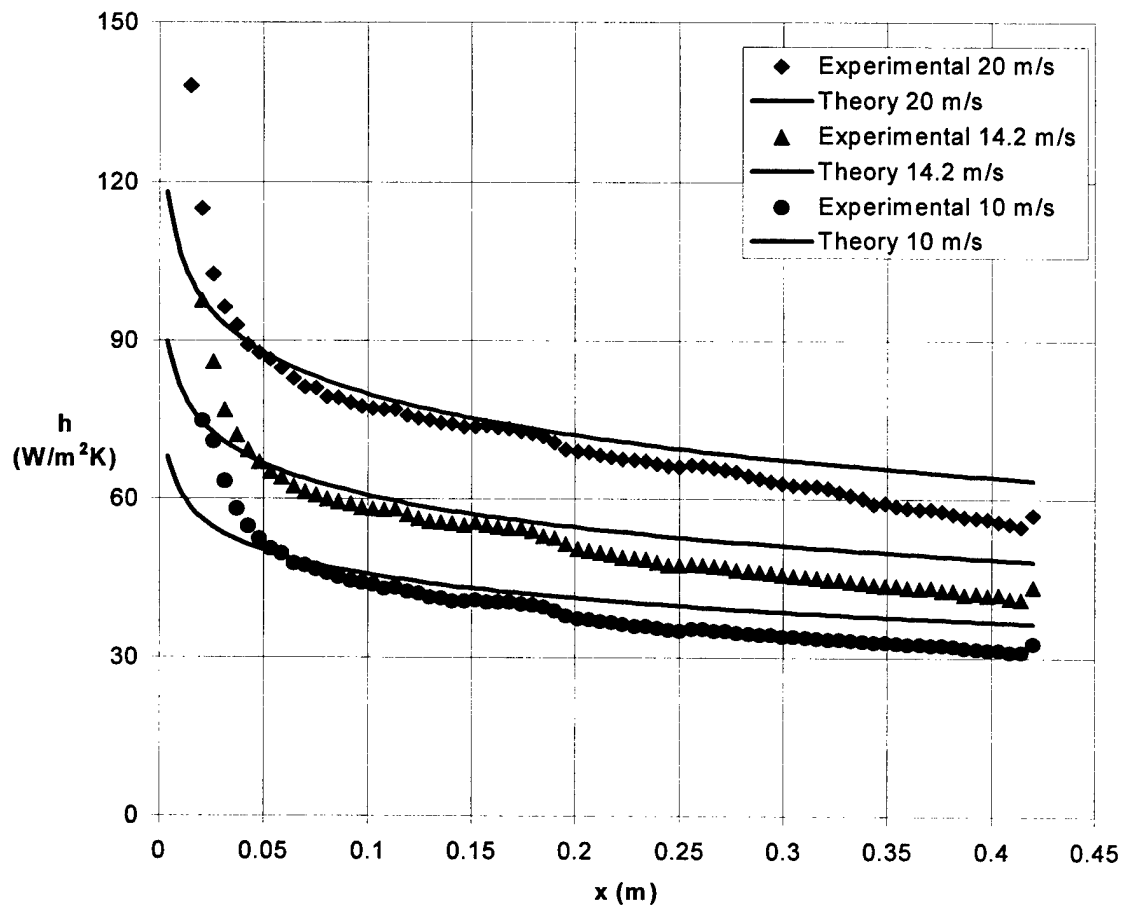
Figure 8 Flat Plate Experimental Results: Comparison to Theory

In both cases, agreement was quite good between experimental results and theory, especially in the region

between 0.05 m and 0.2 m. The forward region (under 0.05m) is experiencing several phenomena worth

mentioning. The boundary layer is being artificially tripped to turbulence, with wall Reynolds numbers in

this forward region of $1.6 \cdot 10^5$ or less. This is below that normally associated with transition to a turbulent

boundary layer. Hence, turbulent boundary layer theory is unable to provide a good match. Additionally,

this forward region is near the leading edge of the Styrofoam insulation behind the gold film, so end effects

(conduction losses) cause the surface temperature to be lower than in a perfectly insulated case. Also, due

to the steep temperature profile (and correspondingly steep h profile) near the leading edge, high

conduction between neighboring pixels lowers the temperature of adjoining pixels. Both influences cause

the h profile to appear higher than it actually is, which helps explain the variance near the leading edge.

Nevertheless, the results support the validity of the experimental method performed. For the region of the flat plate past 0.05 m, the experimental results for the 10 m/s case are within 9% of theoretical predictions, while the 14.2 m/s and 20 m/s results are within 8% and 5%, respectively. The computed uncertainties in h over the entire plate length are 4.1%, 4.1%, and 3.9%, respectively. The close agreement with flat plate theory allows us to move forward with further tests. We are confident that the temperatures sensed and the convective heat transfer profiles computed are reasonably accurate.

Furthermore, the results for the three flow velocities show proper scaling. Since $h \propto Nu$, and $Nu \propto Re^{0.8}$ from Equation (2), we expect $h \propto Re^{0.8}$. As the velocity increases from 10 m/s to 14.2 m/s, the h values should increase 32%, while the 20 m/s experimental data should show an increase of 74% over the 10 m/s data. In fact, these theoretical increases are closely matched by the experimental data in Figure 8. Actual increases are 33% and 79% for the two velocities.

For the remaining discussion of results, only the 10 m/s experimental data is shown for simplicity. The results from the 14.2 m/s and 20 m/s tests are contained in Appendix F, Effect of Velocity. Additionally, a discussion on the effect of power setting is contained in Appendix G.

B. Flat Plate with Interrupted Heating

Several different heated and unheated lengths were studied in the flat plate models with interrupted heating. First considered is the model with similar spacing to the ribbed model: 38 mm heated sections with 25mm unheated sections. An image from one of the runs is shown below, at a heat flux setting of 709 W/m^2.

heated strips with colorplay   unheated strips between
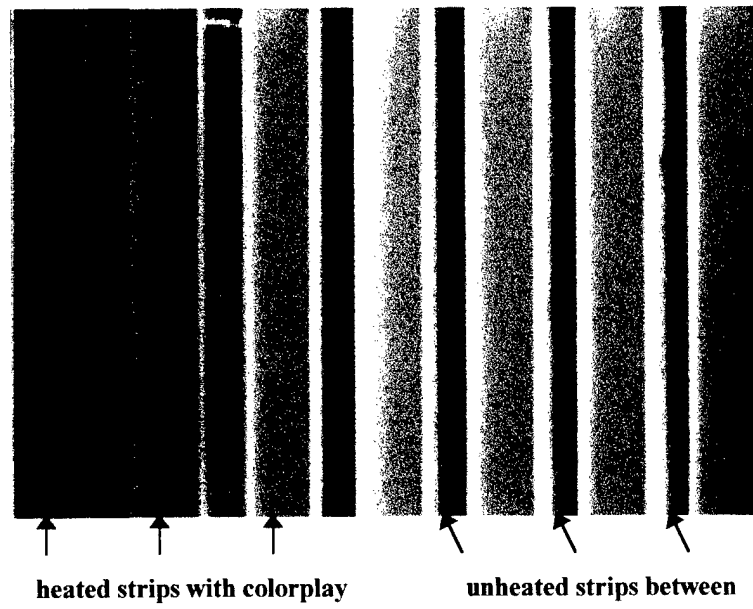
Figure 9 RGB Image of Flat Plate with Interrupted Heating, Spacing #1

To better see how the h profile changes, we can compare the first interrupted heating model to the

uniformly heated flat plate model. The following graph shows the 10 m/s experimental results for this

modification:
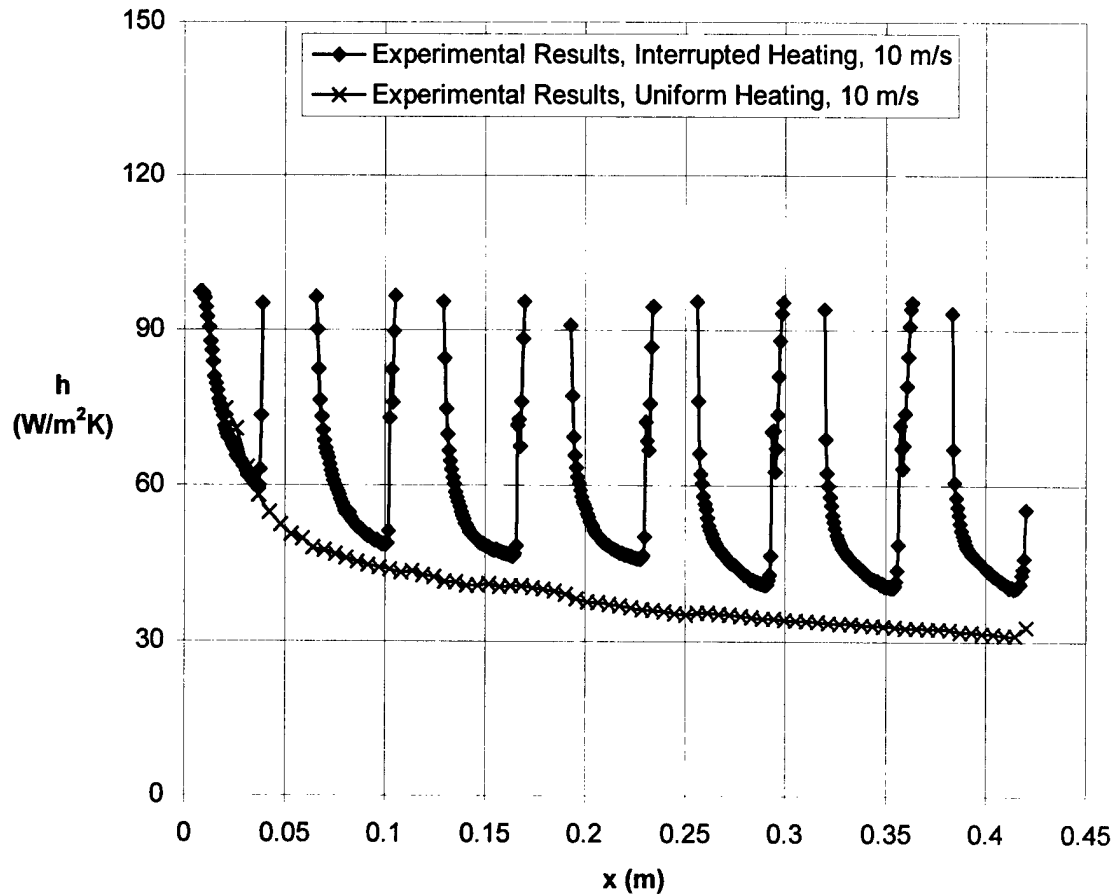
Figure 10 Comparison of h vs. x for Flat Plate Interrupted Heating and Uniform Heating, Spacing #1

As is expected, the h profile is high at the leading edge, like the flat plate model. The absence of heat flux in the unheated regions, however, causes the thermal boundary layer to begin to "reset" and we see a similar h profile repeated on each successive heated section. Although the thermal boundary layer "resets", the freestream air is warmer when it arrives at the second heated strip due to the upstream heating that has occurred. There is evidence of this in the lowest heat transfer coefficients on the trailing edge of each heated section. The minimum h value continues to decrease and stabilizes by about the 5th heated section. This suggests that the profile reaches a steady-state condition, where the freestream air temperature is in balance with the heat transfer from the plate, and the h profiles become self-similar. Similar results have

been seen in the numerical work on this subject (Ang, Yap 1997). The sharp upturn in the h profile at the trailing edge of each heated section may be an artifact of wall conduction and should be ignored.

For this case and those remaining, it is interesting to establish how much of an incrase in h exists, when compared to the flat plate uniform heating model. For comparison purposes, we choose to evaluate the average h value at the 5th heated section (since stability occurs after this) and compare it to the flat plate data at the same location. For this case, on the 5th heated section, there is a 38% average increase in h. It should be noted that the average is higher on the heated strips, but the overall average is lower, due to the absence of any heat transfer on the unheated strips.

We next look at the second spacing tested in the study of the heat transfer coefficient over a flat plate with interrupted heating. This modification involved decreasing the heated length to 25 mm, while increasing the unheated section length to 38 mm. Figure 11, below, shows the experimental results for 10 m/s.
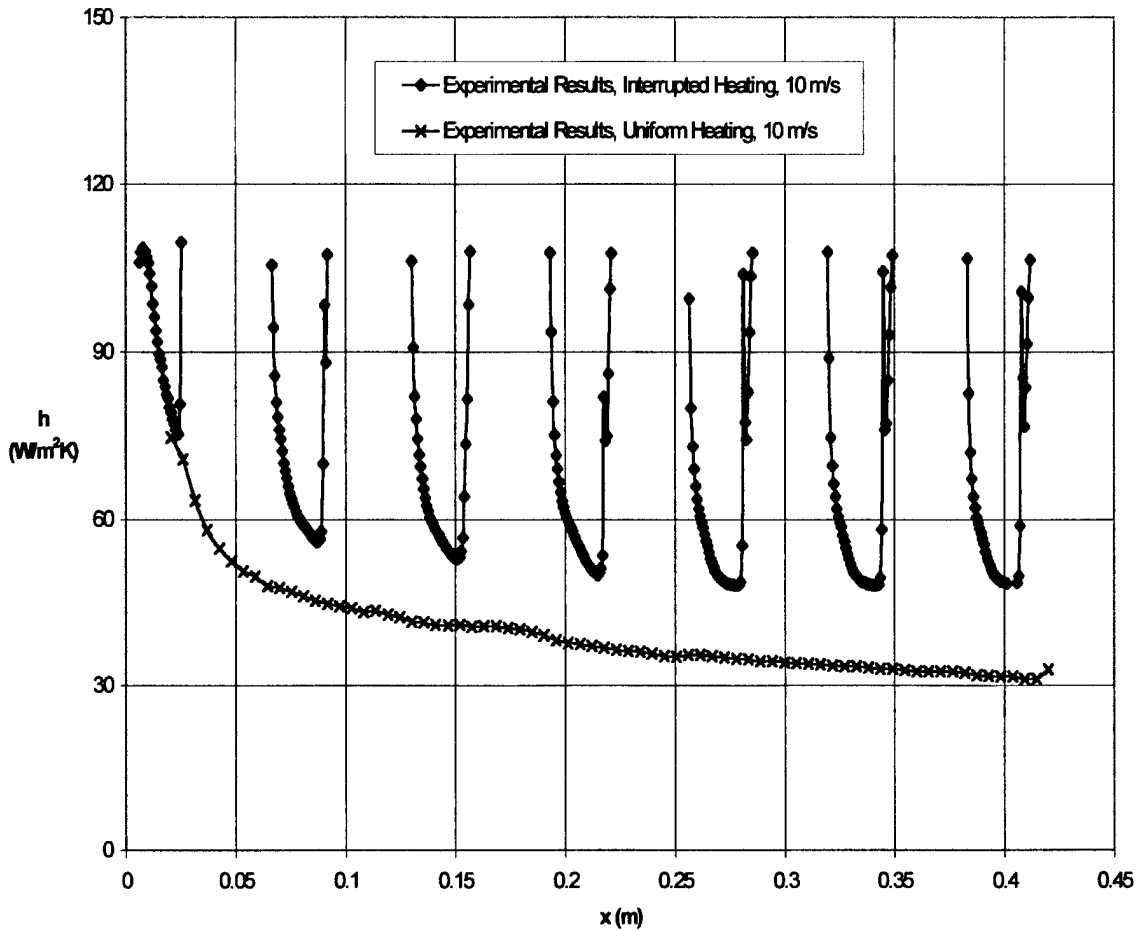
Figure 11 Comparison of h vs. x for Flat Plate Interrupted Heating and Uniform Heating, Spacing #2

As in the previous case, we see a steep h profile for each successive heated section, with the solutions

becoming self-similar after approximately 5 ribs. Again, the trailing edge of each section shows some

bleed-off of the temperature into the non-heated sections, causing an artificial rise in the heat transfer

coefficient over the last 5-10 columns. Because the areas of non-heating are larger, the thermal boundary

layer resets more than in the previous case, hence, the h profile is steeper, with higher maximum h values

and higher average h values across each heated section. When compared to the uniformly heated model,

the average h on the 5th heated section increases approximately 64%.

Finally, the heated strips are reduced in size to 16 mm, with a corresponding increase in the size of the unheated strips to 47 mm. The following figure shows a typical image, at 10 m/s with a heat flux setting of 791 W/m².

heated strips with colorplay   **unheated strips between**
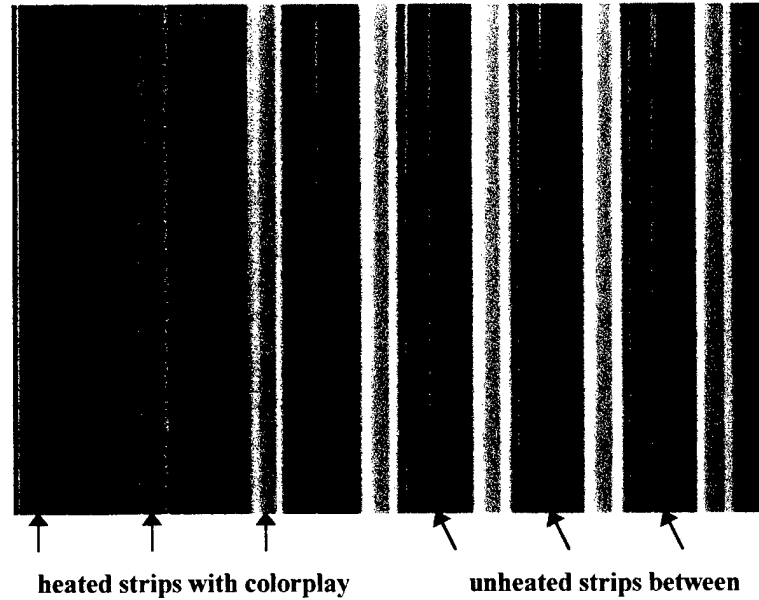
Figure 12 RGB Image of Flat Plate Interrupted Heating, Spacing #3

Figure 13 on the following page shows the experimental results for Spacing #3 at 10 m/s.
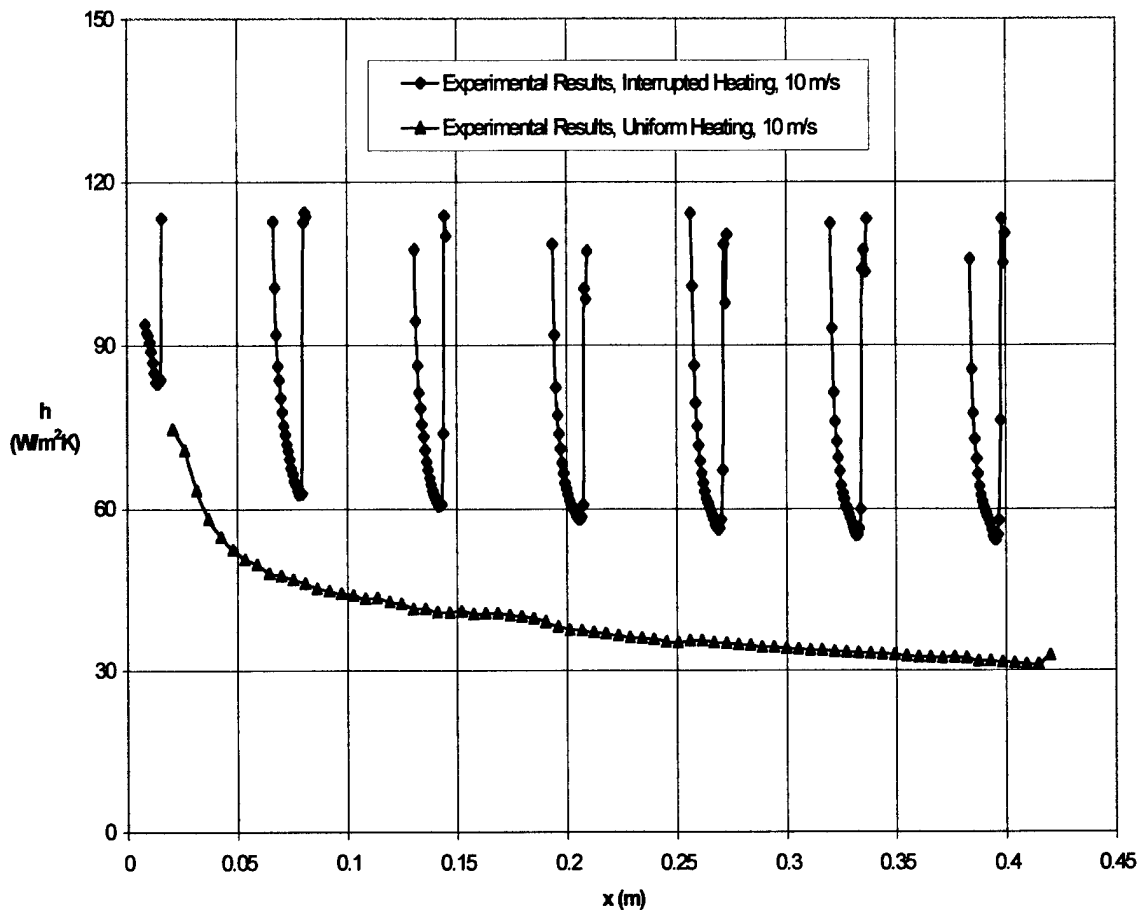
Figure 13 Comparison of h vs. x for Flat Plate Interrupted Heating and Uniform Heating, Spacing #3

In this example, the effect of shortening the heated section and lengthening the unheated section is amplified. The h profile is steeper, and the maximum h values at the leading edge are higher. A steady-state heat transfer profile appears to take shape at the 5th heated section as before. Trailing edge bleed-over into the non-heated sections are observed here as well, with the artificially high h values in the 5 columns aft of the trailing edge of the heated sections.

The average h on the 5th heated strip is nearly double that of the uniform heating case (93%) for this spacing at 10 m/s.

C. Ribbed Model

The ribbed model studied has heated/unheated sections similar to one of the flat plate interrupted heating models (spacing 1). The heated ribs are 38 mm wide, with unheated channels between the heated sections that are 25 mm wide. The channels are recessed 19 mm below the top surface of the ribs. This allows air to circulate in the cavities between the ribs, cooling and effecting the thermal boundary layer. An RGB image from the 10 m/s data set is presented below. Notice the lack of color bleed to the neighboring unheated sections, and the distinct color play that occurs on each heated rib.

heated ribs with colorplay   **unheated channels between**
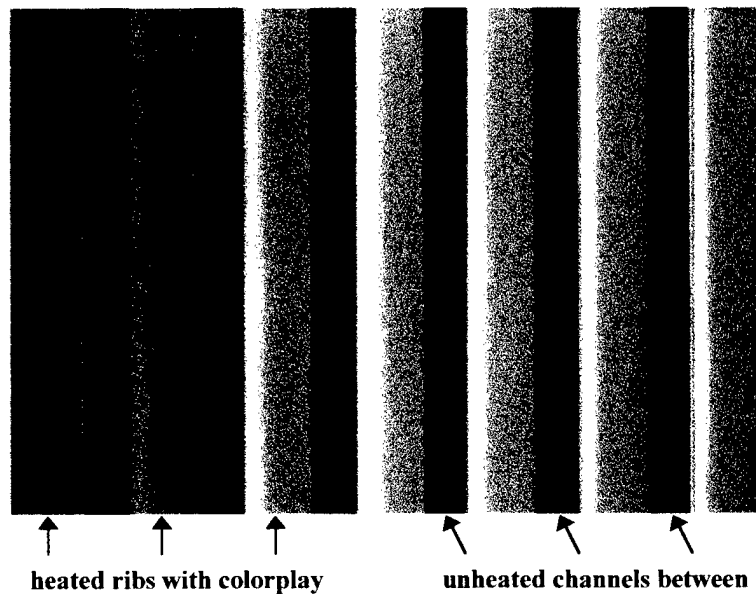
Figure 14 RGB Image of Ribbed Model

The next figure shows the heat transfer coefficient distribution over the ribbed model for 10 m/s flow. Notice the same repeated steep h profile as seen in the interrupted heating flat plate models.
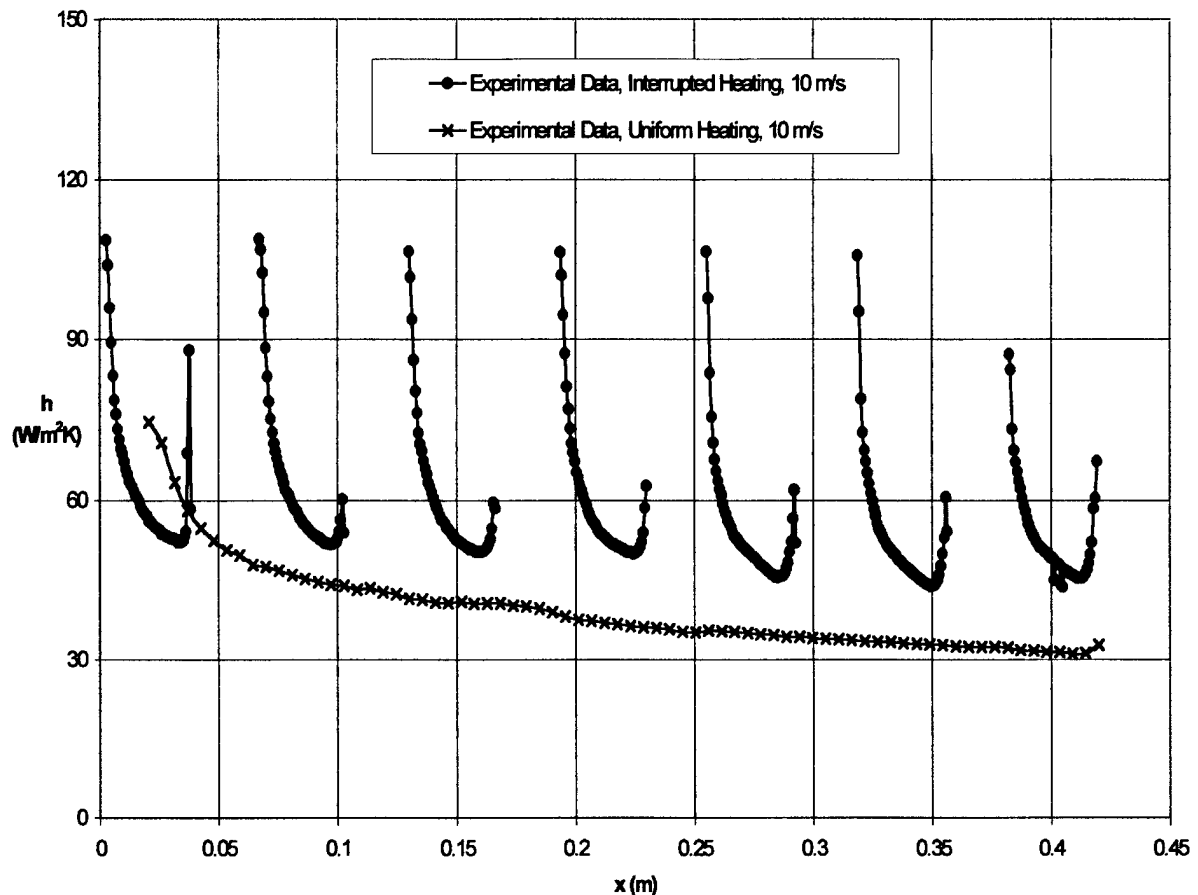
Figure 15 Comparison of h vs. x for Ribbed Model Interrupted Heating and Flat Plate Model Uniform Heating

The downstream edge of each rib shows an upturn in the h profile as well. Again, this is caused by conduction losses. These losses occur in the pixels near the edge of the Styrofoam insulation, much as they did in the flat plate model near the leading edge. Due to these losses, the surface is cooler there than in a perfectly insulated case and the computed h profile shows an upturn, larger than actually exists. Each column is 0.68 mm wide; end effects are seen in approximately the last 8 columns, or 5 mm of the 38 mm rib width.

The average h increase on the 5th heated rib, when compared to the flat plate uniform heating model, is 57%.

It is interesting to compare the ribbed model heat transfer results with the flat plate interrupted heating (spacing 1) results. The dimensions of the heated and unheated sections are the same. Therefore, the comparison shows the effect of the cavities on heat transfer. As stated previously, we would expect the ribs to increase circulation and mixing of the thermal boundary layer, thereby bringing cooler air to the surface, and increasing heat transfer when compared to a surface without the ribs. In fact, this does occur. The following figure shows a comparison between the flat plate interrupted heating and the ribbed model results. Heat transfer is 13% higher along the entire profile for the ribbed model, apparently due to the increased flow mixing which promotes lower thermal boundary layer temperatures and higher heat transfer coefficients. Note that the two h profiles are very similar in shape and are simply shifted higher for the ribbed case (heated sections 2 through 7).
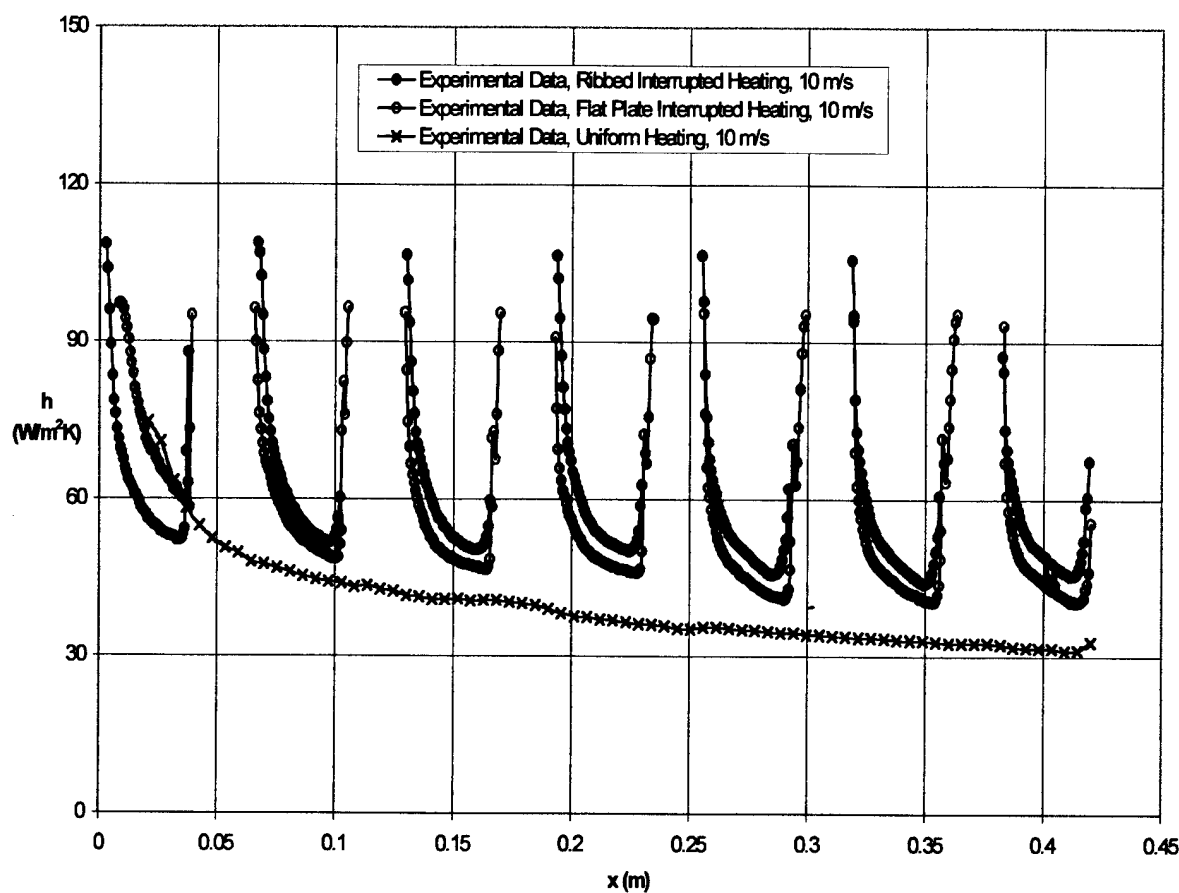
Figure 16 Comparison of h vs. x for Ribbed and Flat Plate Interrupted Heating

Although we do not place much confidence in the heat transfer results near the leading edge of the flat plate due to end effects and the breakdown of our turbulent boundary layer heat transfer theory, it is interesting to note the difference between the ribbed model and flat plate interrupted heating cases on the first heated section. The ribbed model heat transfer is actually lower than the flat plate interrupted heating case. This is probably due to the flow dynamics occurring at the leading edge of the plate versus those occurring at the first rib, where each meets the wind tunnel wall. Perhaps the juncture with the flat plate was smoother, and the ribbed model caused some separation to occur.

This section has focused on results obtained for the 10 m/s freestream velocity condition. Data was also collected for 14.2 m/s and 20 m/s test conditions, and can be found in Appendices F and G. This data agrees well with the 10 m/s data, with only a few exceptions.

The following table summarizes the increase in average h value at the 5th heated section, when compared to the flat plate uniform heating case.

Table 2 Summary of h profile results

Model Configuration	Flow Velocity, m/s	% Change
Flat Plate with Interrupted Heating, Spacing #1	10	38
Flat Plate with Interrupted Heating, Spacing #2	10	64
Flat Plate with Interrupted Heating, Spacing #3	10	93
Ribbed Model	10	57

V Conclusions

Studies of local convective heat transfer were conducted for three cases with a turbulent boundary layer. These studies yielded the following results:

- For a flat plate with uniform heating, good agreement (better than 10%) was found between flat plate uniform heat flux theory and the experimental results. The small difference is easily explained by the experimental uncertainty and the lower than normal Reynolds numbers for the tripped turbulent boundary layer.

- For a flat plate with interrupted heating, the heat transfer was found to be significantly higher on each heated strip, compared to the uniform heating case. As the heated sections become narrower, (and the non-heated sections wider), the h profile increased further.

- For a ribbed model, the heat transfer from the top of the ribs is also higher than that for the flat plate with uniform heating. It is slightly greater than the heat transfer over the flat plate with interrupted heating (same heated and unheated lengths). The cavities enhance flow circulation, increasing heat transfer from the top surface of the ribs.

- The studies show that for a known surface heat flux, the heat transfer is higher, and the corresponding temperature is lower, for surface-mounted modules than would be predicted with flat plate uniform heating theory. Interruption of the heating has a significant effect on the local heat transfer, far more than the rib/cavity effects.

- The heated-coating method with TLC's proved to be an excellent means of mapping the local heat transfer coefficient data.

- The uncertainty in h for all three models studied, with a 95% confidence level, is approximately 5%.

- The benefits of future studies in this field are clear: better heat transfer in electronic packaging and other applications, and reduction of problems caused by high operating temperatures.

- It is hoped that numerical calculations can be performed for comparison with the specific cases studied here. This would help validate these results, as well as help advance the capabilities of predicting interrupted thermal boundary condition heat transfer results on flat and ribbed surfaces.

VI References

1. Agonafer, D., and Moffat, D. F. 1985, "Numerical Modeling of Forced Convection Heat Transfer For Modules Mounted on Circuit Board," *Numerical Simulation of Electronic Equipment Cooling,* ASME, HTD-Vol. 121, pp. 1-5.

2. Ang, C.C. and Yap, C., 1997, "The Effect of Geometric Parameters and an Implanted Barrier on the Cooling of Chip Arrays," *Transport Phenomena in Thermal Science and Process Engineering,* Vol. 3, pp. 851-856, Japan: Pacific Center of Thermal-Fluids Engineering.

3. Anon. 1993, *Guide to the Expression of Uncertainty in Measurement,* International, Organization for Standardization, Geneva, Switzerland, ISBN 92-67-10188-9.

4. Arkin, H., and Colton, R. R. 1970, *"Statistical Methods,"* Barnes and Noble, Inc.

5. Bar-Cohen, A., and Witzman, S., 1993, "Analysis and Prevention of Thermally Induced Stresses in Electronic Equipment," *Thermal Management of Electronic Systems,* pp. 25-42.

6. Baughn, J. W., 1995, "Liquid Crystal Methods for Studying Turbulent Heat Transfer," *International Journal of Heat and Fluid Flow,* Vol. 16, pp. 365-375.

7. Baughn, J. W., Anderson, M. R., Mayhew, J. E., and Wolf, J. D. 1998, "Hysteresis and Uncertainty of Thermochromic Liquid Crystal Temperature Measurement Based On Hue," Proceedings of the 5th ASME/JSME Joint Thermal Engineering Conference, March 15-19, 1999, San Diego, CA. Also submitted to ASME *Journal of Heat Transfer.*

8. Baughn, J. W., Takahashi, R. K., Hoffman, M. A., and McKillop, A. A. 1985, "Local Heat Transfer Measurement Using an Electrically Heated Thin Gold-Coated Plastic Sheet," ASME *Journal of Heat Transfer,* Vol. 107, pp. 953-959.

9. Brown, K. K., Coleman, H. W., Steele, W. G., and Taylor, R. P., 1996, "Evaluation of Correlated Bias Approximations in Experimental Uncertainty Analysis," *AIAA Journal,* Vol. 34, No. 5, pp 1013-1018.

10. Butler, R. J. 1995, "The Effects of the Thermal Boundary Condition and Turbulence on Heat Transfer from a Cylinder, Flat Plate, and Turbine Blade Using the Transient Shroud and Heated-Coating Techniques," Ph. D. Dissertation, University of California, Davis.

11. Coleman, H. W., and Steele, W. G., 1995, "Engineering Application of Experimental Uncertainty Analysis," *AIAA Journal*, Vol. 33, No. 10, pp. 1888-1896.

12. Coleman, H. W., and Steele, W. G. 1989, *Experimentation and Uncertainty Analysis for Engineers*, Wiley, New York.

13. Hacker, J. M., and Eaton, J. K. 1997, "Measurements of Heat Transfer in a Separated and Reattaching Flow with Spatially Varying Thermal Boundary Conditions," International Journal of Heat and Fluid Flow, Vol. 18, No. 1, pp. 131-141.

14. Incropera , F. P., and DeWitt, D. P. 1990, *Fundamentals of Heat and Mass Transfer*, 3rd ed., Wiley, New York.

15. Kang, B. H., Jaluria, Y., and Tewari, S. S. 1990, "Mixed Convection Transport from an Isolated Heat Source Module on a Horizontal Plate," Transactions of the ASME. Journal of Heat Transfer, Vol. 112, No. 3, pp. 653-661.

16. Kays, W. M., and Crawford, M. E. 1980, *Convective Heat and Mass Transfer*, McGraw-Hill, New York.

17. Kline, S. J., and McClintock, F. A., 1953, "Describing Uncertainties in Single-Sample Experiments," *Mechanical Engineering*, Vol. 75, pp. 3-8.

18. Schenck, H., 1979, *Theories of Engineering Experimentation*, 3rd ed., McGraw-Hill, New York.

19. Siegel, R., and Howell, J. R. 1992, *Thermal Radiation Heat Transfer*, 3rd ed., Hemisphere, Washington D.C.

20. Sparrow, E. M., Niethammer, J. E., and Chaboki, A. 1982, "Heat Transfer and Pressure Drop Characteristics of Arrays of Rectangular Modules Encountered in Electronic Equipment," *International Journal of Heat and Mass Transfer*, Vol. 25, pp. 961-973.

21. Taylor, R. P., Coleman, H. W., Hosni, M. H., and Love, P. H. 1989, "Thermal Boundary Condition Effects on Heat Transfer in the Turbulent Incompressible Flat Plate Boundary Layer," *Int. Journal of Heat and Mass Transfer*, Vol. 32, pp. 1165-1174.

22. Wirtz, R. A., and Chen, W. 1992, "Laminar-transitional Convection From Repeated Ribs in a Channel," *Journal of Electronic Packaging*, Vol. 114, pp. 29-34.

Appendix A: Liquid Crystal Selection

Hallcrest BM/R30C10W/C17-10 TLC's were chosen for this application, for several reasons. First, broad-band liquid crystals allow visualization of a wide range of surface temperatures. Because the TLC's used in this application have a ten degree bandwidth, a wide range of temperatures and heat transfer coefficients can be captured in one image with a particular power setting. This is useful, as both the data collection and data reduction are simplified. The following graph shows several different liquid crystals and their corresponding h ratios, for ambient temperatures of 25°C-30°C. The h ratio shown is the ratio of the maximum measurable h to the minimum measurable h.
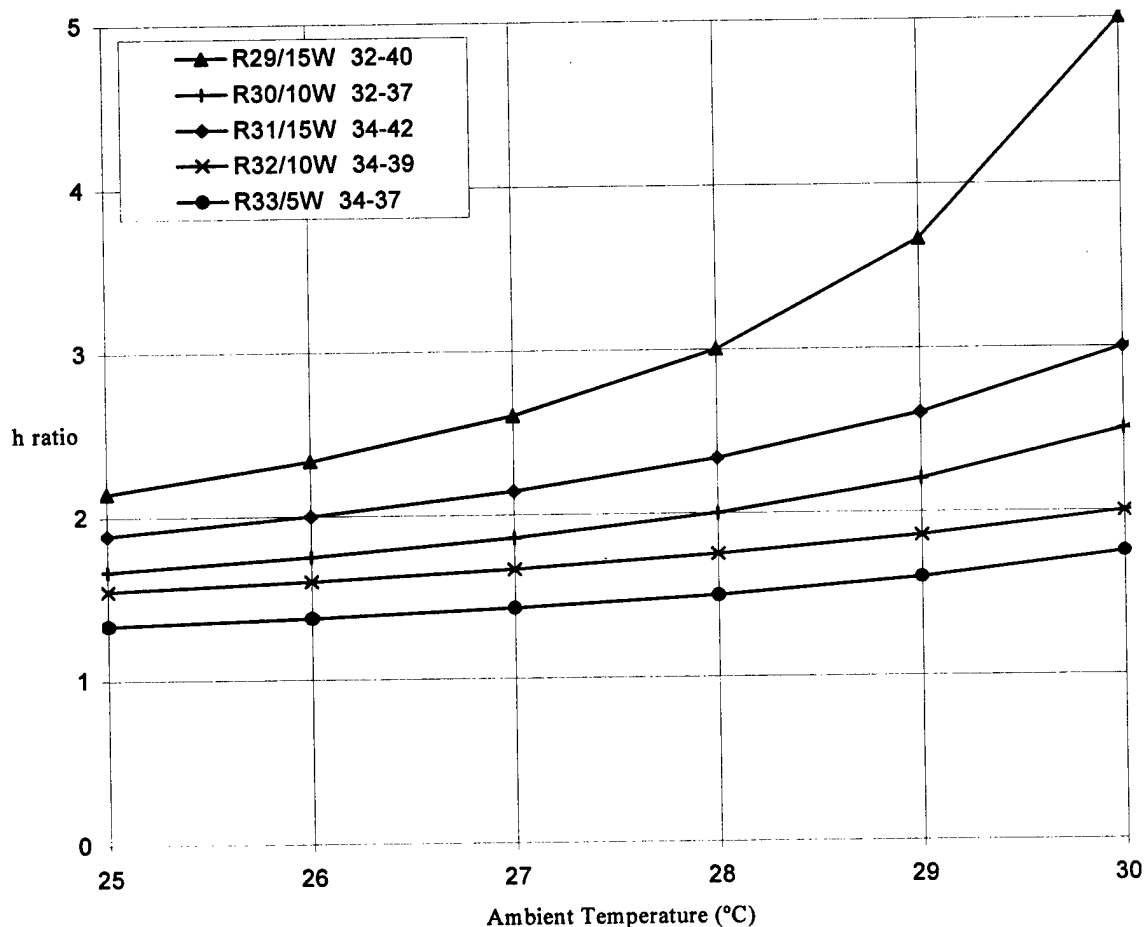
Figure 17 Measurable h ratios for Several TLC's vs. Ambient Temperature

The reader will note that the broad-band TLC's, when compared to the narrow-band ones, produce the largest ratios. Additionally, lower "red start" temperatures increase the h ratio even more, and are desirable.

A red start temperature of 30°C was also beneficial in affording lower uncertainties in our results. From the previous work of Baughn et al. (1998), calibration of wide band liquid crystals which avoids high temperatures and hysteresis can achieve uncertainties in temperature on the order of 4% of the useful range. Using this predicted value of surface temperature uncertainty, and the anticipated freestream air temperature of 25°C to 31°C in the wind tunnel lab, the following equation was used to determine the "relative uncertainty" in surface temperature difference.

$$\frac{U_{Tsurface}}{(T_s - T_\infty)} = \frac{0.04 \cdot (T_{High} - T_{Low})}{(T_s - T_\infty)} \tag{5}$$

Estimating a color play range of 32°C to 38°C for the R30C10W TLC, a relative uncertainty of 5% or less is possible with lab temperatures as high as 27°C. Figure 18 shows this relative uncertainty for a range of ambient temperatures.
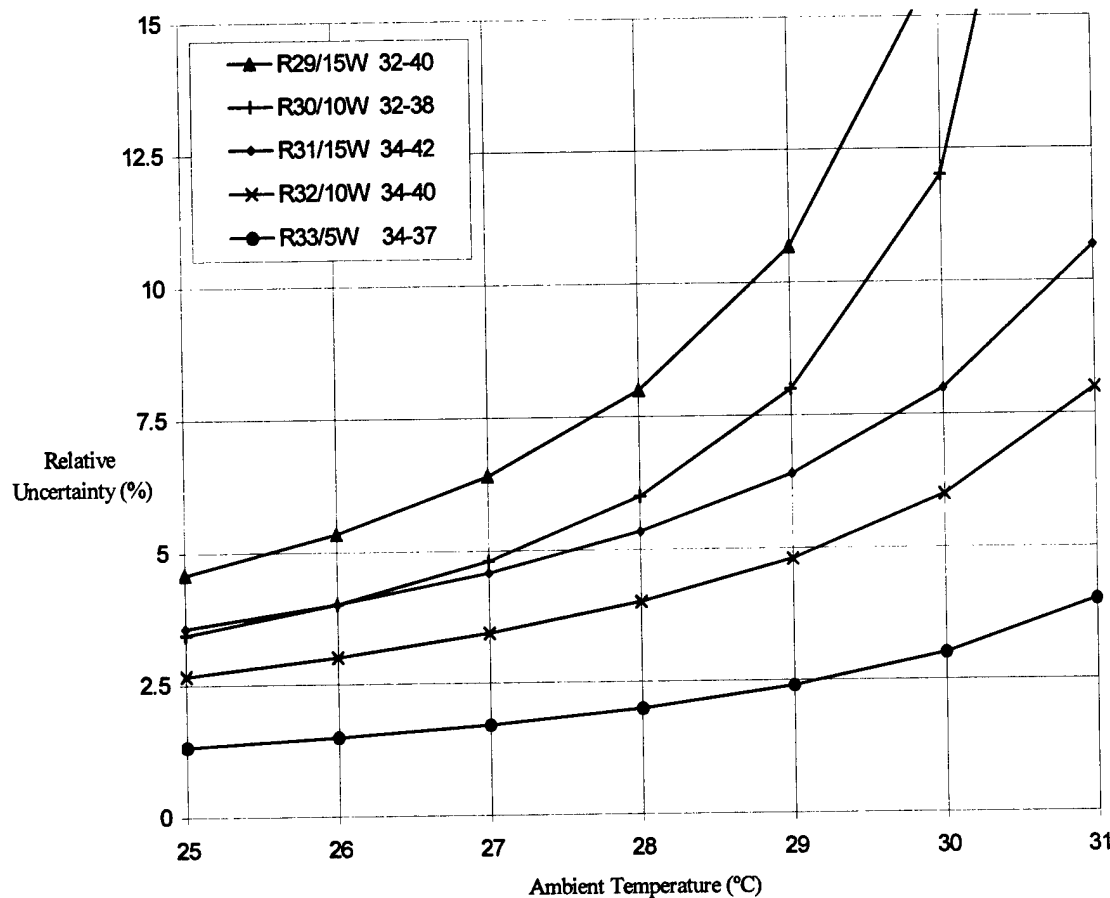
Figure 18 Uncertainty in Temperature for Several TLC's vs. Ambient Temperature

Minimizing uncertainty for all measured temperatures at high ambient temperatures is a priority; therefore, the R30C10W TLC provided low uncertainty levels along with a large measurable h range. Another liquid crystal which performed well in terms of uncertainty and h range is the R31C15W. The 10W crystal was chosen over the 15W liquid crystal because of the author's experience with 10W liquid crystals, and because of the anticipated range of surface temperatures that would be present during testing.

Appendix B: Liquid Crystal Calibration and Calibration Image Processing

Calibration of the Hallcrest BMR30C/10W liquid crystal began with a series of tests conducted to determine its hysteresis characteristics. The tests were conducted alongside several other liquid crystals in a separate calibration apparatus. This apparatus was used previously in such tests as described in the paper, "Hysteresis and Uncertainty of Thermochromic Liquid Crystal Temperature Measurement Based on Hue" (Baughn et al. 1998). The tests revealed, as previously experienced with other wide band liquid crystals, that hysteresis on cooling does occur with this liquid crystal, but only when heated to 52.5°C or higher. Although the models would be heated in actual tests, it was determined that calibration of this liquid crystal could be done using a cooling procedure, as long as the initial temperature for cooling was kept under about 50°C to avoid hysteresis. The author further reduced this temperature to provide an extra margin of safety, allowing the calibration block to reach a maximum temperature of only 43°C during all phases of calibration conducted.

An in-situ calibration was performed to expose the liquid crystal to the same lighting and camera angles, as well as the same amount and quality of incident light, as falls on the on the models themselves. With regard to this last item, camera adjustment was performed to ensure the recorded hues matched those of the MacBeth Color Checker standard. Four gray squares (having equal amounts of red, green, and blue components) were photographed, and the output RGB values matched with camera gain settings to ensure a neutral color balance. A red gain setting of -27 and blue gain setting of +42 provided a close match.

The lighting used for the calibration as well as the data collection runs were two GE Soft White lights, with Spectrum 574 UV filters in place to eliminate transmission of wavelengths below 400 nm. The magenta-colored filter (it reduces the green component of the light), when combined with the Soft White lights, produces a nearly flat spectrum in the 400 nm to 700 nm range. This is ideal for a balanced calibration curve that is nearly linear in the temperature vs hue relation.

Hallcrest BB-G1 black paint (4:1 water to paint ratio) was airbrushed onto the copper calibration block, and allowed to dry. Liquid crystal (2:1 water to LC ratio) was then applied, with the desired coverage assessed during painting using a heat gun. The amounts of coverage were recorded, so that the models could be painted with the same amount (per area) as the copper calibration block. This ensured equal reflectivity of the liquid crystal, as well as an equal contribution to the perceived hue by the black background. Amounts used per 100 in^2 area (0.07 m^2) were: black paint: one 4 oz glass jar. Liquid crystal: 6 thimbles. Care was taken to ensure an even coverage of paint and liquid crystal, to reduce the standard deviation as well as any end-to-end variations on the calibration block.

The total length of the flat plate and ribbed models is 0.42 m. It was necessary to collect calibration data with the 0.23 m calibration block in two positions: left and right. This data were then combined to form calibration data for the entire area of interest. Since the camera and lighting angles change from left to right across the plate, is was necessary to form separate calibration curves for different areas. There are seven heated sections on the flat plate model, and 7 ribs on the ribbed model. Therefore, seven different areas were chosen to calculate individual calibration curves. Each area corresponds to one heated section and its neighboring downstream, unheated section. This breakdown allows a more precise calibration of each point on the plate. Figure 18 shows how the calibration runs were broken down into seven areas.
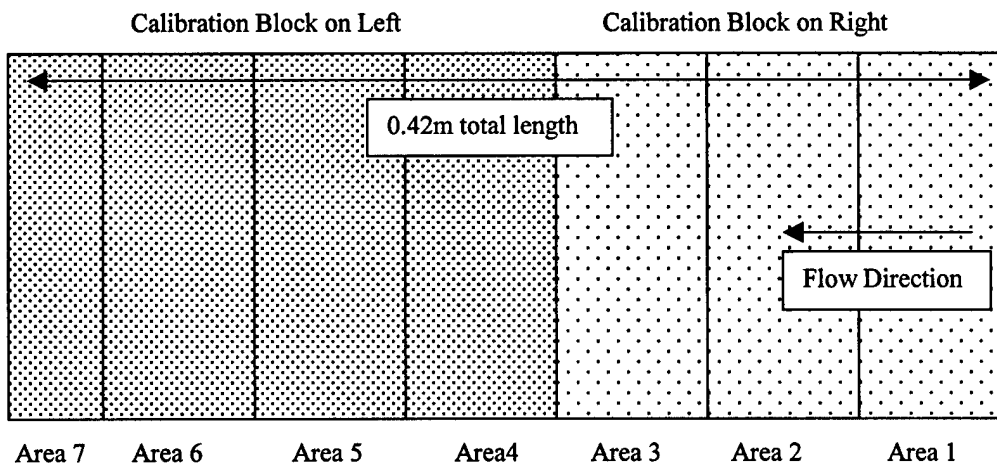
Figure 19 Area Distribution of Calibration Runs

Figure 20 shows how the standard deviation of the mean hue varies across the areas of calibration. The peaks at areas 1, 4, and 7 may occur because of calibration block conduction losses near the edges, and the influence of lighting reflections from neighboring tunnel walls at the block ends.
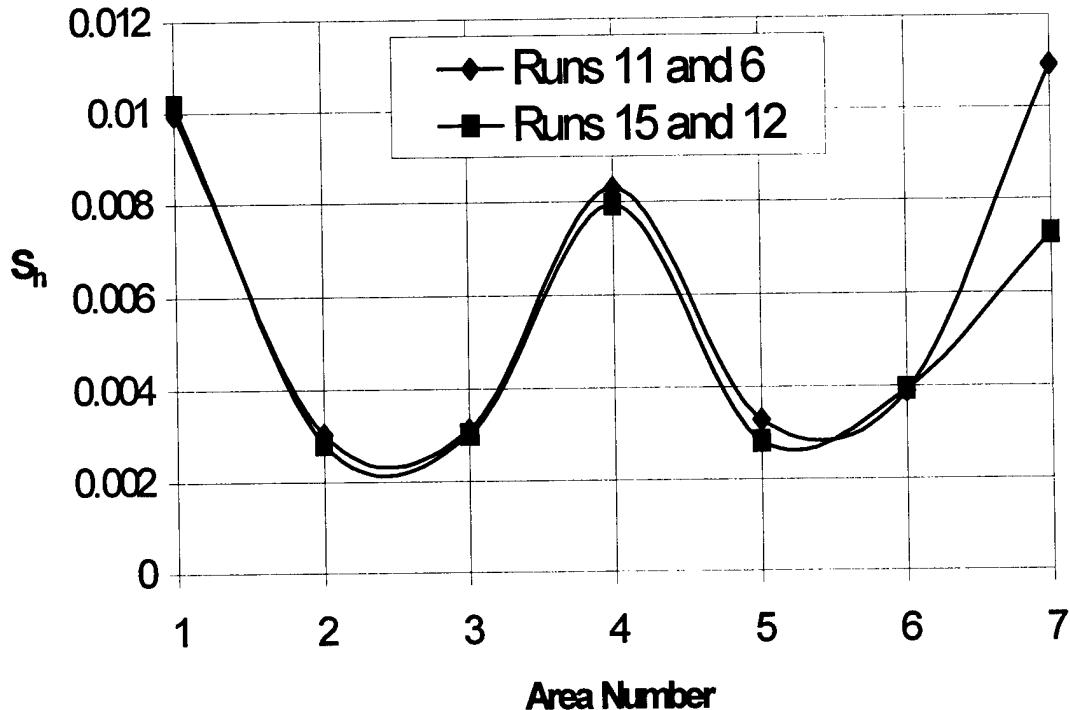
Figure 20 Standard Deviation in Hue for 7 Calibration Regions

The calibration block height matches the area of interest at 15 cm. However, sufficient variation was seen top to bottom, to warrant the choice of a smaller area to calibrate and collect data. This desire for a smaller area size is balanced by the fact that more pixels in a sample actually lowers the standard deviation of the mean hue. The standard deviation of the mean hue is reduced by the square root of the number of items in the sample (Coleman, Steele 1989):

$$S_{h\,mean} = \frac{S_h}{\sqrt{N}}$$

(6)

To better study the effects of area size and relative position on the plate, we analyzed the mean hue and

standard deviation of five different areas. These areas are shown on Figure 21, below: i) middle 2.5 cm,

ii) middle 5 cm, iii) middle 7.5 cm, iv) 2.5 cm above the hole, v) 5 cm above the hole.
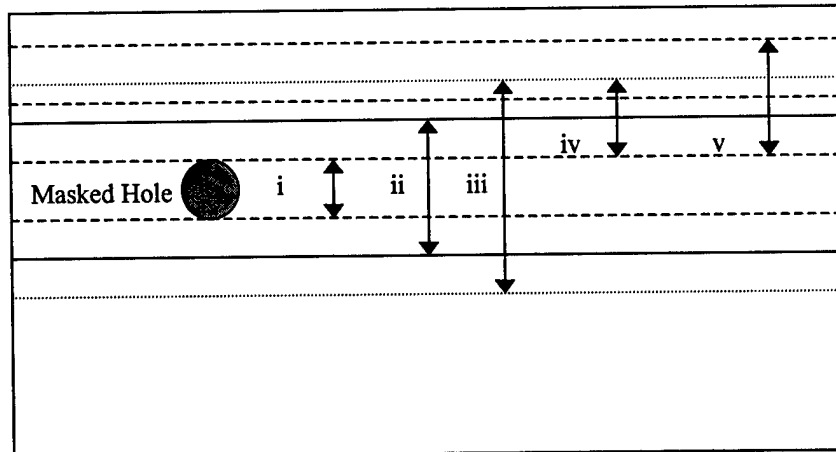
Figure 21 Plate Areas Used for Standard Deviation Comparison

Figure 22 on the following page shows a comparison of the average pixel-to-pixel standard deviation

throughout the 10°C calibration range for the five different plate areas.
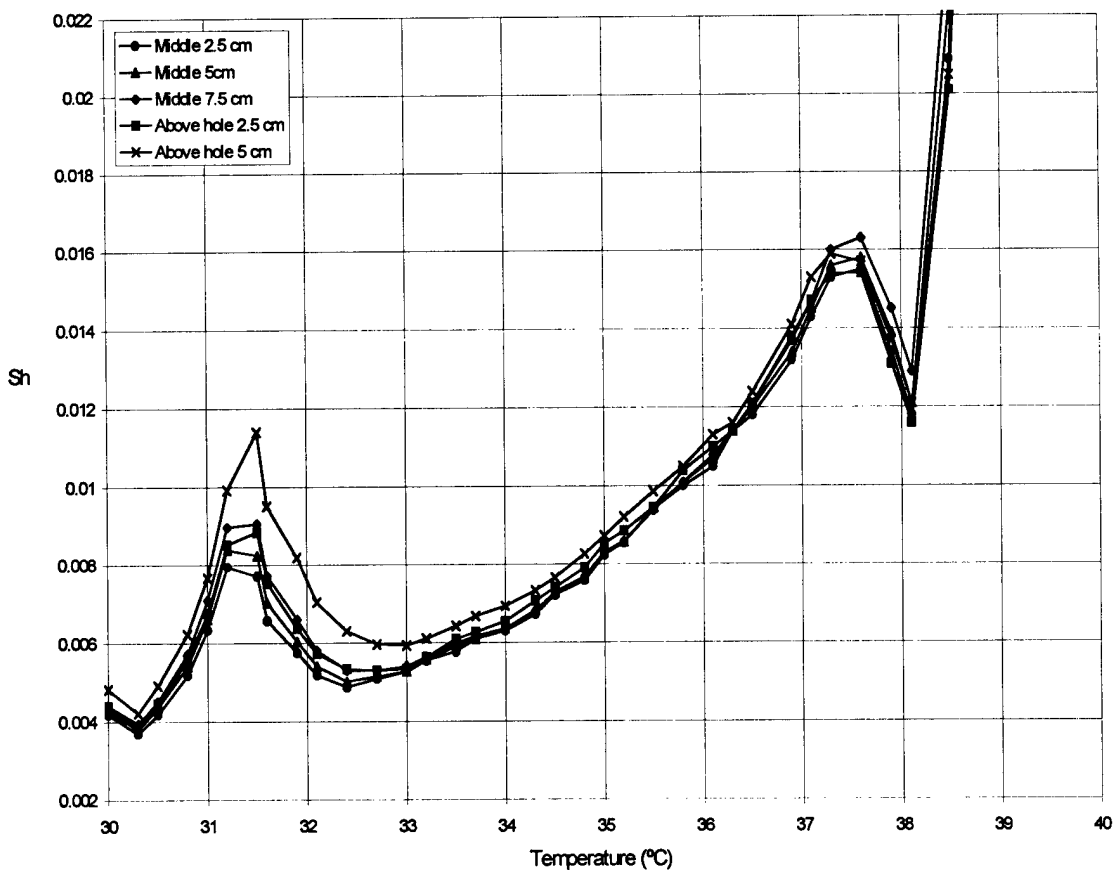
Figure 22 Standard Deviation in Hue for Various Plate Areas

It is expected that the middle 2.5 cm (Area i) would show the lowest standard deviation. From a calibration and data reduction standpoint, it is simpler to use an area above the existing masked hole in the Plexiglas window. The graph shows that the standard deviation of this 2.5 cm portion (Area iv) is within 10% of the best area (i), so we chose to use this area for the present study.

Related to the standard deviation in hue of each area is the method we use to analyze the mean hue and the standard deviation for the specified area. According to a recent paper on the subject (Baughn et al. 1998), a median filter is a good method to use. The median filter takes an [N x M] area about a selected pixel and computes the median hue of the block, assigning that value to the selected pixel. The effect of the median filter is to reduce the standard deviation from pixel to pixel, with an associated loss in spatial resolution.

If a median filter is used the standard deviation of the sample is related to the standard deviation of the population by the following equation (Arkin, Colton 1970).

$$S_{h\,median} = 1.2533 \frac{S_h}{\sqrt{N}} \qquad (7)$$

The median does not reduce the standard deviation as much as a mean. However Arkin and Colton (1970) point out that the median has several advantages over a mean including the fact that "It is not distorted in value by unusual items." In TLC images bad pixels in the CCD camera, regions with poor TLC coverage, or dust can introduce "outliers" or wild readings. The use of a median filter reduces the effect of these "outliers" at the cost of less reduction in standard deviation than a mean filter.

A median filter degrades the spatial resolution because each pixel now contains information from surrounding pixels. A 3×3 and a 5×5 block degrades the spatial resolution by a factor of 3 and 5, respectively. Whether this loss in spatial resolution is worth the reduced standard deviation (and corresponding reduced uncertainty) depends on the application. Figure 23 shows the effect of a median filter on the hue standard deviation of one of the seven calibration areas studied. The advantage of a 5×5 median filter is clear, especially in the absence of any spatial resolution requirements.
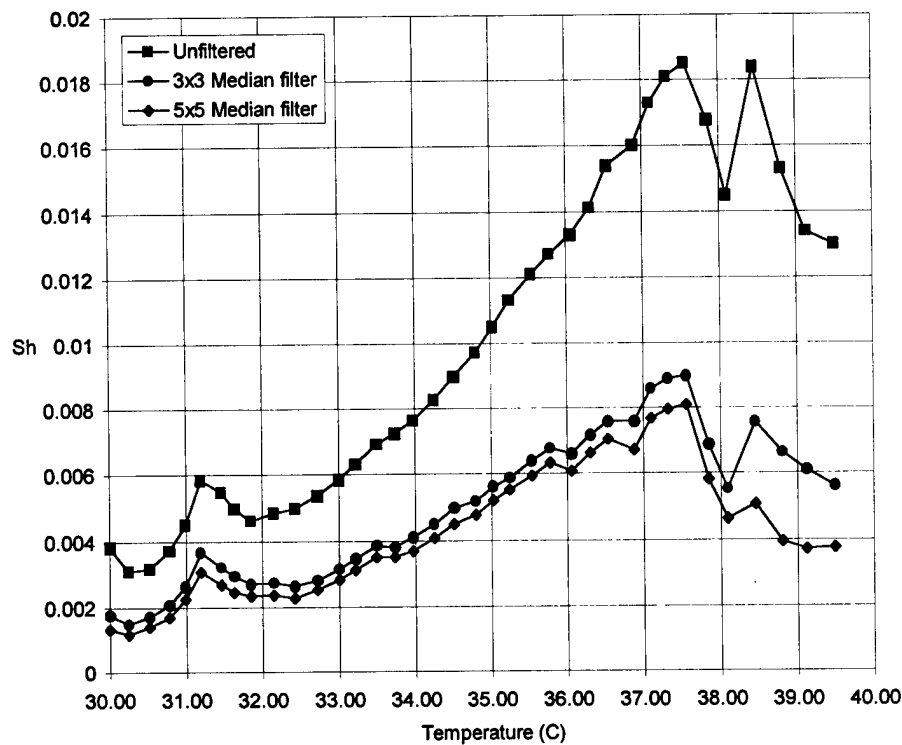
Figure 23 Effect of Median Filter on Standard Deviation for Calibration Area 4

Several calibration runs were performed prior to the tests being conducted. Over a 27-hour period, three calibration runs were made with the block on the left and right sides (6 total runs). These three calibration runs on each side were plotted to determine repeatability. As Figure 24 on the following page shows, they are highly repeatable.

Temperature vs Hue
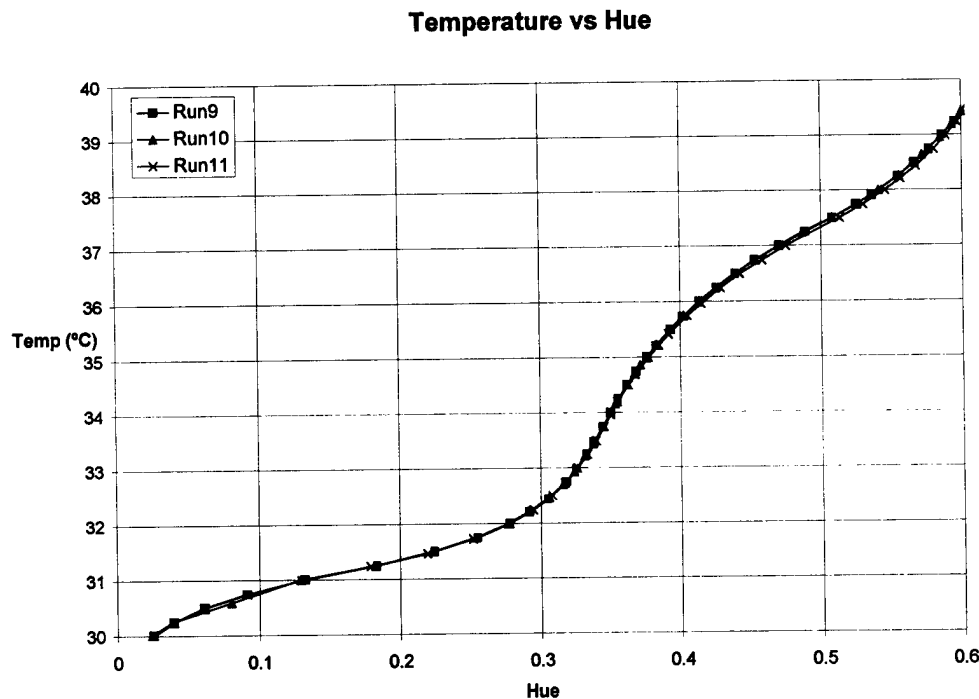
Figure 24 Repeatability of Three Early Calibration Runs

Since all three runs showed identical performance (within 0.1°C), the calibration run having the lowest

standard deviation in hue for the seven areas was chosen for final data analysis. This run was then

combined with a calibration run conducted at the conclusion of testing (approximately 3 weeks later).

This ensured that the average calibration information (actually the curvefit through both sets of data) most

closely approximates the actual output of the liquid crystal on the test models during the testing period.

The "before" and "after" calibration curves for a representative area (3) shows the comparison between

these two data sets. It is clear that the middle and upper portion of the calibration range (33°C -40°C) show

better agreement between the two runs than the lower portion (30°C -33°C). It is this lower portion that

contributes the most to the curvefit Standard Error of Estimate (SEE).
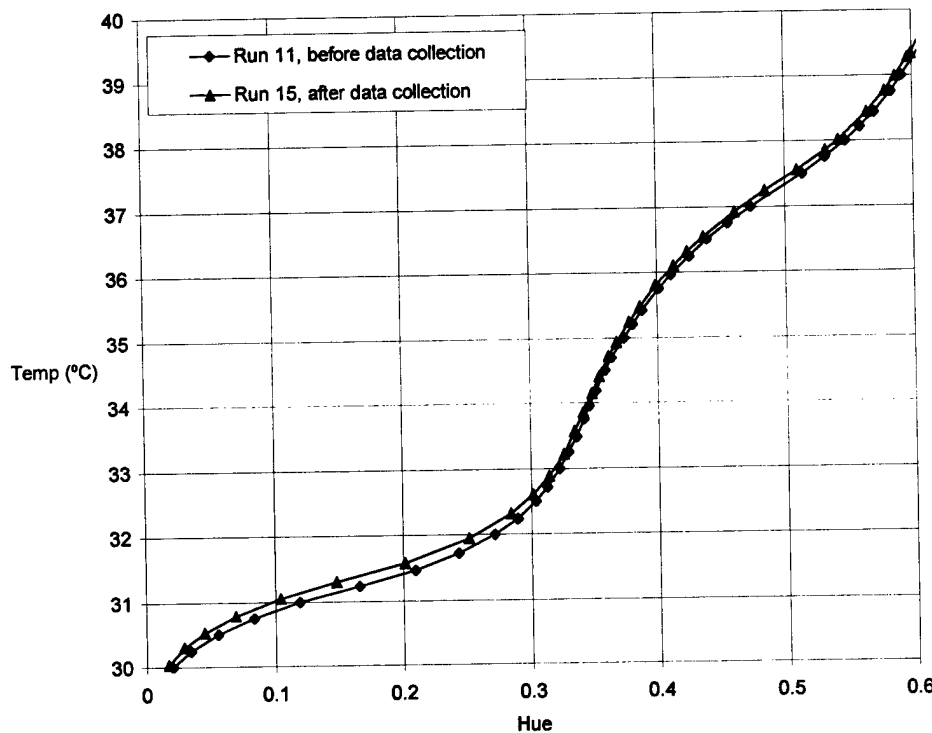
Figure 25 Temperature vs. Hue for "Before" and "After" Calibration Runs

The curvefit performed in Microsoft Excel is a 6th order fit of the data in the calibration range of 30°C - 40°C. The SEE associated with the curvefit is considered a 68% measure of the precision error in the curvefit, only when the bias contribution to the uncertainty is small (Schenck 1979). Because the calibration curve shifted slightly over the course of the two weeks of testing, there is a bias present between the first calibration curve and the second. However, if we want to represent both sets of data with one curvefit, then the SEE is the best means to identify the uncertainty in this curvefit. The SEE is computed using the following equation (Coleman, Steele 1989):

$$SEE_T = \left\{ \frac{\sum_{i=1}^{N} [T_i - (ah_i^6 + bh_i^5 + ch_i^4 + dh_i^3 + eh_i^2 + fh_i + g)]^2}{N-7} \right\}^{1/2} \qquad (8)$$

In the preceding equation, the (N-7) arises in the denominator because we use a 6th order curvefit, with 7

constants in the equation. Therefore, the SEE computation must account for the loss of 7 degrees of

freedom. For the seven curvefit calibration areas, the SEE is:

Table 3 SEE summary

Area #	SEE_T
1	0.098
2	0.109
3	0.103
4	0.124
5	0.112
6	0.112
7	0.143

Using SEE in computing the overall precision limit in T is covered in Appendix E, Uncertainty Analysis.

The following graphs show the calibration curves and 6th order curvefit equations for the seven different

calibration areas used.

$$y = -6.11749641E+04x^6 + 1.53606501E+05x^5 - 1.54917645E+05x^4 + 7.98982682E+04x^3$$
$$- 2.20991549E+04x^2 + 3.11341553E+03x - 1.43881993E+02$$
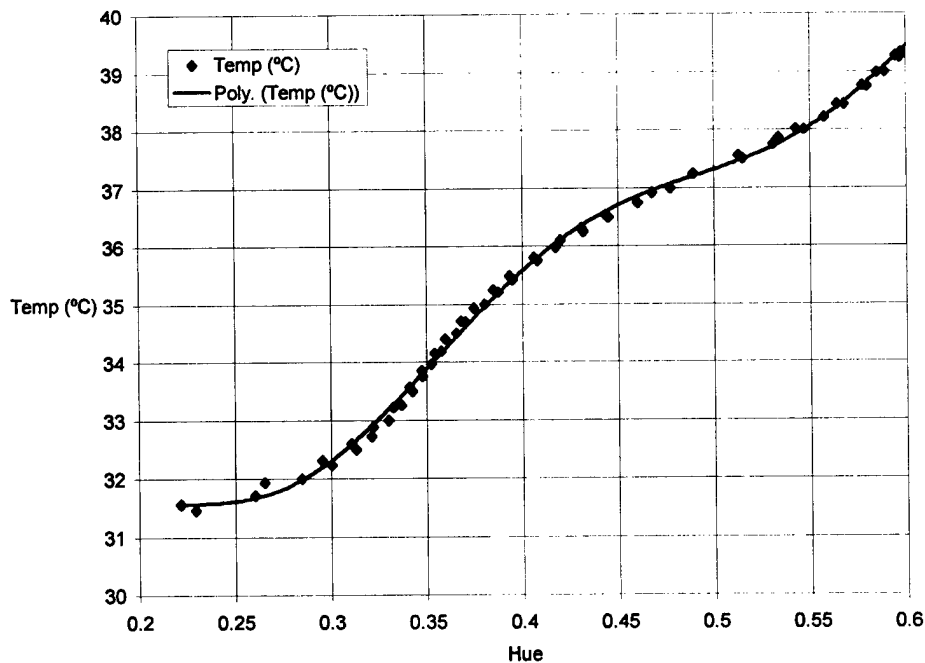
Figure 26 Temperature/Hue Calibration Curve for Area 1

$$y = -6.29137483E+04x^6 + 1.57603036E+05x^5 - 1.58626867E+05x^4 + 8.16780411E+04x^3 - 2.25668414E+04x^2 + 3.17767664E+03x - 1.47404950E+02$$
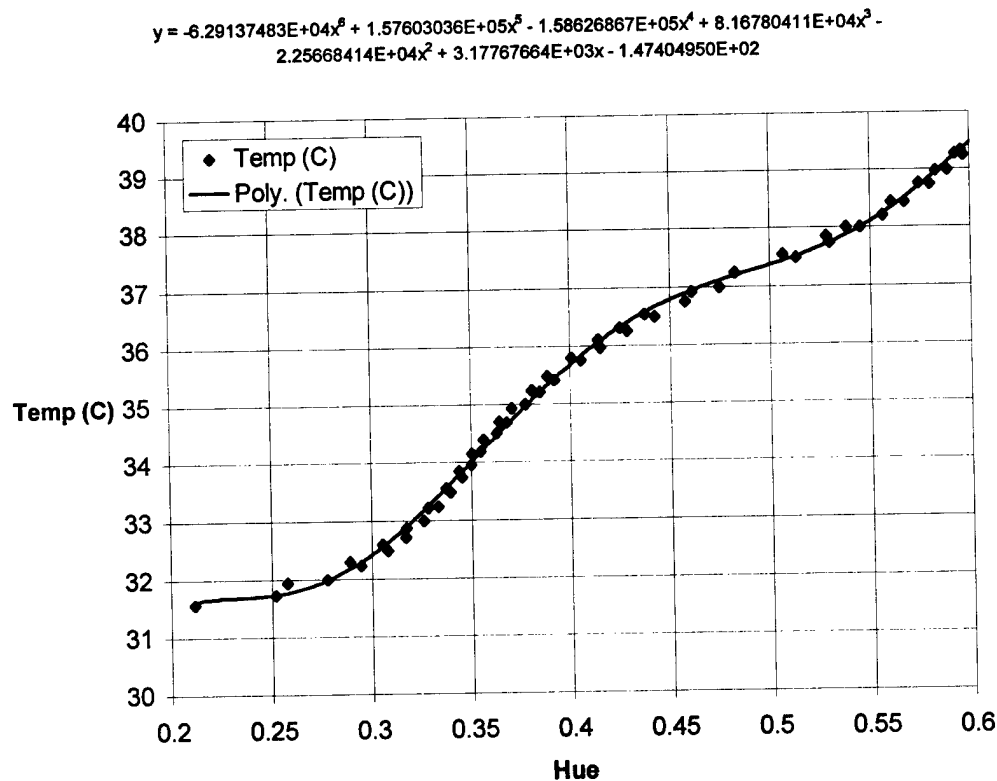
Figure 27 Temperature/Hue Calibration Curve for Area 2

$$y = -5.80519113E+04x^6 + 1.45179306E+05x^5 - 1.45645431E+05x^4 + 7.46018846E+04x^3 - 2.04551439E+04x^2 + 2.85226062E+03x - 1.27181803E+02$$
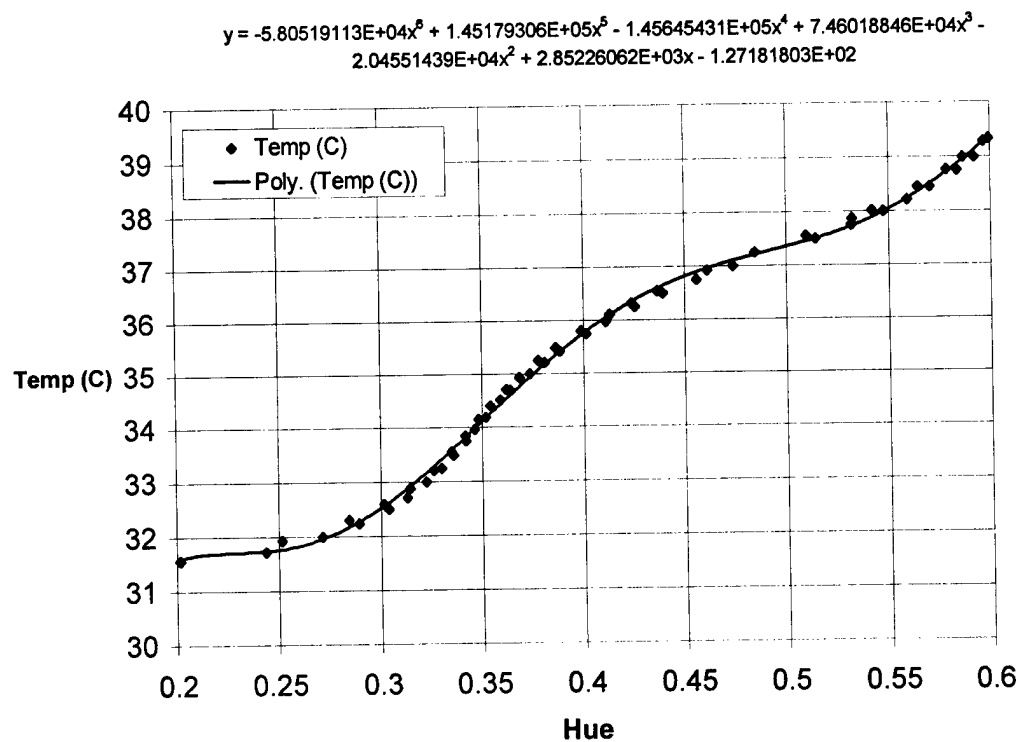
Figure 28 Temperature/Hue Calibration Curve for Area 3

$$y = -6.34531428E+04x^6 + 1.55082411E+05x^5 - 1.51827350E+05x^4 +$$
$$7.56976687E+04x^3 - 2.01174511E+04x^2 + 2.70189801E+03x - 1.12036258E+02$$
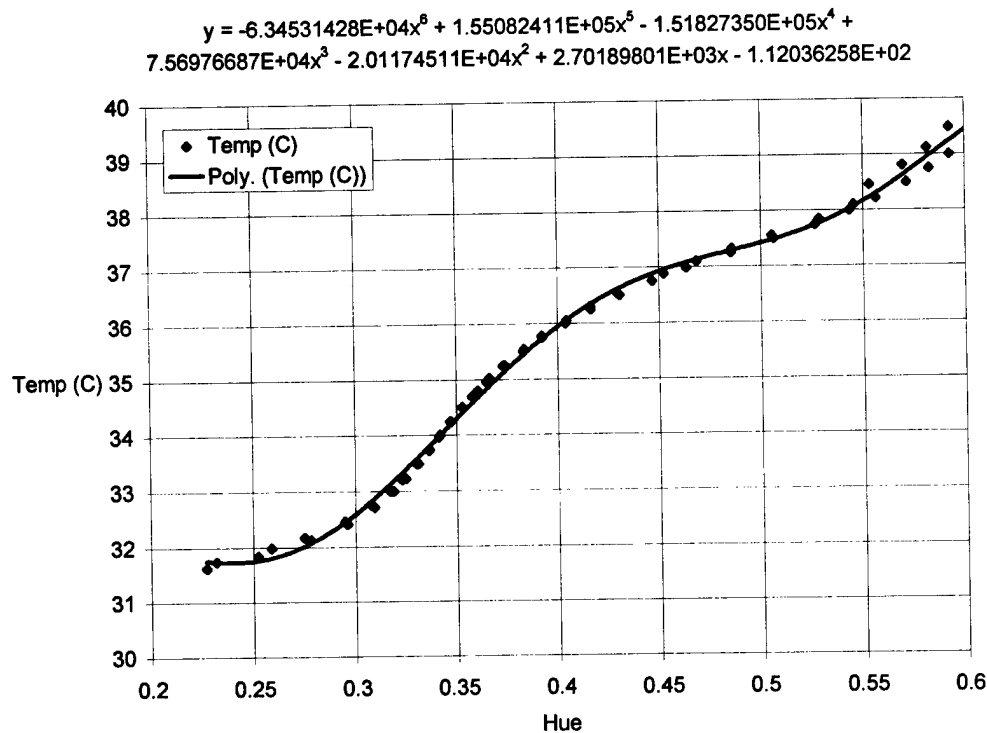
Figure 29 Temperature/Hue Calibration Curve for Area 4

$$y = -6.52716072E+04x^6 + 1.61754319E+05x^5 - 1.61021552E+05x^4 +$$
$$8.19758473E+04x^3 - 2.23848959E+04x^2 + 3.11395078E+03x - 1.41552424E+02$$
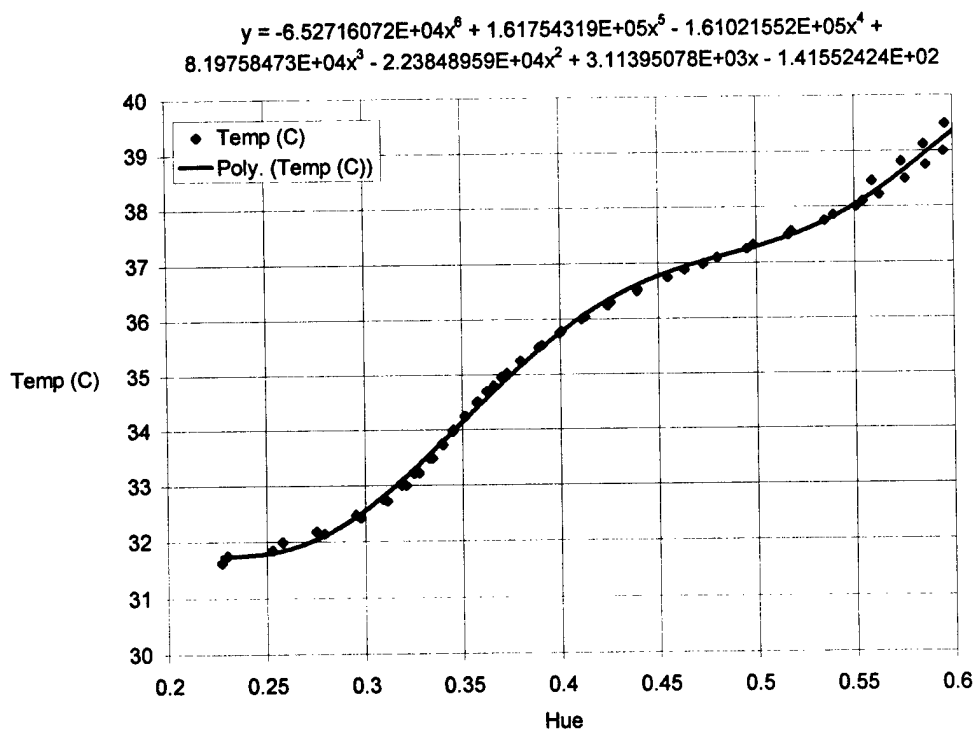
Figure 30 Temperature/Hue Calibration Curve for Area 5

$$y = -6.52990792E+04x^6 + 1.61671200E+05x^5 - 1.60745573E+05x^4 + 8.17115890E+04x^3 - 2.22730509E+04x^2 + 3.09284870E+03x - 1.40105704E+02$$
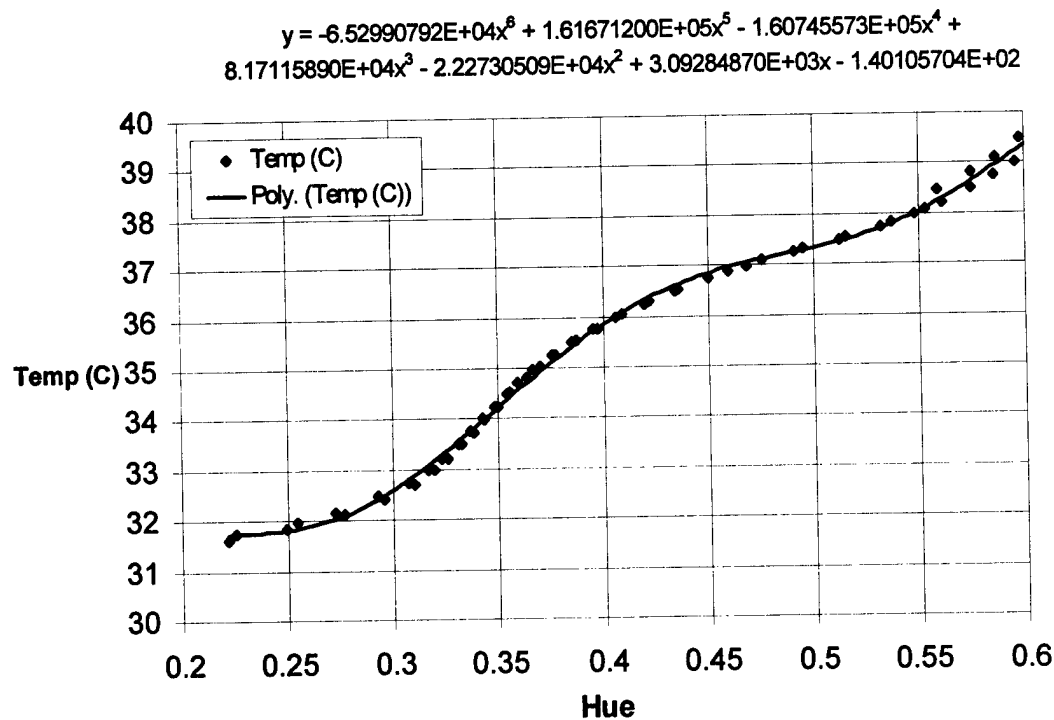
Figure 31 Temperature/Hue Calibration Curve for Area 6

$$y = -5.82801249E+04x^6 + 1.41960605E+05x^5 - 1.38244141E+05x^4 + 6.83793320E+04x^3 - 1.79655155E+04x^2 + 2.37661179E+03x - 9.22813799E+01$$
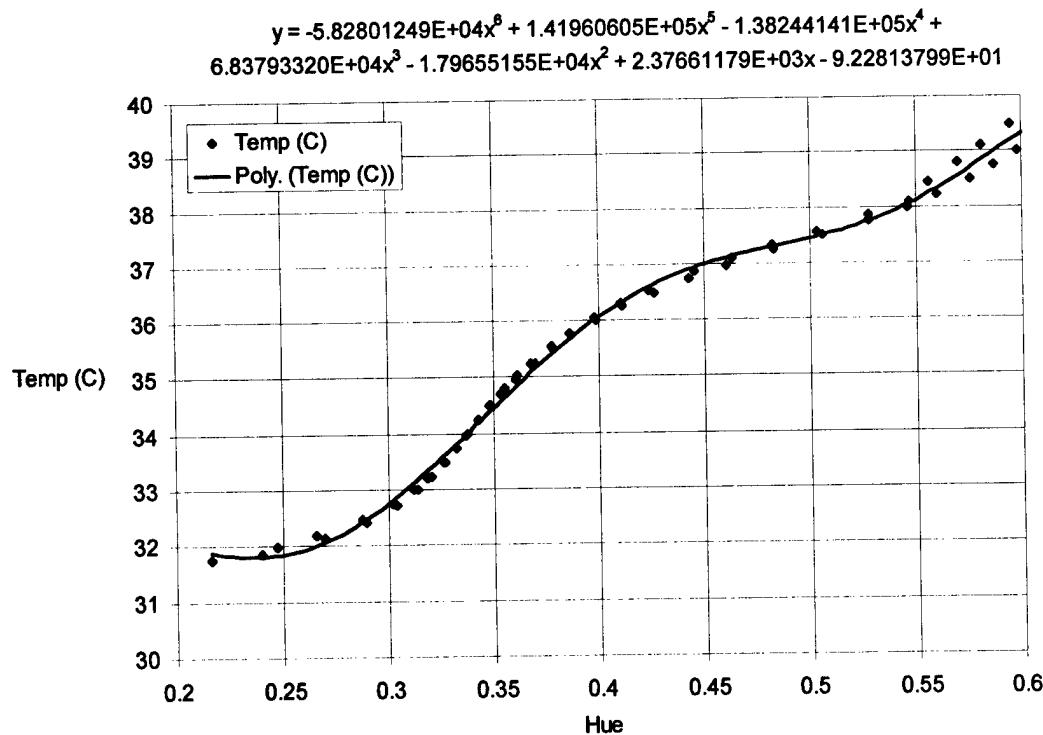
Figure 32 Temperature/Hue Calibration Curve for Area 7

Appendix C: Thermistor Calibration

The same thermistor was used to calibrate the copper block (to obtain the temperature/hue calibration curves) and to measure the freestream air temperature, T_{∞}. The same thermistor was used to reduce the uncertainty in heat transfer coefficient by providing a correlated bias term. It is a glass-coated bead type thermistor from Thermometrics. This particular thermistor is #2 of 10, which were calibrated together against a Rosemount 162CE Platinum Resistance Thermometer (PRT) in a constant temperature oven. The calibration process used 8 points ranging from 20°C to 50°C. Since our calibration and testing were conducted between 30°C and 40°C, this range was suitable for the thermistor calibration used. Both the thermistor 2-wire resistance output and the PRT 4-wire resistance output ran to an HP 3455A DVM, which was controlled by Labview.

From an uncertainty standpoint, there are two elemental bias sources in the temperature measurment: that due to the platinum resistance thermometer used in thermistor calibration, and that due to the DVM resistance measurement accuracy, evaluated at a 6 month interval since calibration. For the first bias source, the PRT manual states that over time, the resistance of the PRT increases due to small scratches, dings, dents, etc. on its surface. To find just how much bias exists, the author prepared an ice bath in a vaccuum-insulated container, and allowed the PRT to stabilize at a 0°C point for several hours. The ice bath was continually drained and repacked over this time as well. Upon reaching the lowest temperature, a PRT reading was made, which corresponded to a temperature of 0.075°C. Assuming this resistance measurement is correct, this becomes the bias limit in the PRT (B_{PRT}=0.075 K, b_{PRT}=0.0375 K). This seems possible, as the PRT was last calibrated in 1977, and this would allow for a modest 0.004 K shift per year since then. The PRT readings could be corrected for this bias, but it is not certain that it remains the same at all resistance levels, and there could be some uncertainty associated with our ice bath method. Realizing that a bias exists in the PRT, which contributes to an uncertainty in temperature, allows us to propogate this throughout our data reduction equation for h.

The DVM used for the thermistor calibration was last calibrated in March, 1998. Since all tests were conducted within six months of the calibration date, the bias limit due to the DVM is calculated using the six-month accuracy table in the HP 3455A manual. The maximum deviation in resistance (dR) from calibration accuracy occurs near the upper end of the copper calibration block range (43°C). This value is used in the thermistor calibration equation (which relates temperature in degrees Celsius to log(resistance)), to find the resulting deviation in temperature. Figure 33 shows the calibration curve and equation for this thermistor.

$$y = 0.0053x^3 - 0.0927x^2 + 0.5515x - 1.0929$$
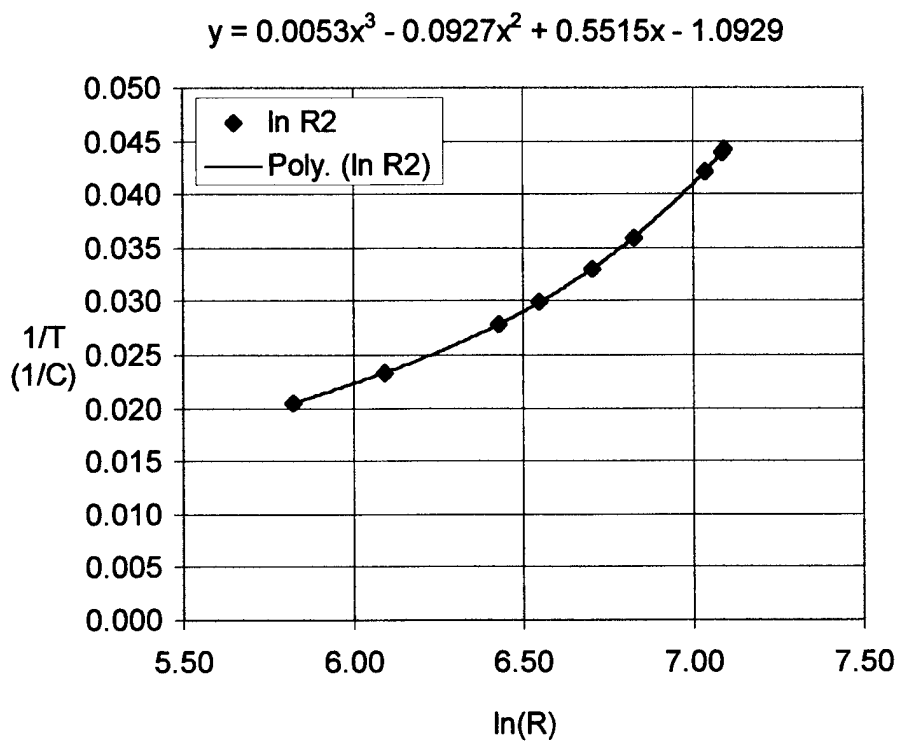
Figure 33 Thermistor #2 3rd Order Calibration

The calibration equation used is 3rd order, as recommended by the thermistor manufacturer for best accuracy. When the maximum dR value of 0.0204 Ω is inserted in this equation, the value of dT is 0.0107°C, which is a 95% confidence estimate. Therefore, the 68% confidence level estimate for the bias in temperature due to DVM calibration is b_{dvm}=0.0535°C.

One conservative approach is to consider the DVM and PRT uncertainties independent and combine them using the root-sum-square method. This yields an overall 68% bias limit in the temperature measurements of $b_{TLC} = b_{T\infty} = 0.0653°C$, which is used in the uncertainty analysis equations in Appendix E.

In terms of the precision limit associated with the thermistor calibration, there are two sources which affect temperature: the readability of the Labview screen display, and the curvefit performed to obtain the thermistor calibration curve and equation. The first source yields a precision limit of 0.02°C, at a 95% confidence level. Our 68% level precision limit is therefore 0.01°C. Second, the curvefit of temperature versus the logarithm of resistance has a standard error of estimate (SEE) of 0.065°C. This is plotted in Figure 34, below.
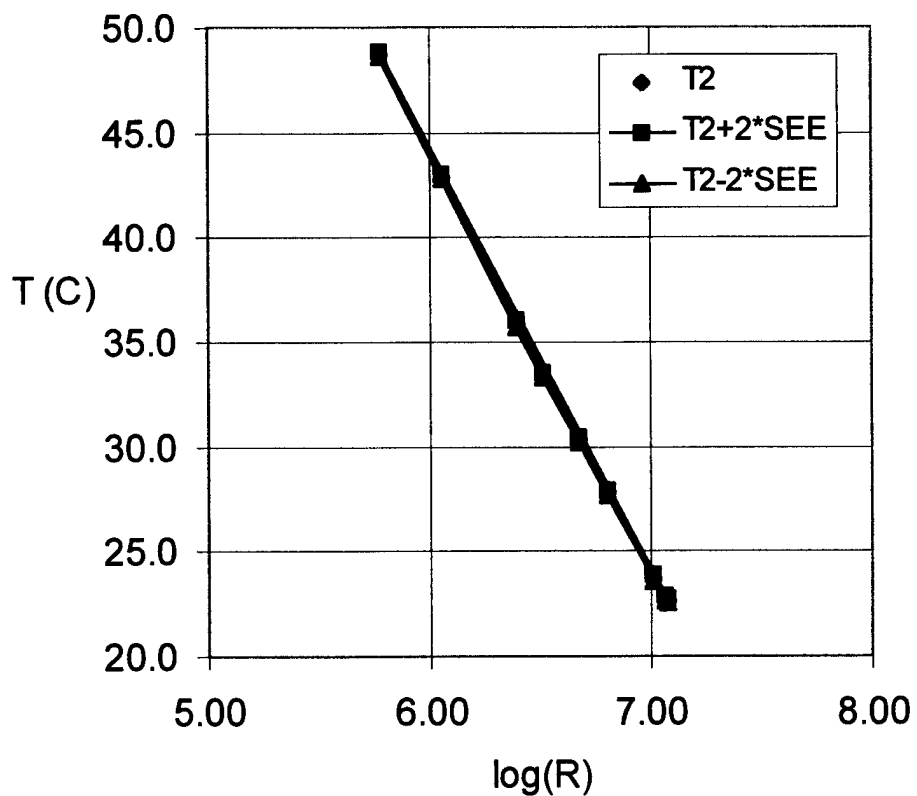
Figure 34 Thermistor #2 Calibration with 95% Uncertainty Limits

The +/- 2*SEE bands shown on the calibration curve in Figure 34 represent a 95% confidence estimate of the uncertainty associated with the curvefit shown (Schenck 1979). As can be seen, the SEE bounds are small. When the two precision limit sources are combined using the root-sum-square method, an overall precision limit in temperature of 0.066°C is calculated, with 68% confidence. This value is used in the uncertainty analysis of h as well.

Appendix D: Calculation of radiation correction term

There are two methods one can use to solve for the absorbed radiation incident on the surface

from the fluorescent lights used in the experiments. The first method is based on an assump-

tion that for a given set of tests at multiple power settings, at a constant wind tunnel speed,

the convective heat transfer coefficient will be constant as well. Therefore, one can solve the

following equation N times (for N power settings):

$$(q1 + qradinlight) - \epsilon p \cdot \sigma \cdot \left(Tlc1^4 - Tinf1^4\right) = h \cdot (Tlc1 - Tinf1) \qquad (9a)$$

where   qradinlight is the absorbed radiation incident from the lights
         q1 is the electrically-supplied heat flux to the surface
         Tlc1 is the temperature of the liquid crystal
         Tinf1 is the freestream air temperature

We choose to solve this equation three times, using information from four columns

across the plate: #100, #200, #300, #400.

100	200	300	400
Tlc1 := 308.434	Tlc1 := 307.93	Tlc1 := 307.605	Tlc1 := 307.052
Tlc2 := 310.899	Tlc2 := 310.27	Tlc2 := 309.402	Tlc2 := 308.568
Tlc3 := 306.782	Tlc3 := 306.28	Tlc3 := 305.513	Tlc3 := 304.7450

The three liquid crystal temperatures and freestream air temperatures listed below

correspond to the three power settings used on these runs.

Power settings: Freestream air temperatures:

I_1 := 5.033
                                                        Tinf1 := 299.23
I_2 := 5.598 $\sigma := 5.67 \cdot 10^{-8}$
                                                        Tinf2 := 299.3
I_3 := 4.404 $\epsilon p := .95$ Tinf3 := 299.35

Plate dimensions:

$$l := 7.68751 \qquad\qquad w := 16.5$$

$$lwratio := \frac{l}{w} \qquad lwratio = 0.466 \qquad Aplate := l \cdot \frac{w}{1550} \qquad\qquad Aplate = 0.082$$

Plate resistance information:

$$Rprime := 2.42$$

$$Rplate := Rprime \cdot lwratio$$

$$Rplate = 1.128$$

Current from three power settings:

$$q1 := I\_1^2 \cdot \frac{Rplate}{Aplate} \qquad q1 = 349.006$$

$$q2 := I\_2^2 \cdot \frac{Rplate}{Aplate} \qquad q2 = 431.763$$

$$q3 := I\_3^2 \cdot \frac{Rplate}{Aplate} \qquad q3 = 267.223$$

Now we have all the information needed to solve equations (9a,b,c) simultaneously for 3 different power settings. There are three equations for only two unknowns, so the system of two equations can be solved 3 times, obtaining three answers for h and qradinlight. The answers should be reasonably close (assuming h remains constant regardless of the power setting). The system of equations below yields one of the three solutions:

$$(q2 + qradinlight) - \varepsilon p \cdot \sigma \cdot \left(Tlc2^4 - Tinf2^4\right) = h \cdot (Tlc2 - Tinf2) \qquad\qquad (9b)$$

$$(q3 + qradinlight) - \varepsilon p \cdot \sigma \cdot \left(Tlc3^4 - Tinf3^4\right) = h \cdot (Tlc3 - Tinf3) \qquad\qquad (9c)$$

Unfortunately, this procedure does not work well. Instead, h does appear to vary slightly from power setting to power setting. Therefore, several different values of the radiation term are obtained, although it should be a constant. The average radiation term (for all power settings and locations on the plate) is on the order of 10 W/m².

Another method is tried to estimate the radiation term.

The overall radiation power output from the flourescent lights used in the experiments is primarily in the visible spectrum. When the light is energized, the gases inside give off UV which excite phosphors on the tube, which change state and give off light. The phosphors in the fluorescent light are largely opaque in the visible and IR regions of the spectrum. Because we have UV filters covering the light, no UV is transmitted through the Plexiglas. Roughly half of the tubes' circumferences are visible to the plate, and the light sources have an approximate color temperature of 4500K.

Consulting Thermal Radiation Heat Transfer (Siegel, Howell 1995), we find that at this temperature, 27% of the light's total energy is emitted in the visible spectrum. We estimate the transmissivity of the Plexiglas in this region of the spectrum to be 0.95. The shape factor, evaluated from a light to the model, is calculated using Hottel's String Method to be 0.201.

$$\text{Power} := 20 \quad \text{Watts} \qquad \text{ShapeFactor} := 0.201$$

$$\text{partial} := 0.5 \qquad\qquad \varepsilon := 0.95$$

$$\text{number} := 2 \qquad\qquad \text{visible} := 0.27$$

When these terms are combined in the following equation, we get:

$$\text{Qlight} := \text{Power} \cdot \text{partial} \cdot \text{ShapeFactor} \cdot \text{number} \cdot \text{visible} \cdot \varepsilon \tag{10}$$

$$\text{Qlight} = 1.031 \ \text{W}$$

$$\text{qlight} := \frac{\text{Qlight}}{\text{Aplate}}$$

$$\text{qlight} = 12.6 \quad \frac{\text{Watts}}{\text{m}^2}$$

Since this calculation also yields a radiation correction on the order of 10 W/m^2, this value is used with an uncertainty of +/- 50%. The 68% bias limit is then +/- 2.5 W/m^2. In all cases, this radiation term is small, i.e. less than 4% of the electrical power input per unit area.

Appendix E: Uncertainty Analysis

In analyzing the uncertainty associated with the convective heat transfer coefficient, h, the author consulted Experimentation and Uncertainty Analysis for Engineers, by Coleman and Steele (1989). This book is a good guide to handling many common experimental sources of uncertainty, and serves as a baseline to conduct the analysis. The ISO method of approach (as presented in the Guide to the Expression of Uncertainty in Measurement, published in late 1993) supplements this book with updated ISO-approved procedures. Furthermore, for the latest in uncertainty analysis procedures, Coleman and Steele's methods (1995) are used.

For this discussion, recall that the data reduction equation is:

$$h = \frac{q_e + q_l - \varepsilon \cdot \sigma \cdot (T_{LC}{}^4 - T_\infty{}^4)}{(T_{LC} - T_\infty)} \tag{4b}$$

Where q_e = electrical power in
q_l = radiation in from light source
ε = emissivity of surface
σ = Stephan/Boltzmann constant
T_{LC} = Temperature of liquid crystal-coated surface
T_∞ = Temperature of freestream air

Each of the five items shown above are either constants or are directly measured, with the exception of q_e, which is calculated in the data reduction equation shown below:

$$q_e = \frac{f \cdot I^2 \cdot R_{plate}}{A_{plate}} = \frac{f \cdot I^2 \cdot R' \cdot (l/w)}{(l \cdot w)} = \frac{f \cdot I^2 \cdot R'}{w^2} \tag{11}$$

Where   f = non-uniformity factor for resistance per square, = 1.0
I = current through gold film (amps)
R' = resistance per square of gold film(Ω)
w = width of plate (m)

The overall uncertainty in q_e can be divided into two parts: precision limits, (those due to random phenomenon), and those due to bias. The precision limit in q_e is due to the elemental precision limits of the four variables shown. It is convenient to directly solve for the sensitivity coefficients, as our equation is in the "special form" (Coleman, Steele 1989). Therefore, it is convenient to solve for the relative precision limit in q. For the 68% precision limit, we have:

$$\frac{Sq_e}{q_e} = \sqrt{4 \cdot (\frac{S_I}{I})^2 + (\frac{S_{R'}}{R'})^2 + 4 \cdot (\frac{S_w}{w})^2}$$

(12a)

Beginning with the first term, the precision limit of the current measurement, I derives from the "readability" of the Fluke digital multimeter connected to our HP power supply. During each image acquisition, the power supply was held at a constant power setting for ten minutes to ensure stability. Since there was no "flicker" observed in the output, we could use ½ least digit for this value. However, the reading often would change by as much as 4 milliamps during the ten-minute period. Therefore, the 68% confidence level precision limit in current is estimated at 2 milliamps. The precision limit in R', resistance per square of the gold film, derives from a series of tests conducted on nine identical samples of gold film used in building the ribbed model. A 4-wire resistance measurement was made of each rib, and the standard deviation of the nine measurements was found to be 0.01 Ω. The precision limit for the width measurement is equal to ½ the least division on the ruler used to measure the gold film. This is 1/32 inches for the flat plate model, or a relative precision limit of 0.0019. Notice that Equation (12a) does not contain a term for f, the gold film non-uniformity factor. This variable only contains a bias limit, as it is not measured multiple times nor has random errors associated with it.

An uncertainty of +/-20%, ($v=12.5$) is assigned to our estimate of each of these precision limits with the exception of the precision limit in R', which consisted of nine measurements ($v=8$). Therefore, the result has an overall 11 degrees of freedom.

Combining the elemental precision limits defined above, and solving Equation (12a), we find that:

$$\frac{Sq_e}{q_e} = 0.0056 \tag{12b}$$

Similarly for the bias limit in q_e, we have:

$$\frac{bq_e}{q_e} = \sqrt{(\frac{b_f}{f}) + 4\cdot(\frac{b_I}{I})^2 + (\frac{b_{R'}}{R'})^2 + 4\cdot(\frac{b_w}{w})^2} \tag{13a}$$

In this equation, we are interested in estimating the 68% bias limits of the four elemental sources present in Equation (13a). The first term, the correction factor in resistance per square, we consider accurate within 1%. Since this is a 95% confidence level estimate, our bias limit is ½ this amount for a 68% level. For the second term, current measurement, the HP power supply used in this experiment was last calibrated 3 years ago. However, since we are measuring its current output with a digital multimeter in series with the heated models, we are only interested in the accuracy of this instrument. We consider the Fluke digital multimeter accurate to within 0.5% of the actual current, so this 68% relative bias limit is 0.0025 amps, or one-half of 0.5%. Finally, the ruler used to measure the width of the plate. Since we do not have an exemplary method to compare our ruler against, we must estimate its performance as no better than 1% of the ruler's length, 18 inches. This is a more conservative estimate of the uncertainty than ½ least scale, for a 68% bias limit of 0.09 inches. All of the elemental bias limits are estimated to be within 20% of their actual value, for an overall 13 degrees of freedom in the resulting relative bias limit in q_e.

Combining the elemental precision limits defined above, and solving Equation (13a), we find that:

$$\frac{bq_e}{q_e} = 0.0122 \tag{13b}$$

Similar to the study of the uncertainty in q_e, the uncertainty in h can be broken down into precision and bias

limits as well. We will handle each of these separately, starting with the precision limits. The governing

equation for the overall precision limit (68% coverage) in h is:

$$S_h = \sqrt{(\frac{\partial h}{\partial q_e} * \frac{Sq_e}{q_e} * q_e)^2 + (\frac{\partial h}{\partial T_{LC}} * ST_{LC})^2 + (\frac{\partial h}{\partial T_\infty} * ST_\infty)^2} \tag{14}$$

Similarly, the governing equation for the overall 68% bias limit in h is:

$$b_h = \sqrt{(\frac{\partial h}{\partial q_e} * \frac{bq_e}{q_e} * q_e)^2 + (\frac{\partial h}{\partial q_l} * bq_l)^2 + (\frac{\partial h}{\partial \varepsilon} * b\varepsilon)^2 + (\frac{\partial h}{\partial \sigma} * b\sigma)^2 + (\frac{\partial h}{\partial T_{LC}} * bT_{LC})^2 + (\frac{\partial h}{\partial T_\infty} * bT_\infty)^2}$$

$$\tag{15}$$

The partial derivatives in the above equations are called sensitivity coefficients. We could solve for these

directly, using Equation (4b). However, since the governing equation is somewhat complicated, we chose

instead to encorporate a "jitter program" in the Matlab code to calculate these coefficients numerically.

The program performs this calculation for each of the sensitivity coefficients in Equations (14) and (15)

each time the convective heat transfer coefficient is found. When performing this calculation, we

increment each of the variables a very small amount (0.1% of its value), yielding reliable values for the

coefficients.

In terms of the precision limits of the elemental sources in h, we have already examined the electrical

power in, stating that the relative precision limit is:

$$\frac{Sq_e}{q_e} = 0.0056 \tag{12b}$$

Since we chose to compute a relative precision limit, the first term in Equation (14) contains the value of q_e itself. Next, we consider the precision limit in the temperature of the liquid crystal. This quantity is not directly measured, however. Instead, the standard deviation in T_{LC} must be calculated from two contributors: first, the standard deviation in hue, and second, the SEE_T from the hue/temperature calibration curvefit. This procedure is similar to the one followed in the recent paper by Baughn et al. (1998). For the first part, we have a column averaged hue from N=57 pixels on our models. The standard deviation in the mean hue is simply the measured standard deviation in this column average divided by the square root of N.

This brings up an interesting topic: how do we handle hue values which lie far outside of the rest of our values? What if an outlier occurs due to absence of liquid crystal coverage or damage to the surface which precludes a hue reading, or a random phenomenon causes a "wild" hue value in a pixel, well outside the rest of the data points? We must invoke an accepted method of "throwing out" these data points, on the basis of their deviation from the mean of the 57 pixels in our column. This method is called Chauvenet's criterion, and is well documented (ref. 12). We apply Chauvenet's criterion to the 57 data points, which allows us to discard all points which lie outside the range:

$$h_{mean} \pm (2.62) \cdot S_h \tag{16}$$

Although this criterion is evaluated at each column, it is not used to throw out points in every one. In 200 of the 600 columns across the plate, one point is discarded. In 19 columns, 2 points are discarded. Three of more points are discarded less than 1% of the time. After the points are discarded, a new mean and standard deviation are calculated from the modified data set, and are used in further calculations.

The mean hue is multiplied by the sensitivity coefficient ($\partial T / \partial hue$) computed at this location, which yields the standard deviation in temperature. Since we are now talking about specific values for a column calculation, we will look at column number 300 (the midpoint of the flat plate) on the 20 m/s run. Substituting the specific values for this column into this equation yields:

$$ST_{LC} = \frac{Shue}{\sqrt{57}} \cdot \frac{\partial T_{LC}}{\partial hue} = (\frac{0.0102}{7.55}) \cdot (20.2) = 0.0273°C \qquad (17)$$

For the second part, SEE_T from the temperature/hue calibration curvefit, the correct area must be chosen from the 7 calibration areas determined previously. Since column #300 lies in area four, SEE_4=0.124°C (from Appendix B). This is then combined with the standard deviation in T_{LC} for the following overall precision limit in the liquid crystal temperature:

$$ST_{LC} = \sqrt{(ST_{LC})^2 + (SEE_4)^2} = \sqrt{(0.0273)^2 + (0.124)^2} = 0.127°C \qquad (18)$$

It is apparent that the primary contributor to the result (95%) is the curvefit SEE. It is necessary to represent the temperature/hue calibration information as an equation, so that individual hue values can yield discrete temperature values. It would be nice to reduce this SEE, however, a 6th order curvefit equation is the best available. This represents some segments of the calibration curve well and others poorly.

The final elemental precision limit contributor to h is $S_{T\infty}$. The freestream air temperature is measured using the same thermistor used in the calibration of our liquid crystals. Linked to the HP 3455 DVM, and controled by Labview, the temperature can be read to within 0.02 K. However, temperature fluctuations during a five second segment preceding and following an image acquisition limits our accuracy to no better than 0.05 K, outside this limit. This is a 95% estimate, so we take the 68% estimate of $S_{T\infty}$ to be 0.025 K. Another precision limit exists in both the frestream temperature and calibration block temperature measurement. This is a correlated precision limit of 0.065°C, from the SEE in the thermistor calibration equation. Since this correlated precision limit does not increase the overall precision limit in h, it is removed from Equation (16) and the discussion above on $S_{T\infty}$. For more details on thermistor calibration consult Appendix C.

Combining the precision limits in Equation (14) yields a 68% confidence precision limit in h of 0.988

W/m²·K. The relative impact of each of the variables in (14) relating to the overall precision limit in h is

shown in the following table:

Table 4 Relative contributions to precision limit in h

Variable (x)	δh/δx	Sx	(δh/δx*Sx)²	Relative (%)
q_e, electrical power in: 776 W/m²	0.0944	0.0056	0.1684	17.3
T_{LC}, temperature of liquid crystal	-6.9433	0.127	0.7776	79.7
T_∞, freestream air temperature	6.8833	0.025	0.0296	3.0
Overall			Σ=0.9756	100

Next, the bias limits of the elemental sources in h are considered. Recall that:

$$b_h = \sqrt{(\frac{\partial h}{\partial q_e} \cdot \frac{bq_e}{q_e} \cdot q_e)^2 + (\frac{\partial h}{\partial q_l} \cdot bq_l)^2 + (\frac{\partial h}{\partial \varepsilon} \cdot b\varepsilon)^2 + (\frac{\partial h}{\partial \sigma} \cdot b\sigma)^2 + (\frac{\partial h}{\partial T_{LC}} \cdot bT_{LC})^2 + (\frac{\partial h}{\partial T_\infty} \cdot bT_\infty)^2}$$

Equation (15)

We have already studied electrical power in, stating that

$$\frac{bq_e}{q_e} = 0.0122 \tag{13b}$$

Again, this is a relative bias limit in qe, which means that the first term in Equation (15) must include the

actual value of q_e. The second term pertains to the radiative power in from the light source, q_l. This value,

10 W/m², was calculated in two separate manners outlined in Appendix D, Radiation Correction. We

assign a 95% confidence estimate of +/-5.0 W/m² (+/-50%) to this value, for a resulting 68% estimate of

+/-2.5 W/m². The third term pertains to the emissivity of the model. An experimentally determined

emissivity has not been found for the surface with black paint and liquid crystal coverage. Instead,

experience with the TLC, and tables for the emissivity of various black painted surfaces were consulted

(ref. 19), and a mean value of 0.95 +/-0.03 was chosen. The 68% bias limit for this quantity is then 0.015.

The next term is the Stefan-Bolzman constant, σ. This constant has only a fossilized bias limit associated

with it, which will be estimated at 0.5% of the value, or 2.835×10^{-10} W/ $m^2 \cdot K^4$. The last two terms in

Equation (17) are the bias limits associated with the temperature measurements, both of the liquid crystal,

and of the freestream air. Since both measurements used the same thermistor, DVM, and Labview display,

these biases are not only identical, but are also perfectly correlated, an advantage we will see shortly.

Next, it is necessary to identify the elemental sources of bias which combine to form the bias in

temperature measurement. Appendix C provides details of thermistor calibration, and resulting biases. The

68% bias limit in the temperature measurement is $b_{TLC}=b_{T\infty}=0.0653°C$.

The correlated bias term has been removed from under the radical of Equation (15) for simplicity, but will

be shown here for refence in the upcoming discussion:

$$b_{TC} = \sqrt{2 \cdot \frac{\partial h}{\partial T_{LC}} \cdot \frac{\partial h}{\partial T_\infty} \cdot b_{TLC} \cdot b_{T\infty}}$$ (19)

This correlated bias term, when included in the bias limit estimate for h, removes the combined bias

contribution from the elemental temperature sources. This reduces the overall bias in the result, h, by

47.1%, and is the primary reason for using the same thermistor probe to measure both the temperature of

the liquid crystal calibration block and the freestream air temperature.

All degrees of freedom for this bias limit study were considered to be 13, which indicates that our estimates

are within 20% of the true estimates of elemental bias limits. Table 5 shows the relative contributions of

the 6 variables to the bias limit in h.

Table 5 Relative contributions to bias limit in h

Variable (x)	δh/δx	bx	(δh/δx*bx)²	Relative (%)
q_e, electrical power in: 776 W/m²	0.0944	0.0122	0.7987	92.4
q_l, radiative power from lights	0.0944	2.5	0.0557	6.4
ε, emissivity of models	-6.4229	0.015	0.0093	1.1
σ, Stephan-Boltzman constant	-1.076E08	2.835E-10	9.31E-04	0.1

T_{LC}, temperature of liquid crystal	-6.9433	0.0653	0.2056	23.7
T_∞, freestream air temperature	6.8833	0.0653	0.2020	23.4
Correlated bias of T_{LC}, T_∞			(-) 0.4076	(-) 47.1
Overall			$\Sigma = 0.8645$	100

The 68% bias and precision limits are combined in the following equation to obtain the overall uncertainty in h, with 95% coverage (ref

$$U_h = k \cdot \sqrt{(S_h^2 + b_h^2)} \tag{20a}$$

where k is the coverage factor, = 2.0

Because the number of degrees of freedom in our elemental sources of all the valiables in the precision and bias limits in h were estimated to be greater than 9, the number of degrees of freedom in the result, h, is greater than 9. Therefore, the "large sample assumption" holds, and the coverage factor does not need to be calculated using the Welch-Satterthwaite formula (Coleman, Steele 1995). Instead, for 95% coverage, the coverage factor is set equal to 2.0, and used to calculate the overall uncertainty in h:

$$U_h = 2.0 \cdot \sqrt{(.9877^2 + .9298^2)} = 2.71 \frac{W}{m^2 \cdot K} \tag{20b}$$

At this particular location on our 20 m/s flat plate run (column #300), the h value is 68.24 W/m²·K, yielding a relative uncertainty of 4.0%. For the entire length of the plate, the average uncertainty is calculated to be 3.9%. Average uncertainty values are presented in the table below for the entire series of tests.

Table 6 Relative Uncertainty in h for All Tests

Model	Velocity (m/s)	Average U_h/h (%)
Flat Plate	10	4.1
	14.2	4.1
	20	3.9
Flat Plate with Interrupted Heating	10	4.1
(Geometry 1)	14.2	4.0
	20	4.0
Flat Plate with Interrupted Heating	10	3.8
(Geometry 2)	14.2	3.7
	20	3.7

Model	Velocity (m/s)	Average Uh/h (%)
Flat Plate with Interrupted Heating	10	4.0
(Geometry 3)	20	5.2
	10	4.1
Ribbed	14.2	4.5
	20	4.2

Appendix F: Effect of Velocity

Results have been presented for the 10 m/s flow velocity for all models tested. Also, the results for all three velocities for the flat plate uniform heating model have shown that the h profile scales as $Re^{0.8}$, or $(V_2/V_1)^{0.8}$ as the velocity increases. We now look at the effect of velocity on the interrupted heating results. Because no fundamental change has occurred in the freestream conditions or the models, the scaling relationship should hold true here as well.

Figure 35 on the next page shows the flat plate model (spacing #1) at 14 m/s. Notice that again, the heat transfer from the interrupted heating case is greater than that of the uniform heating model. Here, comparing the average h over heated strip #5, an increase of 31% is observed.
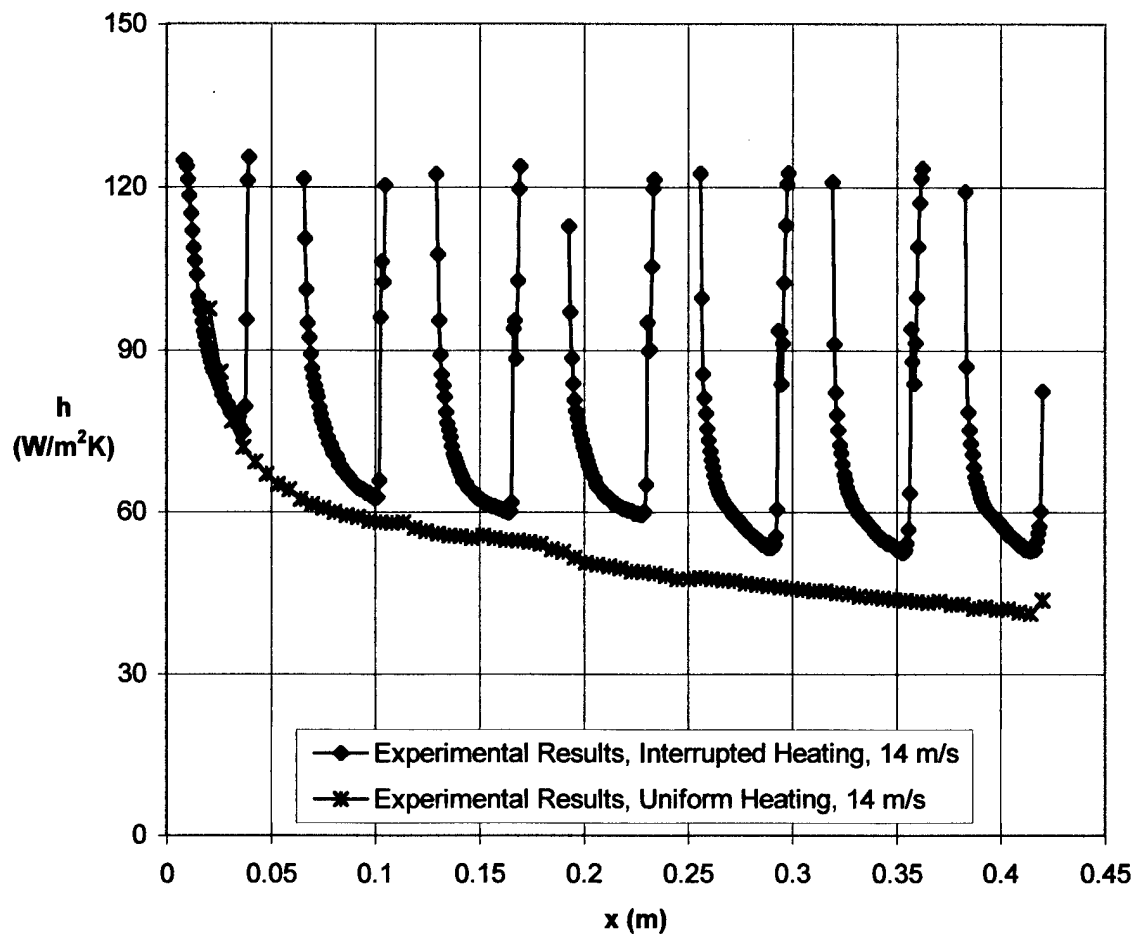
**Figure 35 Comparison of h vs. x at 14 m/s for Flat Plate Interrupted Heating
and Uniform Heating, Spacing #1**

This spacing was also run at a speed of 20 m/s. The results for this test condition are shown in Figure 36, on the following page.
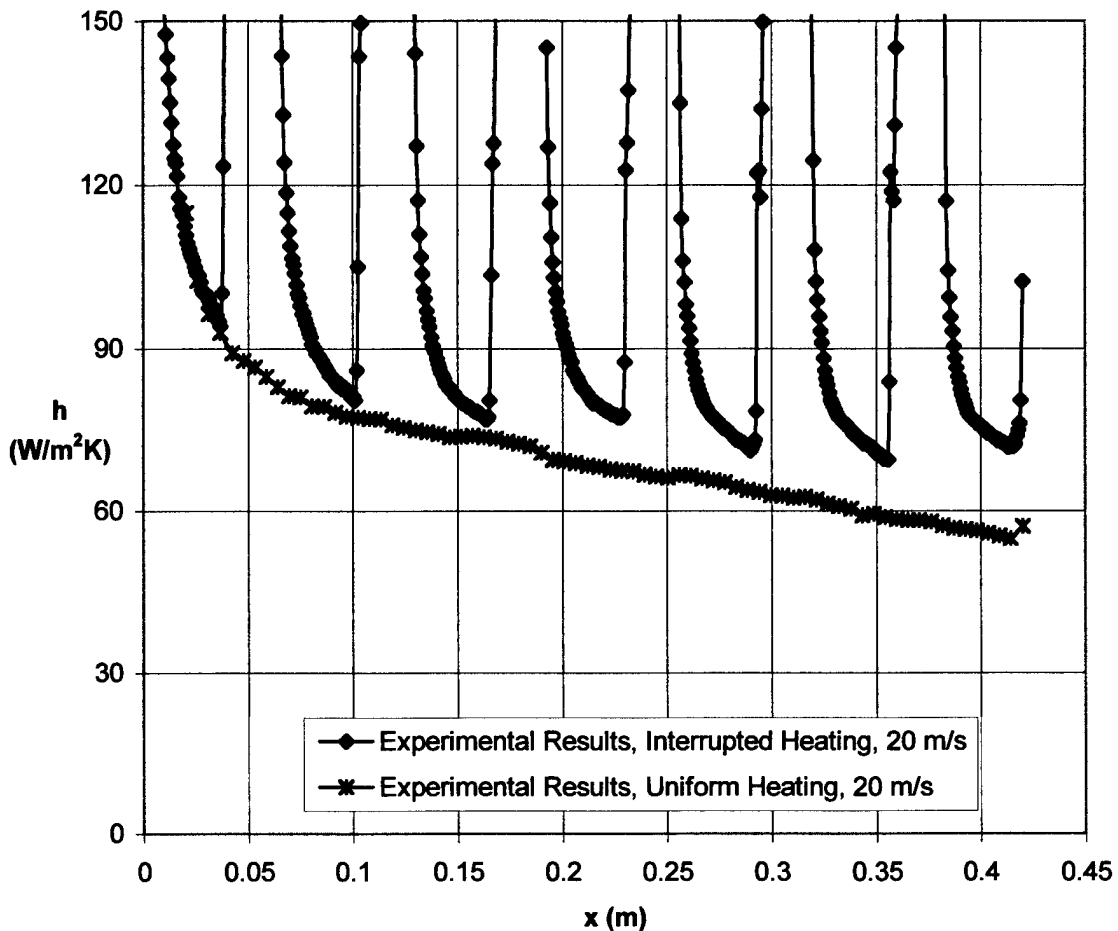
Figure 36 Comparison of h vs. x at 20 m/s for Flat Plate Interrupted Heating

and Uniform Heating, Spacing #1

The reader will notice that the results from this test condition matched the trend of the previous runs. The

heat transfer coefficients once again increase when evaluated at the heated sections. The average increase

over the uniform heating of the flat plate model, for heated section #5 is 26%.

Results from the flat plate with interrupted heating (spacing #2) are considered next. First, results from the

14 m/s test condition are shown in the figure below. Notice that this test condition shows a greater

increase than spacing #1 for the interrupted heating versus the flat plate uniform heating. The 10 m/s

results showed an increase of 64%, whereas the increase on heated section #5 is about 56% for this test

condition.
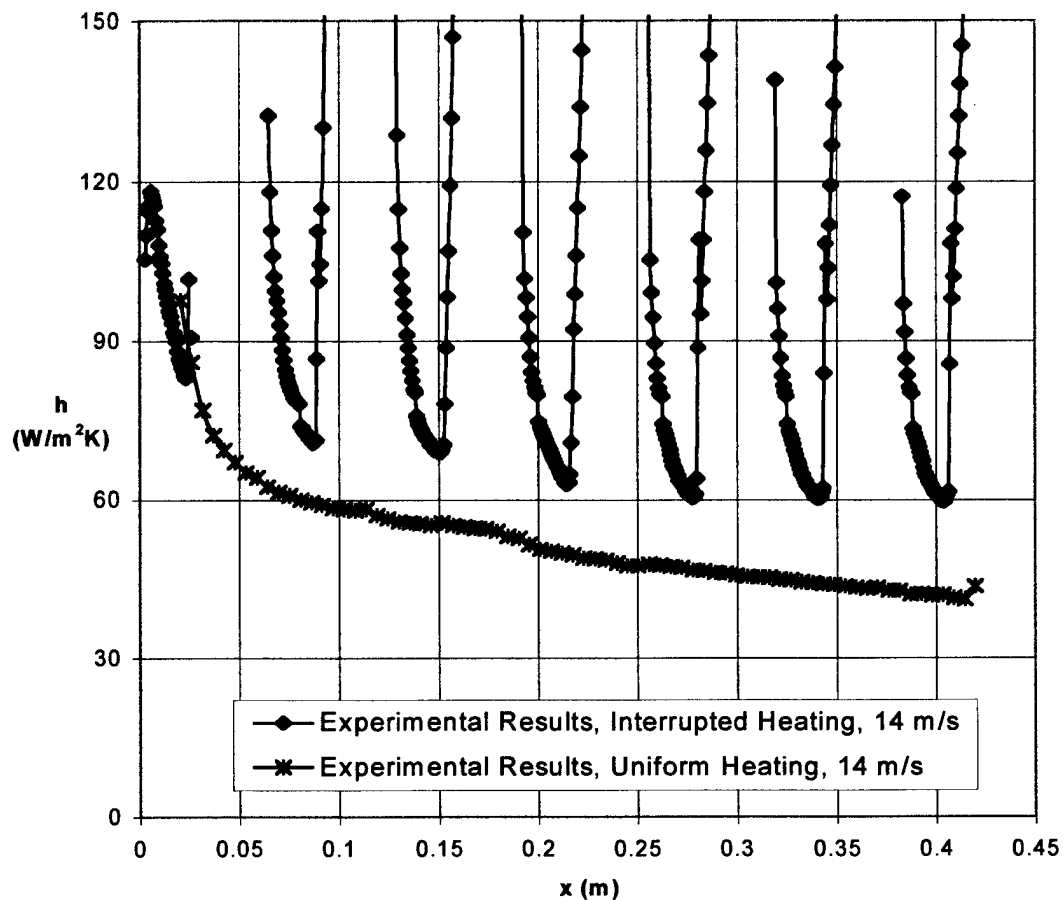
Figure 37 Comparison of h vs. x at 14 m/s for Flat Plate Interrupted Heating

and Uniform Heating, Spacing #2

The results from the 20 m/s test condition for spacing #2 are shown in figure 38, below. The interrupted heating heat transfer profile is fully above the uniform heating profile. An increase in h of 43% is observed this time.
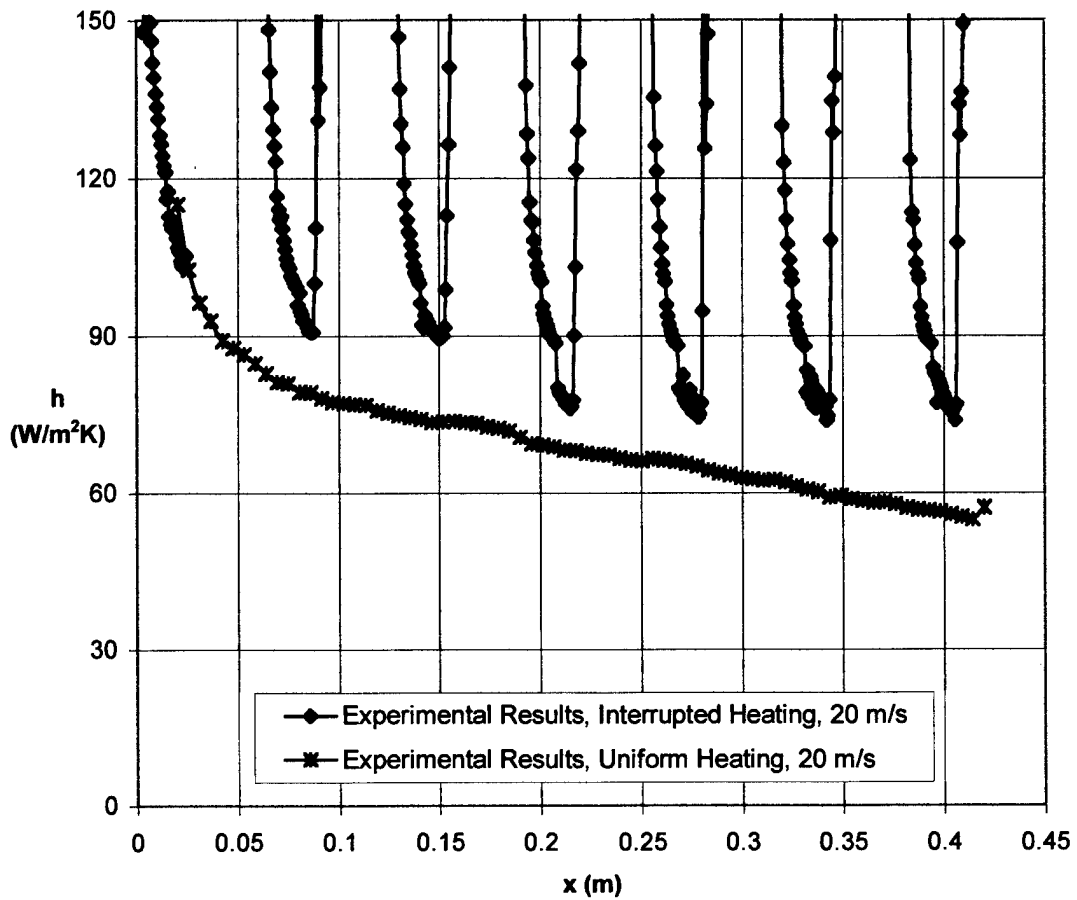
. **Figure 38 Comparison of h vs. x at 20 m/s for Flat Plate Interrupted Heating**

and Uniform Heating, Spacing #2

The heat transfer profiles in both the 14 m/s and 20 m/s runs appear to stabilize after the 4th or 5th rib, which

has been noted in the 10 m/s data as well.

For the final flat plate interrupted heating case, the 20 m/s test condition for spacing #3 is considered. Test

data at 14 m./s was not gathered. Once again, the h profile increases above that seen in the uniform heating

data set. The magnitude of this increase is 69%, less than that seen for this spacing at 10 m/s (93%).
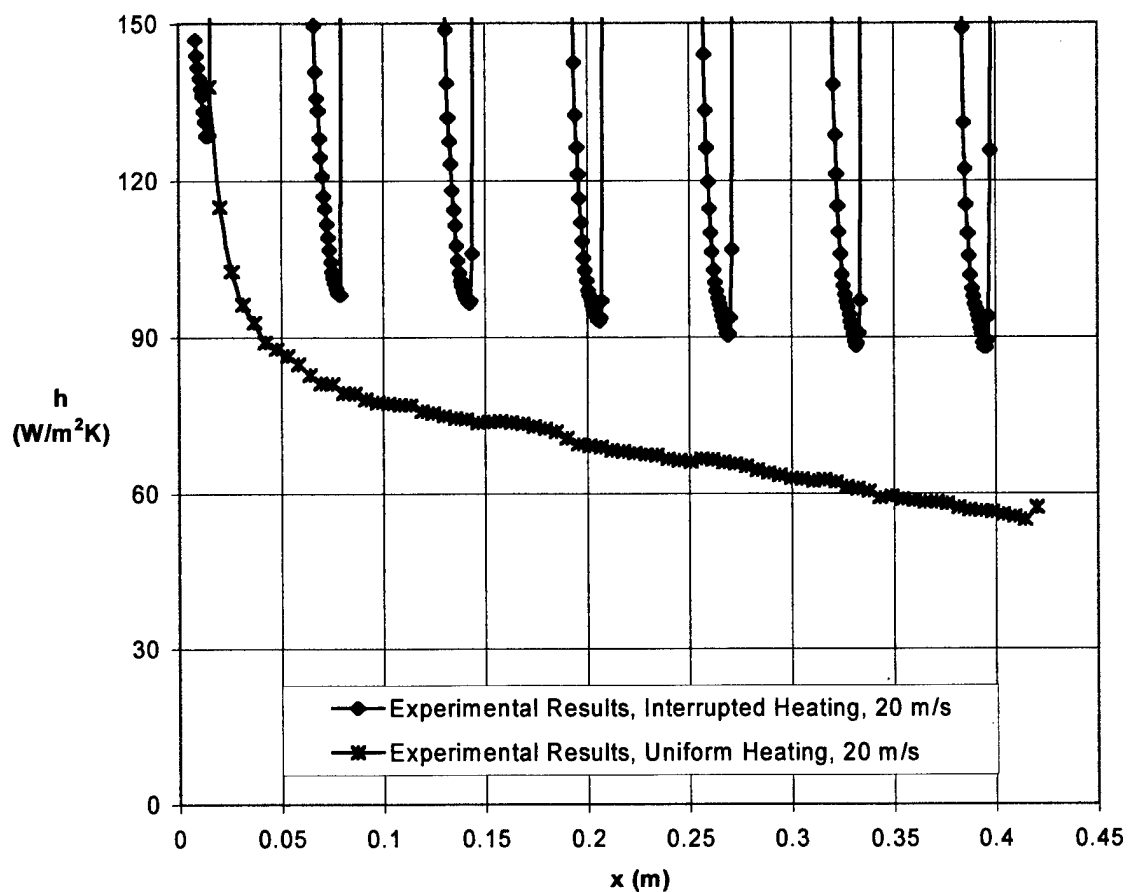
Figure 39 Comparison of h vs. x at 20 m/s for Flat Plate Interrupted Heating

and Uniform Heating, Spacing #3

Finally, the ribbed model heat transfer at various speeds is studied. Recall that the 10 m/s case showed an increase of 57% over the flat plate uniform heating data. The 14 m/s data is presented in the figure below.
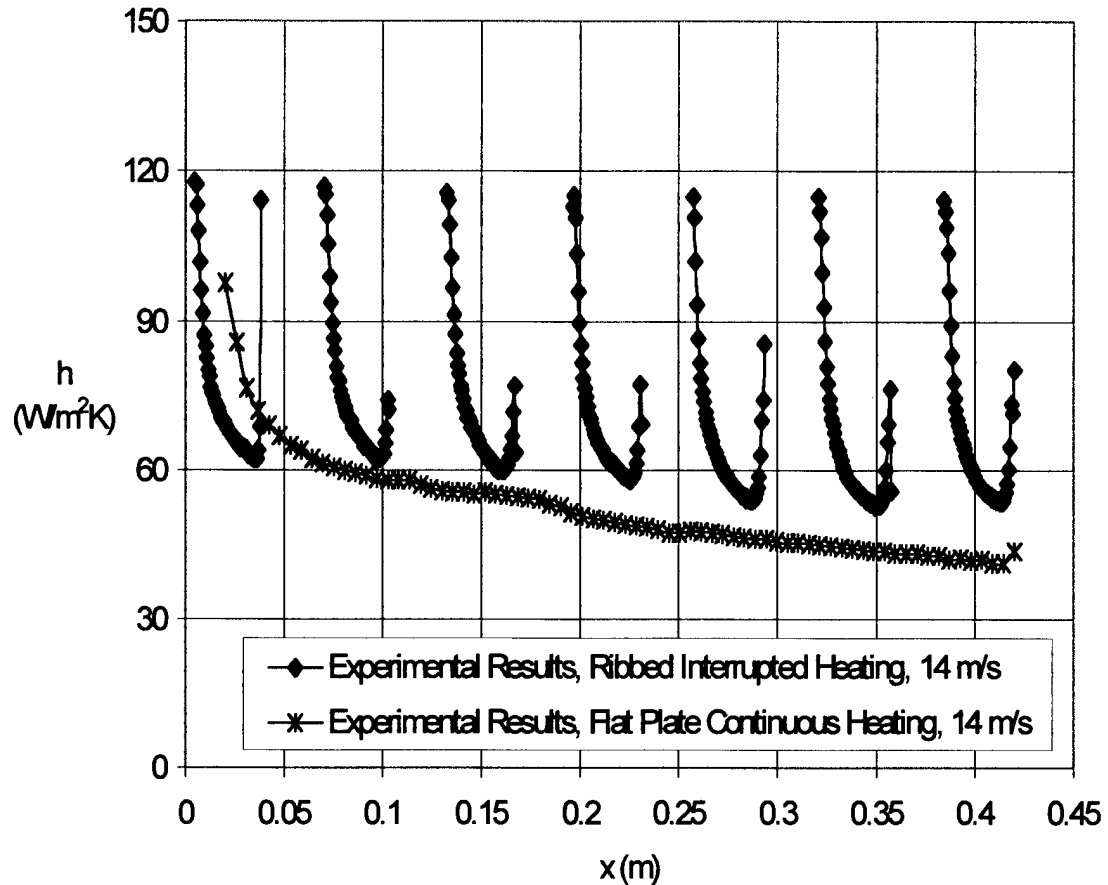
Figure 40 Comparison of h vs. x at 14 m/s for Ribbed Model Interrupted Heating

and Flat Plate Uniform Heating

It is noted that the heat transfer increases for this case, similar to the 10 m/s flow velocity. Stability is seen after 5 ribs, as before. The magnitude of the heat transfer coefficient increase is 36%, evaluated at rib #5.
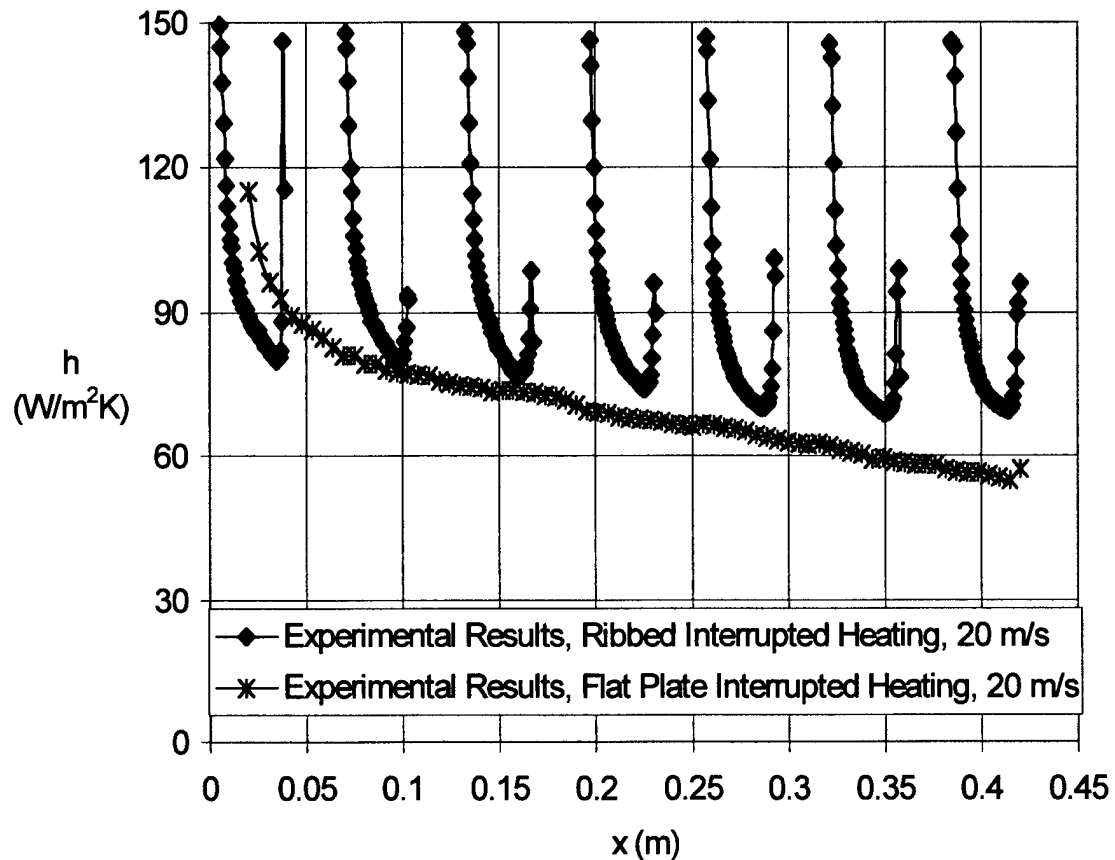
Figure 41, Comparison of h vs. x at 20 m/s for Ribbed Model Interrupted Heating

and Flat Plate Uniform Heating

The increase in h over the flat plate uniform heating case for this test condition is not as great, and is calculated to be 27%.

As before, we can compare the ribbed results to the flat plate with interrupted heating results, since the spacing of heated and unheated sections is the same. In the 10 m/s case, recall that the ribbed model showed a 13% increase, likely because of the additional mixing that takes place, and the cooler air that reaches the heated surfaces. At the two higher flow velocities, the ribbed model does not appear to make as large of a difference in heat transfer. The 14 m/s results are shown on the following page.
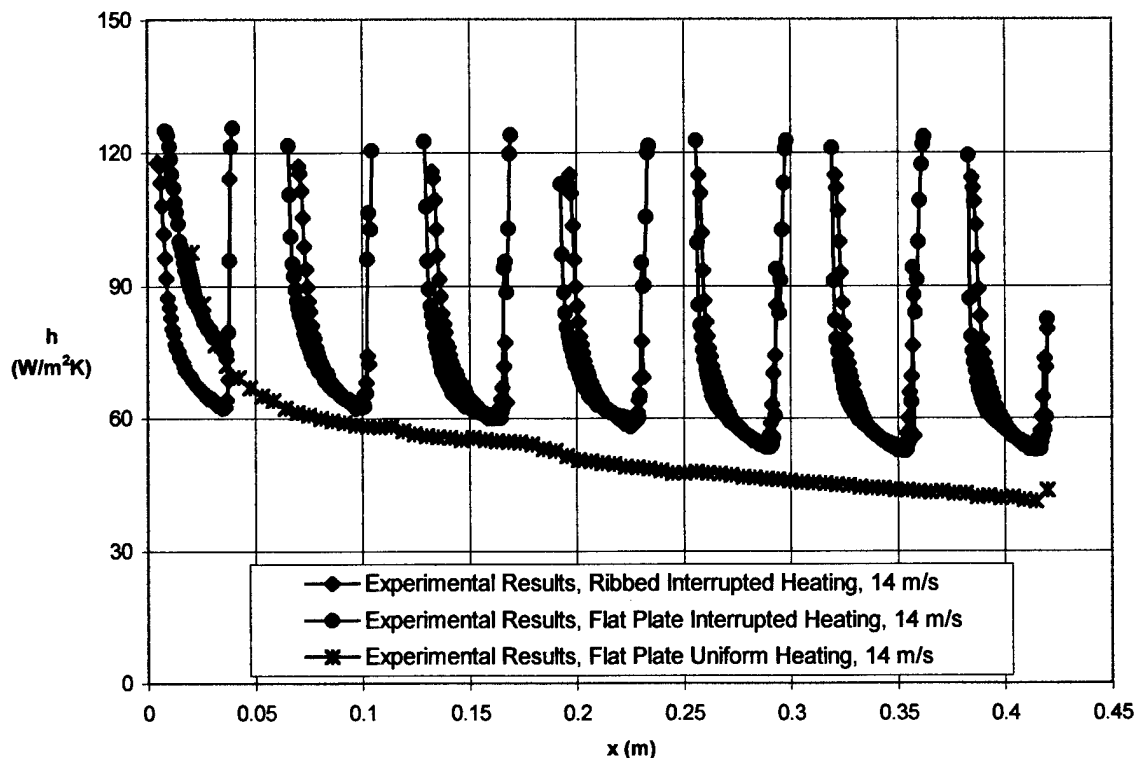
Figure 42 Comparison of h vs. x at 14 m/s for Flat Plate Interrupted Heating and Ribbed Interrupted Heating

In spite of the addition of cavities to promote circulation, a large increase in h is not seen. Over ribs 2 through 7, the increase is only 7% over the flat plate with interrupted heating. The h profile appears to be slightly greater toward the leading edge of each rib, which could be attributed to conduction losses on the leading edge of the rib that would not occur on the flat plate

This spacing was also evaluated at the 20 m/s flow velocity. Figure 43 on the following page shows the h profiles for the flat plate with interrupted heating compared to the ribbed interrupted heating. Again, only a slight increase in h is seen for the ribbed model (4% over ribs 2 through 7). Although the profile is greater toward the leading edge, conduction losses out the front of the rib could explain this.
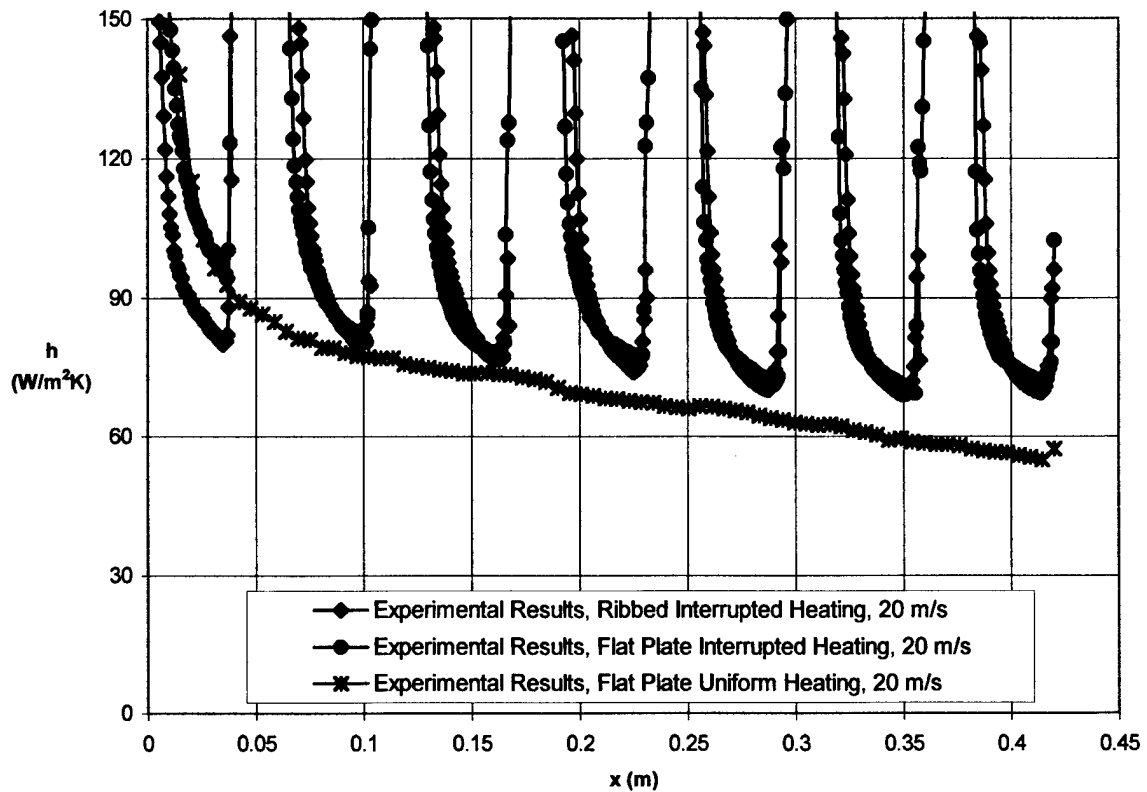
Figure 43 Comparison of h vs. x at 20 m/s for Flat Plate Interrupted Heating and Ribbed

Interrupted Heating

The following table shows a summary of all h profile results.

Table 7 Summary of h profile results for all speeds

Model Configuration	Flow Velocity	% Increase
Flat Plate with Interrupted Heating, Spacing 1	10 m/s	38
	14 m/s	31
	20 m/s	26
Flat Plate with Interrupted Heating, Spacing 2	10 m/s	64
	14 m/s	56
	20 m/s	43
Flat Plate with Interrupted Heating, Spacing 3	10 m/s	93
	20 m/s	69
Ribbed Model	10 m/s	57
	14 m/s	36
	20 m/s	27

Appendix G: Effect of Power Setting

The calculation of heat transfer coefficient across each test model used this equation from section II:

$$h = \frac{q_e + q_l - \varepsilon \cdot \sigma \cdot (T_{LC}{}^4 - T_\infty{}^4)}{(T_{LC} - T_\infty)} \qquad (4b)$$

Where q_e = heat flux from electrical power in (W/m^2)
q_l = heat flux from the incident lighting (W/m^2)
ε = emissivity of model surface
σ = Stefan-Boltzman constant
T_{LC} = temperature of the liquid crystal surface

Because the specific power setting used should not influence the value of h, data collection at each test velocity was done multiple times, each at different power settings. It was thought that a lower power setting would give better results at the trailing edge of each heated section (where the surface temperatures are higher), and a higher power setting would allow for more complete data at the leading edge. The uncertainty in each h value was calculated in the Matlab code (as explained in section III). A larger uncertainty in h was associated with those values obtained at a lower power setting (primarily from the low temperature difference between the surface and the freestream air). Due to this high uncertainty, h data for each column position was usually chosen from the higher power settings for each run.

The graph below shows one curve for each of the four power settings used on the 10 m/s ribbed model test.
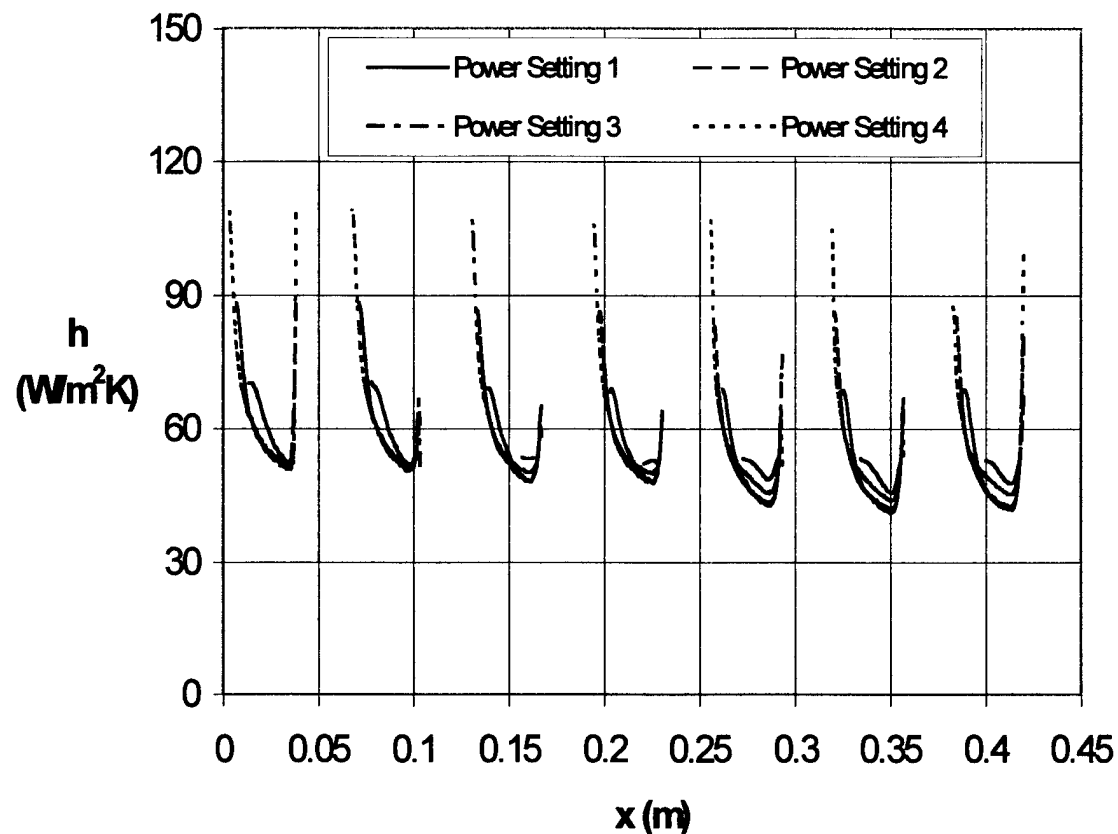
Figure 44 Comparison of Four Power Settings Used in Calculating h

The reader will notice that all four power settings yield results for h that are very similar, so that choosing the one with the lowest uncertainty is a reasonable practice. Again, it is usually the run with the highest power setting that has the lowest uncertainty, and is therefore chosen in most of the graphs presented in this paper.

Appendix H: Matlab Data Analysis Code

%Wolf Master's Thesis
%Flat Plate Image Files a35.tif-a37.tif

clear

%Step 1. Read in images (at different power settings) for one tunnel speed
path=['E:\FLATPLATE\']; %Change according to folder name

fileprefix='a';

filedata=dir(path);
filenamesall={filedata.name}';
y=strncmp(filenamesall,fileprefix,1);
filenames=filenamesall(y==1);

```
for i=35:37 %image numbers
    image=imread([path,fileprefix, int2str(i),'.tif']);
    %Step 2. Crop image from 480x640 to 57x640, approx. 3.8 cm x 42 cm
    imagesmall=image(180:236,lower:upper,:);
    %Step 3. Convert cropped image from R,G,B to Hue, Saturation, Value
    clear H S V;
    [H S V]=rgb2hsv(imagesmall); %get HSV from smallimage

    for c=1:numcol %count through the columns, one at a time
        k=0;
        Hcol=H(:,c);

        %Step 4. Considering one column at a time, calculate the mean hue
        %       and standard deviation in hue.
        hueout(i,c,:)=huestats(Hcol);
        huemean=hueout(i,c,1); %(mean hue is the first component of hueout,
        %       standard deviation is the second component)
        [counts,x]=imhist(Hcol); %determine the center of the Hcol data
        center=x(find(counts==max(counts)));
        center=center(1)/length(x);
        %shift the data so that it is centered about the midpoint
        if center<.5
            Hcol=Hcol-(Hcol>=(center+.5));
        end
        if center>.5
            Hcol=Hcol+(Hcol<=(center-.5));
        end

        %Step 5. Apply Chauvenet's Criterion to the column data and recalcu-
        %       late hue mean and standard deviation.
        k=find((Hcol>(huemean-(2.62*hueout(i,c,2))))&(Hcol<(huemean+(2.62*
            hueout(i,c,2)))));    %use 2.62 because we have 57 points
        chauvenet(i,c,1)=mean(Hcol(k)); %returns the mean of all data within
        %       %2.62 Standard Deviations of the mean
        %now wrap it back around if it fell a bit outside the (0,1) bounds
        if chauvenet(i,c,1)<0
            chauvenet(i,c,1)=chauvenet(i,c,1)+1;
        end
        if chauvenet(i,c,1)>1
            chauvenet(i,c,1)=chauvenet(i,c,1)-1;
        end
```

```
        chauvenet(i,c,2)=std2(Hcol(k)); %find new standard dev of data
        %chauvenet(i,c,3)=chauvenet(i,c,2)/sqrt(57); %find Sh bar
        %chauvenet(i,c,4)=CF*sqrt(chauvenet(i,c,3)^2+SEEh^2); % combine SEE
            %and Sh bar to get total Uh
    end
    filenumber(i)=i;
end


%Step 6. If hue is outside calibration range (0.2 to 0.63), make it a NaN
huecal min=0.20;
huecal max=0.63;

for i=35:37
    huecalmask=(squeeze(chauvenet(i,:,1))>=huecal min)&
        (squeeze(chauvenet(i,:,1))<=huecal max);
    huechauvfin(i,:,1)=(chauvenet(i,:,1)).*(0./huecalmask+1);
        %Nan the means outside the calibration range
    huechauvfin(i,:,2)=(chauvenet(i,:,2)).*(0./huecalmask+1);
        %Nan the St Dev's outside the calibration range
end


%Step 7. Define the areas of interest - where the leading edge is, where
        %the ribs and spaces lie on the plate.
%All areas are the 4 cm portion above the plexiglas hole blockage, 57 pix
%All areas have format (xstart, xfinish, ystart yfinish)

area(1,:)=[180 236 540 628];   %first rib and space 52+37=89
area(2,:)=[180 236 447 539];   %second rib and space 56+37=93
area(3,:)=[180 236 354 446];   %third rib and space 56+37=93
area(4,:)=[180 236 261 353];   %fourth rib and space 56+37=93
area(5,:)=[180 236 168 260];   %fifth rib and space 56+37=93
area(6,:)=[180 236 75 167];    %sixth rib and space 56+37=93
area(7,:)=[180 236 19 74];     %seventh rib 56
lower=19;
upper=628;
numcol=upper-lower+1;


%Step 8. Load in the 6th order polynomial calibration curves and SEE data
        %for each of the 7 areas.
%Area 1 Calibration Equation and SEE from Excel:
p1=[8.80478482E+03 -1.38428428E+04 7.29109023E+03 -1.30776721E+03
    5.71414179E-01 2.13746093E+01 2.95127204E+01];
SEE1=0.167;
%Area2
p2=[8.55366000E+03 -1.33118574E+04 6.87361050E+03 -1.15776036E+03
    -2.46697444E+01 2.35552657E+01 2.94612103E+01];
SEE2=0.167;
%Area3
p3=[7.81519249E+03 -1.19736547E+04 5.97227115E+03 -8.89325561E+02
    -5.64021901E+01 2.42047098E+01 2.95643830E+01];
SEE3=0.166;
%Area4
p4=[5.40806030E+03 -7.43086865E+03 2.71619085E+03 2.00804817E+02
    -2.23735106E+02 3.40999374E+01 2.94437101E+01];
SEE4=0.214;
%Area5
p5=[5.61044299E+03 -8.02456290E+03 3.32458898E+03 -7.15036413E+01
    -1.71679095E+02 3.04392207E+01 2.95111459E+01];
SEE5=0.197;
```

```
%Area6
p6=[5.44478898E+03 -7.67615223E+03 3.04431247E+03 3.05179786E+01
   -1.86995444E+02 3.10377217E+01 2.95628180E+01];
SEE6=0.201;
%Area7
p7=[4.09617356E+03 -5.10016888E+03 1.16930897E+03 6.63263848E+02
   -2.81896714E+02 3.60627891E+01 2.95874227E+01];
SEE7=0.232;


for i=35:37
    %Step 9. Convert hue to temperature using the calibration data
            %specific to each area.
    tempout(i,522:610,1)=polyval(p1,huechauvfin(i,522:610,1));
    tempout(i,429:521,1)=polyval(p2,huechauvfin(i,429:521,1));
    tempout(i,336:428,1)=polyval(p3,huechauvfin(i,336:428,1));
    tempout(i,243:335,1)=polyval(p4,huechauvfin(i,243:335,1));
    tempout(i,150:242,1)=polyval(p5,huechauvfin(i,150:242,1));
    tempout(i,57:149,1)=polyval(p6,huechauvfin(i,57:149,1));
    tempout(i,1:56,1)=polyval(p7,huechauvfin(i,1:56,1));


    %Step 10. Calculate the 68% uncertainty in temperature
    tempout(i,522:610,2)=(polyval(p1,(huechauvfin(i,522:610,1)+.0001))-
        polyval(p1,(huechauvfin(i,522:610,1)-.0001)))/.0002;
    tempout(i,429:521,2)=(polyval(p2,(huechauvfin(i,429:521,1)+.0001))-
        polyval(p2,(huechauvfin(i,429:521,1)-.0001)))/.0002;
    tempout(i,336:428,2)=(polyval(p3,(huechauvfin(i,336:428,1)+.0001))-
        polyval(p3,(huechauvfin(i,336:428,1)-.0001)))/.0002;
    tempout(i,243:335,2)=(polyval(p4,(huechauvfin(i,243:335,1)+.0001))-
        polyval(p4,(huechauvfin(i,243:335,1)-.0001)))/.0002;
    tempout(i,150:242,2)=(polyval(p5,(huechauvfin(i,150:242,1)+.0001))-
        polyval(p5,(huechauvfin(i,150:242,1)-.0001)))/.0002;
    tempout(i,57:149,2)=(polyval(p6,(huechauvfin(i,57:149,1)+.0001))-
        polyval(p6,(huechauvfin(i,57:149,1)-.0001)))/.0002;
    tempout(i,1:56,2)=(polyval(p7,(huechauvfin(i,1:56,1)+.0001))-
        polyval(p7,(huechauvfin(i,1:56,1)-.0001)))/.0002;


    for c=1:610
        tempout(i,c,2)=tempout(i,c,2)*(huechauvfin(i,c,2)/sqrt(57));
    end
    %Use a coverage factor of 1 to get 68% UT, using ST and SEE
    cf=1;
    for c=522:610
        tempout(i,c,3)=cf*sqrt((tempout(i,c,2))^2+(SEE1^2));
    end
    for c=429:521
        tempout(i,c,3)=cf*sqrt((tempout(i,c,2))^2+(SEE2^2));
    end
    for c=336:428
        tempout(i,c,3)=cf*sqrt((tempout(i,c,2))^2+(SEE3^2));
    end
    for c=243:335
        tempout(i,c,3)=cf*sqrt((tempout(i,c,2))^2+(SEE4^2));
    end
    for c=150:242
        tempout(i,c,3)=cf*sqrt((tempout(i,c,2))^2+(SEE5^2));
    end
    for c=57:149
        tempout(i,c,3)=cf*sqrt((tempout(i,c,2))^2+(SEE6^2));
    end
```

```
    for c=1:56
        tempout(i,c,3)=cf*sqrt((tempout(i,c,2))^2+(SEE7^2));
    end
end

hresult(:,:)=tempout(35,:,:);
hprofile=tempout;

%Step 11. Input power setting, qe and freestream air temperature,
        %T infinity, for the specified runs.
q1=349.006;
q2=431.763;
q3=267.223;
Tinf1=299.23;
Tinf2=299.3;
Tinf3=299.35;

%Step 12. Input uncertainty analysis data - bias and precision limits
        %for each of the elemental source in h.
%qe, electric power in:
relplq=0.0056;
relblq=0.0122;
%ql, power from light radiation:
ql=10;
absblql=2.5;
%emissivity of block:
eps=0.95;
abspleps=0;
absbleps=0.015;
%Stephan-Boltzman constant, sigma:
sigma=5.67E-08;
absblsigma=2.835E-10;
dsig=5.67E-11;
%Liquid Crystal temp, Tlc:
%absolute precision limit contained in tempout(:,:,3) (combined ST, SEE)
absbltlc=0.067;
%Freestream air temp:
absbltinf=0.067;
abspltinf=0.025;
k=2;

%Step 13 Compute h profile
for c=1:610
    %first image:
    hprofile(35,c,1)=(q1+ql-eps*sigma*((tempout(35,c,1)+273.15)^4-
        (Tinf1)^4))/(tempout(35,c,1)+273.15-Tinf1);
    % Step 14. Calculate h sensitivity coefficients for uncert. analysis
    dhdq=(((q1+.1)-eps*sigma*((tempout(35,c,1)+273.15)^4-(Tinf1)^4))/
        (tempout(35,c,1)+273.15-Tinf1)-((q1-.1)-eps*sigma*((tempout(35,c,1)
        +273.15)^4-(Tinf1)^4))/(tempout(35,c,1)+273.15-Tinf1))/.2;
    dhdql=((q1+(ql+.01)-eps*sigma*((tempout(35,c,1)+273.15)^4-(Tinf1)^4))/
        (tempout(35,c,1)+273.15-Tinf1)-(q1+(ql-.01)-eps*sigma*((tempout
        (35,c,1)+273.15)^4-(Tinf1)^4))/(tempout(35,c,1)+273.15-Tinf1))/.02;
    dhde=((q1-(eps+.001)*sigma*((tempout(35,c,1)+273.15)^4-(Tinf1)^4))/
        (tempout(35,c,1)+273.15-Tinf1)-(q1-(eps-.001)*sigma*((tempout
        (35,c,1)+273.15)^4-(Tinf1)^4))/(tempout(35,c,1)+273.15-Tinf1))/.002;
    dhds=((q1-eps*(sigma+dsig)*((tempout(35,c,1)+273.15)^4-(Tinf1)^4))/
        (tempout(35,c,1)+273.15-Tinf1)-(q1-eps*(sigma-dsig)*((tempout(35,
        c,1)+273.15)^4-(Tinf1)^4))/(tempout(35,c,1)+273.15-Tinf1))/(2*dsig);
```

```
    dhdtlc=((q1-eps*sigma*((tempout(35,c,1)+273.25)^4-(Tinf1)^4))/
        (tempout(35,c,1)+273.25-Tinf1)-(q1-eps*sigma*((tempout(35,c,1)
        +273.05)^4-(Tinf1)^4))/(tempout(35,c,1)+273.05-Tinf1))/.2;
    dhdtinf=((q1-eps*sigma*((tempout(35,c,1)+273.15)^4-(Tinf1+.1)^4))/
        (tempout(35,c,1)+273.15-(Tinf1+.1))-(q1-eps*sigma*((tempout(35,c,1)
        +273.15)^4-(Tinf1-.1)^4))/(tempout(35,c,1)+273.15-(Tinf1-.1)))/.2;
    %the line below puts the 68% precision limit in h into 2nd indice
    hprofile(35,c,2)=sqrt((dhdq*q1*relplq)^2+(dhdtlc*tempout(35,c,3))^2+
        (dhdtinf*abspltinf)^2);
    %the line below puts the 68% bias limit in h into the 3rd indice
    hprofile(35,c,3)=sqrt((dhdq*q1*relblq)^2+(dhdql*absblql)^2+
        (dhde*absbleps)^2+(dhds*absblsigma)^2+(dhdtlc*absbltlc)^2+
        (dhdtinf*absbltinf)^2+2*dhdtlc*dhdtinf*absbltlc*absbltinf);
    %the next line puts the combined uncertainty in h into the 4th indice
    hprofile(35,c,4)=k*sqrt(hprofile(35,c,2)^2+hprofile(35,c,3)^2);

    %second image: perform same steps as first image
    %third image: perform same steps as first and second image

    %Step 15. Compare h values at each column position, for different
        %power settings. Choose h that has lowest associated uncertainty.
    hresult(c,2)=min(hprofile(35:37,c,4)); %holds the min Uh value
    for i=35:37
        if hprofile(i,c,4)==hresult(c,2);
            hresult(c,1)=(hprofile(i,c,1)); %holds corresponding h value
        end
    end

end

%Step 16. Calculate relative uncertainty, save to 3rd position in hresult
for c=1:610
    hresult(c,3)=(hresult(c,2)/hresult(c,1))*100;
end

%plot temps
for i=35:37
    figure;
    plot(tempout(i,:,1)); hold on;
end

%plot all three solutions for h
figure;
for i=35:37
    plot(hprofile(i,:,1)); hold on;
end
%plot all three solutions for h
%plot all h profiles and U bars
figure;
i=35;
plot(hprofile(i,:,1),'r'); hold on;
plot(hprofile(i,:,1)+hprofile(i,:,4),'r'); hold on;
plot(hprofile(i,:,1)-hprofile(i,:,4),'r'); hold on;
i=36;
plot(hprofile(i,:,1),'g'); hold on;
plot(hprofile(i,:,1)+hprofile(i,:,4),'g'); hold on;
plot(hprofile(i,:,1)-hprofile(i,:,4),'g'); hold on;
i=37;
plot(hprofile(i,:,1),'b'); hold on;
plot(hprofile(i,:,1)+hprofile(i,:,4),'b'); hold on;
plot(hprofile(i,:,1)-hprofile(i,:,4),'b'); hold on;
```

```
%plot the resulting h profile and uncertainty bars
figure;
plot(hresult(:,1)); hold on;
plot(hresult(:,1)+hresult(:,2)); hold on;
plot(hresult(:,1)-hresult(:,2));

%Step 17. Output results (h profile and uncertainty for each data point)
        %to a file for use in Excel.
dataout=(hresult(:,:)); %the last two remove the first dimension
    %(which incidentally is called a singleton dimension because it exists
    %but does not contain any data) resulting in a 2-D matrix output
save (['E:\Thesis\hprofileFP10.dat'],'dataout','-ascii','-tabs');
```

Appendix I: Data for Flat Plate

10 m/s

Air Properties:			Universal Gas Constant:		2.87E+02
Pressure (mb)		1006.16	T (C)		26.15
Pressure (N/m^2)		100616	T(K)		299.3
density (kg/m3)		1.17E+00	Pr		0.707
viscosity (kg/ms)		1.85E-05	k (W/mK)		2.63E-02
Velocity (m/s)		10	ZI (Unheated starting length, m)		0.2

Position Data		Experimental Results:			Theoretical Results:				Difference
x (m)	x+ZI	h	Uh	Uh/h (%)	Re(x)	Nu(x)	Nu(x) USL	h	in h (%)
0.420	0.620	32.81	1.51	4.6	3.93E+05	820.78	862.69	36.59	10.34
0.415	0.615	31.21	1.43	4.58	3.90E+05	814.98	857.03	36.68	14.91
0.409	0.609	31.15	1.42	4.57	3.86E+05	809.17	851.36	36.76	15.27
0.404	0.604	31.49	1.44	4.56	3.83E+05	803.35	845.68	36.85	14.54
0.398	0.598	31.57	1.44	4.57	3.80E+05	797.52	839.99	36.94	14.53
0.393	0.593	31.75	1.45	4.56	3.76E+05	791.67	834.29	37.02	14.25
0.387	0.587	31.78	1.45	4.55	3.73E+05	785.82	828.59	37.11	14.37
0.382	0.582	32.32	1.36	4.21	3.69E+05	779.96	822.88	37.20	13.13
0.376	0.576	32.46	1.36	4.2	3.66E+05	774.08	817.16	37.30	12.97
0.371	0.571	32.44	1.36	4.2	3.62E+05	768.19	811.44	37.39	13.24
0.365	0.565	32.51	1.36	4.19	3.59E+05	762.30	805.71	37.49	13.27
0.360	0.560	32.54	1.36	4.19	3.55E+05	756.39	799.97	37.58	13.42
0.354	0.554	32.73	1.37	4.2	3.52E+05	750.47	794.22	37.68	13.14
0.349	0.549	32.96	1.38	4.2	3.48E+05	744.53	788.47	37.78	12.76
0.343	0.543	33.04	1.39	4.19	3.45E+05	738.59	782.71	37.88	12.78
0.338	0.538	33.2	1.39	4.19	3.41E+05	732.63	776.94	37.99	12.60
0.332	0.532	33.37	1.4	4.2	3.38E+05	726.66	771.16	38.09	12.39
0.327	0.527	33.46	1.4	4.2	3.34E+05	720.68	765.38	38.20	12.40
0.321	0.521	33.55	1.41	4.2	3.31E+05	714.69	759.59	38.31	12.42
0.316	0.516	33.73	1.42	4.21	3.27E+05	708.68	753.79	38.42	12.20
0.311	0.511	33.84	1.42	4.2	3.24E+05	702.66	747.98	38.53	12.17
0.305	0.505	34.05	1.43	4.21	3.20E+05	696.63	742.17	38.65	11.89
0.300	0.500	34.1	1.43	4.21	3.17E+05	690.59	736.35	38.76	12.03
0.294	0.494	34.37	1.45	4.21	3.14E+05	684.53	730.53	38.88	11.60
0.289	0.489	34.41	1.45	4.21	3.10E+05	678.46	724.69	39.00	11.78
0.283	0.483	34.69	1.46	4.22	3.07E+05	672.37	718.86	39.13	11.34
0.278	0.478	34.86	1.47	4.22	3.03E+05	666.27	713.01	39.25	11.19
0.272	0.472	35.09	1.48	4.23	3.00E+05	660.16	707.16	39.38	10.90
0.267	0.467	35.24	1.49	4.23	2.96E+05	654.03	701.31	39.51	10.82
0.261	0.461	35.49	1.5	4.22	2.93E+05	647.89	695.44	39.65	10.49
0.256	0.456	35.54	1.5	4.23	2.89E+05	641.74	689.58	39.79	10.67
0.250	0.450	35.18	1.54	4.39	2.86E+05	635.57	683.71	39.93	11.89
0.245	0.445	35.32	1.55	4.38	2.82E+05	629.38	677.83	40.07	11.86
0.239	0.439	35.8	1.57	4.4	2.79E+05	623.18	671.95	40.22	10.98
0.234	0.434	36.04	1.59	4.4	2.75E+05	616.96	666.06	40.37	10.72
0.228	0.428	36.13	1.59	4.4	2.72E+05	610.73	660.18	40.52	10.84
0.223	0.423	36.45	1.61	4.42	2.68E+05	604.48	654.28	40.68	10.40
0.218	0.418	36.84	1.63	4.42	2.65E+05	598.22	648.39	40.84	9.80
0.212	0.412	37.06	1.64	4.43	2.61E+05	591.94	642.50	41.01	9.63
0.207	0.407	37.43	1.66	4.44	2.58E+05	585.64	636.60	41.18	9.10
0.201	0.401	37.6	1.67	4.45	2.55E+05	579.33	630.71	41.35	9.08
0.196	0.396	38.16	1.7	4.46	2.51E+05	572.99	624.81	41.53	8.12

Position	Data	Experimental	Results:		Theoretical	Results:			
x (m)	x+Zl	h	Uh	Uh/h (%)	Re(x)	Nu(x)	Nu(x) USL	h	diff (%)
0.190	0.390	39.07	1.64	4.19	2.48E+05	566.65	618.92	41.72	6.35
0.185	0.385	39.67	1.67	4.2	2.44E+05	560.28	613.03	41.91	5.35
0.179	0.379	40.1	1.69	4.22	2.41E+05	553.89	607.14	42.11	4.77
0.174	0.374	40.28	1.7	4.21	2.37E+05	547.49	601.26	42.31	4.80
0.168	0.368	40.68	1.72	4.22	2.34E+05	541.07	595.39	42.52	4.33
0.163	0.363	40.66	1.72	4.23	2.30E+05	534.63	589.52	42.74	4.86
0.157	0.357	40.58	1.72	4.24	2.27E+05	528.16	583.67	42.96	5.54
0.152	0.352	41.01	1.74	4.24	2.23E+05	521.68	577.83	43.19	5.05
0.146	0.346	40.79	1.72	4.21	2.20E+05	515.18	572.00	43.43	6.08
0.141	0.341	40.84	1.72	4.22	2.16E+05	508.66	566.20	43.68	6.50
0.135	0.335	41.37	1.75	4.22	2.13E+05	502.12	560.41	43.94	5.85
0.130	0.330	41.51	1.76	4.24	2.09E+05	495.55	554.65	44.21	6.10
0.124	0.324	42.37	1.85	4.37	2.06E+05	488.97	548.93	44.49	4.77
0.119	0.319	42.76	1.87	4.37	2.02E+05	482.36	543.24	44.78	4.52
0.114	0.314	43.45	1.91	4.4	1.99E+05	475.73	537.59	45.09	3.64
0.108	0.308	43.31	1.9	4.38	1.95E+05	469.08	531.99	45.41	4.63
0.103	0.303	43.92	1.93	4.39	1.92E+05	462.40	526.45	45.75	4.01
0.097	0.297	44.28	1.95	4.4	1.89E+05	455.70	520.98	46.11	3.97
0.092	0.292	44.76	1.98	4.43	1.85E+05	448.97	515.59	46.49	3.73
0.086	0.286	45.34	2.01	4.44	1.82E+05	442.22	510.29	46.89	3.31
0.081	0.281	46.12	2.06	4.47	1.78E+05	435.44	505.11	47.32	2.54
0.075	0.275	46.86	2.09	4.46	1.75E+05	428.64	500.06	47.78	1.93
0.070	0.270	47.62	2.14	4.5	1.71E+05	421.81	495.18	48.28	1.36
0.064	0.264	48.03	2.17	4.52	1.68E+05	414.95	490.50	48.81	1.60
0.059	0.259	49.74	2.17	4.37	1.64E+05	408.06	486.07	49.39	0.71
0.053	0.253	50.7	2.24	4.43	1.61E+05	401.14	481.95	50.03	1.34
0.048	0.248	52.52	2.32	4.43	1.57E+05	394.20	478.23	50.74	3.51
0.042	0.242	54.86	2.47	4.5	1.54E+05	387.22	475.02	51.54	6.45
0.037	0.237	58.21	2.69	4.62	1.50E+05	380.21	472.49	52.45	10.99
0.031	0.231	63.46	2.98	4.7	1.47E+05	373.17	470.91	53.51	18.60
0.026	0.226	70.81	3.45	4.88	1.43E+05	366.09	470.70	54.78	29.27
0.021	0.221	74.69	3.71	4.97	1.40E+05	358.98	472.62	56.37	32.51
0.015	0.215				1.36E+05	351.84	478.18	58.48	
0.010	0.210				1.33E+05	344.66	491.21	61.64	
0.004	0.204				1.30E+05	337.44	526.92	67.90	

Avg Uh 4.06545

Avg Diff (%) 8.74

Appendix J: Data for Flat Plate with Interrupted Heating

10 m/s

Air Properties:			Universal Gas Constant:	2.87E+02
Pressure (mb)	1006.16		T (C)	26.15
Pressure (N/m^2)	100616		T (K)	299.3
density (kg/m3)	1.17E+00		Pr	0.707
viscosity (kg/ms)	1.85E-05		k (W/mK)	2.63E-02
Velocity (m/s)	10		ZI (unheated starting length, m	0.2

Position Data		Experimental Results (section #7):			Flat Plate Continuous Heating Results		
x (m)	x+ZI (m)	h	Uh	Uh/h (%)	x	h	diff (%)
0.420	0.620	55.487	3.326	6.00	0.420	32.81	69.12
0.419	0.619	46.148	1.988	4.31	0.415	31.21	47.86
0.419	0.619	43.967	1.916	4.36	0.409	31.15	41.15
0.418	0.618	42.917	1.824	4.25	0.404	31.49	36.29
0.417	0.617	41.148	1.721	4.18	0.398	31.57	30.34
0.417	0.617	40.92	1.716	4.19	0.393	31.75	28.88
0.416	0.616	40.556	1.687	4.16	0.387	31.78	27.61
0.415	0.615	40.421	1.686	4.17	0.382	32.32	25.06
0.415	0.615	40.317	1.687	4.19	0.376	32.46	24.21
0.414	0.614	40.179	1.674	4.17	0.371	32.44	23.86
0.413	0.613	40.57	1.678	4.14	0.365	32.51	24.79
0.412	0.612	40.609	1.683	4.15	0.360	32.54	24.80
0.412	0.612	40.403	1.675	4.14	0.354	32.73	23.44
0.411	0.611	40.833	1.696	4.15	0.349	32.96	23.89
0.410	0.610	40.885	1.693	4.14	0.343	33.04	23.74
0.410	0.610	41.048	1.714	4.18	0.338	33.2	23.64
0.409	0.609	41.25	1.715	4.16	0.332	33.37	23.61
0.408	0.608	41.507	1.732	4.17	0.327	33.46	24.05
0.408	0.608	41.625	1.733	4.16	0.321	33.55	24.07
0.407	0.607	41.769	1.741	4.17	0.316	33.73	23.83
0.406	0.606	42.028	1.751	4.17	0.311	33.84	24.20
0.406	0.606	42.272	1.766	4.18	0.305	34.05	24.15
0.405	0.605	42.498	1.778	4.18	0.300	34.1	24.63
0.404	0.604	42.589	1.773	4.16	0.294	34.37	23.91
0.404	0.604	42.751	1.78	4.16	0.289	34.41	24.24
0.403	0.603	43.185	1.803	4.18	0.283	34.69	24.49
0.402	0.602	43.351	1.81	4.18	0.278	34.86	24.36
0.402	0.602	43.51	1.818	4.18	0.272	35.09	24.00
0.401	0.601	43.77	1.834	4.19	0.267	35.24	24.21
0.400	0.600	44.034	1.848	4.20	0.261	35.49	24.07
0.399	0.599	44.323	1.859	4.20	0.256	35.54	24.71
0.399	0.599	44.522	1.866	4.19	0.250	35.18	26.55
0.398	0.598	44.97	1.889	4.20	0.245	35.32	27.32
0.397	0.597	45.222	1.9	4.20	0.239	35.8	26.32
0.397	0.597	45.374	1.908	4.21	0.234	36.04	25.90
0.396	0.596	45.645	1.919	4.20	0.228	36.13	26.34
0.395	0.595	45.975	1.937	4.21	0.223	36.45	26.13
0.395	0.595	46.187	1.946	4.21	0.218	36.84	25.37
0.394	0.594	46.432	1.957	4.22	0.212	37.06	25.29
0.393	0.593	46.649	1.97	4.22	0.207	37.43	24.63

Position Data		Experimental Results (section #7):			Flat Plate Continuous Heating Results		
x (m)	x+Zl (m)	h	Uh	Uh/h (%)	x	h	diff (%)
0.393	0.593	47.013	1.989	4.23	0.201	37.6	25.03
0.392	0.592	47.334	2.007	4.24	0.196	38.16	24.04
0.391	0.591	47.864	2.036	4.26	0.190	39.07	22.51
0.391	0.591	48.252	2.06	4.27	0.185	39.67	21.63
0.390	0.590	48.812	2.091	4.28	0.179	40.1	21.73
0.389	0.589	49.688	2.141	4.31	0.174	40.28	23.36
0.389	0.589	50.394	2.187	4.34	0.168	40.68	23.88
0.388	0.588	51.525	2.259	4.39	0.163	40.66	26.72
0.387	0.587	52.887	2.331	4.41	0.157	40.58	30.33
0.386	0.586	54.431	2.426	4.46	0.152	41.01	32.73
0.386	0.586	55.94	2.516	4.50	0.146	40.79	37.14
0.385	0.585	57.808	2.635	4.56	0.141	40.84	41.55
0.384	0.584	60.635	2.831	4.67	0.135	41.37	46.57
0.384	0.584	67.064	3.263	4.87	0.130	41.51	61.56
0.383	0.583	93.271	5.359	5.75	0.124	42.37	120.13
0.382	0.582				0.119	42.76	-100.00
0.382	0.582				0.114	43.45	-100.00
0.381	0.581				0.108	43.31	-100.00
0.380	0.580				0.103	43.92	-100.00
0.380	0.580				0.097	44.28	-100.00
0.379	0.579				0.092	44.76	-100.00
0.378	0.578				0.086	45.34	-100.00
0.378	0.578				0.081	46.12	-100.00
0.377	0.577				0.075	46.86	-100.00
0.376	0.576				0.070	47.62	-100.00
0.376	0.576				0.064	48.03	-100.00
0.375	0.575				0.059	49.74	-100.00
0.374	0.574				0.053	50.7	-100.00
0.373	0.573				0.048	52.52	-100.00
0.373	0.573				0.042	54.86	-100.00
0.372	0.572				0.037	58.21	-100.00
0.371	0.571				0.031	63.46	-100.00
0.371	0.571				0.026	70.81	-100.00
0.370	0.570				0.021	74.69	-100.00
0.369	0.569						
0.369	0.569						
0.368	0.568						
0.367	0.567						
0.367	0.567						
0.366	0.566						
0.365	0.565						
0.365	0.565						
0.364	0.564	Section #6:					
0.363	0.563	95.423	4.724	4.95			
0.363	0.563	94.207	4.634	4.92			
0.362	0.562	90.847	4.405	4.85			
0.361	0.561	84.956	3.998	4.71			
0.360	0.560	79.275	3.616	4.56			
0.360	0.560	73.895	3.277	4.44			
0.359	0.559	67.843	2.926	4.31			
0.358	0.558	63.305	2.663	4.21			

Position Data		Experimental Results:		
x (m)	x+Zl (m)	h	Uh	Uh/h (%)
0.358	0.558	67.126	3.117	4.64
0.357	0.557	71.588	3.599	5.03
0.356	0.556	48.694	1.933	3.97
0.356	0.556	43.792	1.687	3.85
0.355	0.555	41.702	1.602	3.84
0.354	0.554	40.825	1.56	3.82
0.354	0.554	40.424	1.546	3.82
0.353	0.553	40.371	1.545	3.83
0.352	0.552	40.418	1.541	3.81
0.352	0.552	40.622	1.551	3.82
0.351	0.551	40.627	1.549	3.81
0.350	0.550	40.619	1.55	3.82
0.350	0.550	40.637	1.554	3.82
0.349	0.549	41.128	1.573	3.83
0.348	0.548	41.266	1.579	3.83
0.347	0.547	41.097	1.57	3.82
0.347	0.547	41.444	1.587	3.83
0.346	0.546	41.723	1.597	3.83
0.345	0.545	41.753	1.605	3.84
0.345	0.545	41.837	1.606	3.84
0.344	0.544	42.053	1.61	3.83
0.343	0.543	42.074	1.616	3.84
0.343	0.543	42.184	1.616	3.83
0.342	0.542	42.429	1.632	3.85
0.341	0.541	42.734	1.641	3.84
0.341	0.541	42.785	1.645	3.84
0.340	0.540	43.078	1.654	3.84
0.339	0.539	43.245	1.663	3.85
0.339	0.539	43.58	1.676	3.85
0.338	0.538	43.969	1.692	3.85
0.337	0.537	44.199	1.702	3.85
0.337	0.537	44.552	1.718	3.86
0.336	0.536	44.588	1.718	3.85
0.335	0.535	44.699	1.72	3.85
0.334	0.534	45.06	1.736	3.85
0.334	0.534	45.391	1.751	3.86
0.333	0.533	45.754	1.766	3.86
0.332	0.532	45.897	1.771	3.86
0.332	0.532	46.273	1.788	3.86
0.331	0.531	46.54	1.798	3.86
0.330	0.530	46.991	1.82	3.87
0.330	0.530	47.278	1.832	3.88
0.329	0.529	47.585	1.846	3.88
0.328	0.528	48.115	1.872	3.89
0.328	0.528	48.662	1.898	3.90
0.327	0.527	49.18	1.923	3.91
0.326	0.526	49.837	1.957	3.93
0.326	0.526	50.517	1.992	3.94
0.325	0.525	51.836	2.069	3.99
0.324	0.524	53.098	2.132	4.01
0.324	0.524	54.386	2.189	4.03

Position Data		Experimental Results:		
x (m)	x+Zl (m)	h	Uh	Uh/h (%)
0.323	0.523	56.321	2.287	4.06
0.322	0.522	57.883	2.389	4.13
0.321	0.521	59.968	2.484	4.14
0.321	0.521	62.492	2.627	4.20
0.320	0.520	69.06	3.034	4.39
0.319	0.519	94.071	4.63	4.92
0.319	0.519			
0.318	0.518			
0.317	0.517			
0.317	0.517			
0.316	0.516			
0.315	0.515			
0.315	0.515			
0.314	0.514			
0.313	0.513			
0.313	0.513			
0.312	0.512			
0.311	0.511			
0.311	0.511			
0.310	0.510			
0.309	0.509			
0.309	0.509			
0.308	0.508			
0.307	0.507			
0.306	0.506			
0.306	0.506			
0.305	0.505			
0.304	0.504			
0.304	0.504			
0.303	0.503			
0.302	0.502			
0.302	0.502			
0.301	0.501			
0.300	0.500			
0.300	0.500	Section #5:		
0.299	0.499	95.348	4.722	4.95
0.298	0.498	93.25	4.569	4.90
0.298	0.498	87.997	4.208	4.78
0.297	0.497	81.063	3.734	4.61
0.296	0.496	73.69	3.276	4.45
0.296	0.496	67.189	2.881	4.29
0.295	0.495	62.759	2.641	4.21
0.294	0.494	70.595	3.539	5.01
0.293	0.493	70.349	3.527	5.01
0.293	0.493	46.547	1.817	3.90
0.292	0.492	42.894	1.651	3.85
0.291	0.491	41.896	1.61	3.84
0.291	0.491	41.068	1.573	3.83
0.290	0.490	40.894	1.564	3.83
0.289	0.489	41.06	1.569	3.82
0.289	0.489	41.219	1.576	3.82

Position Data		Experimental Results:		
x (m)	x+Zl (m)	h	Uh	Uh/h (%)
0.288	0.488	41.119	1.573	3.83
0.287	0.487	41.23	1.576	3.82
0.287	0.487	41.419	1.589	3.84
0.286	0.486	41.478	1.586	3.82
0.285	0.485	41.545	1.59	3.83
0.285	0.485	41.605	1.593	3.83
0.284	0.484	41.959	1.613	3.85
0.283	0.483	41.918	1.607	3.83
0.283	0.483	42.082	1.62	3.85
0.282	0.482	42.229	1.623	3.84
0.281	0.481	42.518	1.634	3.84
0.280	0.480	42.709	1.638	3.84
0.280	0.480	42.898	1.649	3.85
0.279	0.479	43.183	1.658	3.84
0.278	0.478	43.334	1.669	3.85
0.278	0.478	43.544	1.678	3.85
0.277	0.477	43.768	1.687	3.86
0.276	0.476	44.085	1.701	3.86
0.276	0.476	44.322	1.71	3.86
0.275	0.475	44.718	1.723	3.85
0.274	0.474	44.911	1.735	3.86
0.274	0.474	45.019	1.735	3.86
0.273	0.473	45.08	1.739	3.86
0.272	0.472	45.435	1.755	3.86
0.272	0.472	45.736	1.767	3.86
0.271	0.471	46.089	1.782	3.87
0.270	0.470	46.522	1.802	3.87
0.270	0.470	46.714	1.807	3.87
0.269	0.469	46.998	1.82	3.87
0.268	0.468	47.458	1.841	3.88
0.267	0.467	47.691	1.85	3.88
0.267	0.467	47.957	1.863	3.88
0.266	0.466	48.386	1.88	3.89
0.265	0.465	48.915	1.907	3.90
0.265	0.465	49.332	1.928	3.91
0.264	0.464	49.978	1.957	3.92
0.263	0.463	50.819	2.001	3.94
0.263	0.463	51.475	2.033	3.95
0.262	0.462	52.429	2.079	3.97
0.261	0.461	53.868	2.16	4.01
0.261	0.461	55.484	2.231	4.02
0.260	0.460	56.537	2.303	4.07
0.259	0.459	58.053	2.37	4.08
0.259	0.459	60.45	2.495	4.13
0.258	0.458	62.289	2.6	4.18
0.257	0.457	66.139	2.812	4.25
0.257	0.457	76.353	3.496	4.58
0.256	0.456	95.536	4.738	4.96
0.255	0.455			
0.254	0.454			
0.254	0.454			

Position Data		Experimental Results:		
x (m)	x+ZI (m)	h	Uh	Uh/h (%)
0.253	0.453			
0.252	0.452			
0.252	0.452			
0.251	0.451			
0.250	0.450			
0.250	0.450			
0.249	0.449			
0.248	0.448			
0.248	0.448			
0.247	0.447			
0.246	0.446			
0.246	0.446			
0.245	0.445			
0.244	0.444			
0.244	0.444			
0.243	0.443			
0.242	0.442			
0.241	0.441			
0.241	0.441			
0.240	0.440			
0.239	0.439			
0.239	0.439			
0.238	0.438			
0.237	0.437			
0.237	0.437			
0.236	0.436			
0.235	0.435	Section #4:		
0.235	0.435	94.493	4.972	5.26
0.234	0.434	94.596	4.982	5.27
0.233	0.433	86.817	4.384	5.05
0.233	0.433	75.746	3.591	4.74
0.232	0.432	66.812	3.021	4.52
0.231	0.431	68.689	3.403	4.96
0.231	0.431	72.254	3.891	5.39
0.230	0.430	50.163	2.103	4.19
0.229	0.429	46.623	1.868	4.01
0.228	0.428	46.182	1.845	4.00
0.228	0.428	45.881	1.831	3.99
0.227	0.427	46.004	1.836	3.99
0.226	0.426	45.962	1.836	3.99
0.226	0.426	45.989	1.836	3.99
0.225	0.425	46.089	1.84	3.99
0.224	0.424	46.167	1.845	4.00
0.224	0.424	46.388	1.855	4.00
0.223	0.423	46.451	1.858	4.00
0.222	0.422	46.477	1.859	4.00
0.222	0.422	46.53	1.861	4.00
0.221	0.421	46.69	1.868	4.00
0.220	0.420	46.673	1.867	4.00
0.220	0.420	46.784	1.873	4.00
0.219	0.419	46.954	1.882	4.01

| Position Data | | Experimental Results: | | |
x (m)	x+Zl (m)	h	Uh	Uh/h (%)
0.218	0.418	47.141	1.89	4.01
0.218	0.418	47.137	1.889	4.01
0.217	0.417	47.274	1.896	4.01
0.216	0.416	47.46	1.905	4.01
0.215	0.415	47.608	1.913	4.02
0.215	0.415	47.68	1.917	4.02
0.214	0.414	47.77	1.919	4.02
0.213	0.413	47.973	1.93	4.02
0.213	0.413	48.208	1.943	4.03
0.212	0.412	48.417	1.954	4.04
0.211	0.411	48.585	1.963	4.04
0.211	0.411	48.655	1.965	4.04
0.210	0.410	48.931	1.979	4.04
0.209	0.409	48.996	1.983	4.05
0.209	0.409	49.264	1.998	4.06
0.208	0.408	49.747	2.02	4.06
0.207	0.407	50.103	2.04	4.07
0.207	0.407	50.321	2.057	4.09
0.206	0.406	50.586	2.066	4.08
0.205	0.405	51.014	2.089	4.10
0.205	0.405	51.504	2.113	4.10
0.204	0.404	52.307	2.154	4.12
0.203	0.403	52.72	2.18	4.13
0.202	0.402	53.179	2.205	4.15
0.202	0.402	54.026	2.244	4.15
0.201	0.401	54.595	2.278	4.17
0.200	0.400	55.532	2.332	4.20
0.200	0.400	56.408	2.391	4.24
0.199	0.399	56.934	2.411	4.23
0.198	0.398	57.94	2.467	4.26
0.198	0.398	59.188	2.537	4.29
0.197	0.397	60.445	2.606	4.31
0.196	0.396	61.614	2.693	4.37
0.196	0.396	63.502	2.814	4.43
0.195	0.395	65.796	2.945	4.48
0.194	0.394	69.452	3.183	4.58
0.194	0.394	77.327	3.742	4.84
0.193	0.393	90.915	4.733	5.21
0.192	0.392			
0.192	0.392			
0.191	0.391			
0.190	0.390			
0.189	0.389			
0.189	0.389			
0.188	0.388			
0.187	0.387			
0.187	0.387			
0.186	0.386			
0.185	0.385			
0.185	0.385			
0.184	0.384			

Position Data		Experimental Results:		
x (m)	x+Zl (m)	h	Uh	Uh/h (%)
0.183	0.383			
0.183	0.383			
0.182	0.382			
0.181	0.381			
0.181	0.381			
0.180	0.380			
0.179	0.379			
0.179	0.379			
0.178	0.378			
0.177	0.377			
0.176	0.376			
0.176	0.376			
0.175	0.375			
0.174	0.374			
0.174	0.374			
0.173	0.373			
0.172	0.372			
0.172	0.372			
0.171	0.371			
0.170	0.370	Section #3:		
0.170	0.370	95.517	4.502	4.71
0.169	0.369	88.34	4.052	4.59
0.168	0.368	76.161	3.328	4.37
0.168	0.368	67.519	2.827	4.19
0.167	0.367	72.765	3.51	4.82
0.166	0.366	71.659	3.441	4.80
0.166	0.366	48.453	1.869	3.86
0.165	0.365	47.019	1.774	3.77
0.164	0.364	46.497	1.754	3.77
0.163	0.363	46.486	1.753	3.77
0.163	0.363	46.74	1.763	3.77
0.162	0.362	46.712	1.762	3.77
0.161	0.361	46.801	1.764	3.77
0.161	0.361	47.003	1.773	3.77
0.160	0.360	46.917	1.77	3.77
0.159	0.359	47.075	1.777	3.78
0.159	0.359	47.136	1.779	3.77
0.158	0.358	47.301	1.785	3.77
0.157	0.357	47.316	1.787	3.78
0.157	0.357	47.43	1.793	3.78
0.156	0.356	47.647	1.801	3.78
0.155	0.355	47.65	1.802	3.78
0.155	0.355	47.6	1.8	3.78
0.154	0.354	47.677	1.803	3.78
0.153	0.353	47.771	1.806	3.78
0.153	0.353	47.953	1.815	3.79
0.152	0.352	48.233	1.829	3.79
0.151	0.351	48.336	1.831	3.79
0.150	0.350	48.398	1.834	3.79
0.150	0.350	48.555	1.842	3.79
0.149	0.349	48.836	1.854	3.80

Position Data		Experimental Results:		
x (m)	x+Zl (m)	h	Uh	Uh/h (%)
0.148	0.348	48.794	1.85	3.79
0.148	0.348	48.984	1.863	3.80
0.147	0.347	49.36	1.878	3.81
0.146	0.346	49.626	1.893	3.81
0.146	0.346	49.714	1.898	3.82
0.145	0.345	50.012	1.904	3.81
0.144	0.344	50.521	1.934	3.83
0.144	0.344	50.566	1.935	3.83
0.143	0.343	50.85	1.953	3.84
0.142	0.342	51.143	1.964	3.84
0.142	0.342	51.951	2.007	3.86
0.141	0.341	52.483	2.03	3.87
0.140	0.340	52.778	2.042	3.87
0.140	0.340	53.565	2.081	3.89
0.139	0.339	54.261	2.108	3.88
0.138	0.338	54.979	2.156	3.92
0.137	0.337	55.939	2.195	3.93
0.137	0.337	56.943	2.248	3.95
0.136	0.336	57.833	2.297	3.97
0.135	0.335	58.821	2.336	3.97
0.135	0.335	60.215	2.406	4.00
0.134	0.334	61.506	2.485	4.04
0.133	0.333	63.095	2.553	4.05
0.133	0.333	64.658	2.631	4.07
0.132	0.332	66.708	2.738	4.11
0.131	0.331	69.867	2.929	4.19
0.131	0.331	74.792	3.207	4.29
0.130	0.330	84.611	3.825	4.52
0.129	0.329	95.582	4.508	4.72
0.129	0.329			
0.128	0.328			
0.127	0.327			
0.127	0.327			
0.126	0.326			
0.125	0.325			
0.124	0.324			
0.124	0.324			
0.123	0.323			
0.122	0.322			
0.122	0.322			
0.121	0.321			
0.120	0.320			
0.120	0.320			
0.119	0.319			
0.118	0.318			
0.118	0.318			
0.117	0.317			
0.116	0.316			
0.116	0.316			
0.115	0.315			
0.114	0.314			

Position Data		Experimental Results:		
x (m)	x+Zl (m)	h	Uh	Uh/h (%)
0.114	0.314			
0.113	0.313			
0.112	0.312			
0.111	0.311			
0.111	0.311			
0.110	0.310			
0.109	0.309			
0.109	0.309			
0.108	0.308			
0.107	0.307			
0.107	0.307			
0.106	0.306	Section #2:		
0.105	0.305	96.603	4.742	4.91
0.105	0.305	89.775	4.292	4.78
0.104	0.304	76.093	3.41	4.48
0.103	0.303	82.36	4.189	5.09
0.103	0.303	73.022	3.651	5.00
0.102	0.302	51.32	2.053	4.00
0.101	0.301	48.887	1.891	3.87
0.101	0.301	48.667	1.884	3.87
0.100	0.300	48.658	1.882	3.87
0.099	0.299	48.761	1.886	3.87
0.099	0.299	48.665	1.881	3.86
0.098	0.298	48.99	1.9	3.88
0.097	0.297	49.108	1.904	3.88
0.096	0.296	49.52	1.924	3.89
0.096	0.296	49.492	1.919	3.88
0.095	0.295	49.464	1.921	3.88
0.094	0.294	49.705	1.931	3.89
0.094	0.294	49.852	1.939	3.89
0.093	0.293	50.078	1.953	3.90
0.092	0.292	50.459	1.967	3.90
0.092	0.292	50.311	1.966	3.91
0.091	0.291	50.523	1.972	3.90
0.090	0.290	50.664	1.979	3.91
0.090	0.290	50.977	1.996	3.92
0.089	0.289	51.392	2.016	3.92
0.088	0.288	51.705	2.027	3.92
0.088	0.288	51.791	2.04	3.94
0.087	0.287	51.926	2.045	3.94
0.086	0.286	51.998	2.053	3.95
0.086	0.286	52.327	2.062	3.94
0.085	0.285	52.873	2.097	3.97
0.084	0.284	53.174	2.114	3.98
0.083	0.283	53.434	2.12	3.97
0.083	0.283	53.928	2.142	3.97
0.082	0.282	54.848	2.185	3.98
0.081	0.281	54.737	2.183	3.99
0.081	0.281	54.784	2.187	3.99
0.080	0.280	55.235	2.207	4.00
0.079	0.279	55.986	2.24	4.00

Position Data		Experimental Results:		
x (m)	x+Zl (m)	h	Uh	Uh/h (%)
0.079	0.279	56.64	2.285	4.04
0.078	0.278	57.395	2.321	4.05
0.077	0.277	58.341	2.372	4.07
0.077	0.277	58.892	2.407	4.09
0.076	0.276	59.369	2.416	4.07
0.075	0.275	60.021	2.452	4.08
0.075	0.275	60.832	2.504	4.12
0.074	0.274	61.845	2.567	4.15
0.073	0.273	62.823	2.607	4.15
0.073	0.273	64.102	2.679	4.18
0.072	0.272	65.386	2.758	4.22
0.071	0.271	66.228	2.797	4.22
0.070	0.270	67.136	2.847	4.24
0.070	0.270	68.641	2.96	4.31
0.069	0.269	70.582	3.088	4.37
0.068	0.268	73.204	3.246	4.43
0.068	0.268	76.358	3.46	4.53
0.067	0.267	82.516	3.852	4.67
0.066	0.266	90.086	4.325	4.80
0.066	0.266	96.401	4.728	4.90
0.065	0.265			
0.064	0.264			
0.064	0.264			
0.063	0.263			
0.062	0.262			
0.062	0.262			
0.061	0.261			
0.060	0.260			
0.060	0.260			
0.059	0.259			
0.058	0.258			
0.057	0.257			
0.057	0.257			
0.056	0.256			
0.055	0.255			
0.055	0.255			
0.054	0.254			
0.053	0.253			
0.053	0.253			
0.052	0.252			
0.051	0.251			
0.051	0.251			
0.050	0.250			
0.049	0.249			
0.049	0.249			
0.048	0.248			
0.047	0.247			
0.047	0.247			
0.046	0.246			
0.045	0.245			
0.044	0.244			

Position Data		Experimental Results:		
x (m)	x+Zl (m)	h	Uh	Uh/h (%)
0.044	0.244			
0.043	0.243			
0.042	0.242			
0.042	0.242			
0.041	0.241			
0.040	0.240			
0.040	0.240	Section #1:		
0.039	0.239	95.114	4.359	4.58
0.038	0.238	73.406	3.462	4.72
0.038	0.238	63.163	2.573	4.07
0.037	0.237	60.053	2.387	3.97
0.036	0.236	59.927	2.377	3.97
0.036	0.236	60.118	2.385	3.97
0.035	0.235	60.118	2.387	3.97
0.034	0.234	60.654	2.409	3.97
0.034	0.234	61.155	2.426	3.97
0.033	0.233	62.278	2.493	4.00
0.032	0.232	61.644	2.456	3.98
0.031	0.231	61.85	2.489	4.02
0.031	0.231	62.769	2.503	3.99
0.030	0.230	63.472	2.583	4.07
0.029	0.229	63.702	2.579	4.05
0.029	0.229	64.312	2.609	4.06
0.028	0.228	64.87	2.618	4.04
0.027	0.227	64.881	2.614	4.03
0.027	0.227	65.224	2.649	4.06
0.026	0.226	65.745	2.679	4.08
0.025	0.225	66.784	2.739	4.10
0.025	0.225	67.318	2.764	4.11
0.024	0.224	67.764	2.772	4.09
0.023	0.223	68.804	2.817	4.09
0.023	0.223	69.037	2.861	4.14
0.022	0.222	69.115	2.854	4.13
0.021	0.221	69.93	2.927	4.19
0.021	0.221	70.58	2.924	4.14
0.020	0.220	71.363	2.957	4.14
0.019	0.219	73.298	3.119	4.26
0.018	0.218	74.524	3.16	4.24
0.018	0.218	75.701	3.198	4.22
0.017	0.217	76.503	3.271	4.28
0.016	0.216	78.25	3.374	4.31
0.016	0.216	79.631	3.448	4.33
0.015	0.215	81.034	3.529	4.36
0.014	0.214	83.842	3.711	4.43
0.014	0.214	85.979	3.822	4.45
0.013	0.213	87.806	3.904	4.45
0.012	0.212	90.461	4.067	4.50
0.012	0.212	92.533	4.191	4.53
0.011	0.211	94.374	4.304	4.56
0.010	0.210	96.18	4.418	4.59
0.010	0.210	97.026	4.472	4.61

Position Data		Experimental Results:		
x (m)	x+Zl (m)	h	Uh	Uh/h (%)
0.009	0.209	97.376	4.494	4.62
0.008	0.208	97.312	4.49	4.61
0.008	0.208			
0.007	0.207			
0.006	0.206			
0.005	0.205			
0.005	0.205			
0.004	0.204			
0.003	0.203			
0.003	0.203			
0.002	0.202			
0.001	0.201			
0.001	0.201			
0	0.1	Leading Edge		1693.72
				411.00
			Avg Uh/l	**4.12**

Appendix K: Data for Ribbed Model with Interrupted Heating

10 m/s

Air Properties:			Universal Gas Constant:	2.87E+02
Pressure (mb)	1006.16		T (C)	26.15
Pressure (N/m^2)	100616		T(K)	299.3
density (kg/m3)	1.17E+00		Pr	0.707
viscosity (kg/ms)	1.85E-05		k (W/mK)	2.63E-02
Velocity (m/s)	10		ZI (unheated starting length, m)	0.2

Position Data		Ribbed Results (section 7):			Flat Plate Interrupted		Flat Plate Continuous	
x (m)	x+ZI (m)	h	Uh	Uh/h (%)	h	diff (%)	x	h
0.420	0.520				55.487		0.420	32.81
0.419	0.419	67.266	4.138	6.15	46.148	45.76	0.415	31.21
0.419	0.419	60.425	3.509	5.81	43.967	37.43	0.409	31.15
0.418	0.418	58.47	2.673	4.57	42.917	36.24	0.404	31.49
0.417	0.417	52.165	2.243	4.30	41.148	26.77	0.398	31.57
0.417	0.417	49.981	2.116	4.23	40.92	22.14	0.393	31.75
0.416	0.416	48.303	2.029	4.20	40.556	19.10	0.387	31.78
0.415	0.415	47.129	1.97	4.18	40.421	16.60	0.382	32.32
0.415	0.415	46.311	1.93	4.17	40.317	14.87	0.376	32.46
0.414	0.414	45.655	1.898	4.16	40.179	13.63	0.371	32.44
0.413	0.413	45.403	1.881	4.14	40.57	11.91	0.365	32.51
0.412	0.412	45.414	1.882	4.14	40.609	11.83	0.360	32.54
0.412	0.412	45.371	1.882	4.15	40.403	12.30	0.354	32.73
0.411	0.411	45.375	1.88	4.14	40.833	11.12	0.349	32.96
0.410	0.410	45.738	1.9	4.15	40.885	11.87	0.343	33.04
0.410	0.410	45.87	1.905	4.15	41.048	11.75	0.338	33.2
0.409	0.409	46.005	1.918	4.17	41.25	11.53	0.332	33.37
0.408	0.408	46.215	1.924	4.16	41.507	11.34	0.327	33.46
0.408	0.408	46.436	1.932	4.16	41.625	11.56	0.321	33.55
0.407	0.407	46.61	1.941	4.16	41.769	11.59	0.316	33.73
0.406	0.406	46.871	1.956	4.17	42.028	11.52	0.311	33.84
0.406	0.406	47.017	1.964	4.18	42.272	11.22	0.305	34.05
0.405	0.405	43.732	1.966	4.50	42.498	2.90	0.300	34.1
0.404	0.404	44.187	1.991	4.51	42.589	3.75	0.294	34.37
0.404	0.404	47.87	2.008	4.20	42.751	11.97	0.289	34.41
0.403	0.403	48.136	2.021	4.20	43.185	11.46	0.283	34.69
0.402	0.402	48.356	2.031	4.20	43.351	11.55	0.278	34.86
0.402	0.402	45.014	2.043	4.54	43.51	3.46	0.272	35.09
0.401	0.401	49.047	2.066	4.21	43.77	12.06	0.267	35.24
0.400	0.400	49.312	2.08	4.22	44.034	11.99	0.261	35.49
0.399	0.399	49.492	2.089	4.22	44.323	11.66	0.256	35.54
0.399	0.399	49.869	2.11	4.23	44.522	12.01	0.250	35.18
0.398	0.398	50.232	2.128	4.24	44.97	11.70	0.245	35.32
0.397	0.397	50.421	2.138	4.24	45.222	11.50	0.239	35.8
0.397	0.397	50.672	2.152	4.25	45.374	11.68	0.234	36.04
0.396	0.396	51.045	2.173	4.26	45.645	11.83	0.228	36.13
0.395	0.395	51.198	2.181	4.26	45.975	11.36	0.223	36.45
0.395	0.395	51.712	2.212	4.28	46.187	11.96	0.218	36.84

Position Data		Ribbed Results (section 7):			Flat Plate Interrupted		Flat Plate Continuous	
x (m)	x+Zl (m)	h	Uh	Uh/h (%)	h	diff (%)	x	h
0.394	0.394	52.202	2.237	4.29	46.432	12.43	0.212	37.06
0.393	0.393	52.694	2.269	4.31	46.649	12.96	0.207	37.43
0.393	0.393	53.278	2.304	4.33	47.013	13.33	0.201	37.6
0.392	0.392	53.958	2.342	4.34	47.334	13.99	0.196	38.16
0.391	0.391	54.74	2.389	4.36	47.864	14.37	0.190	39.07
0.391	0.391	55.549	2.438	4.39	48.252	15.12	0.185	39.67
0.390	0.390	56.754	2.509	4.42	48.812	16.27	0.179	40.1
0.389	0.389	57.994	2.586	4.46	49.688	16.72	0.174	40.28
0.389	0.389	59.028	2.649	4.49	50.394	17.13	0.168	40.68
0.388	0.388	60.511	2.738	4.53	51.525	17.44	0.163	40.66
0.387	0.387	62.262	2.851	4.58	52.887	17.73	0.157	40.58
0.386	0.386	63.744	2.949	4.63	54.431	17.11	0.152	41.01
0.386	0.386	65.315	3.057	4.68	55.94	16.76	0.146	40.79
0.385	0.385	67.165	3.187	4.75	57.808	16.19	0.141	40.84
0.384	0.384	69.448	3.337	4.80	60.635	14.53	0.135	41.37
0.384	0.384	73.398	3.635	4.95	67.064	9.44	0.130	41.51
0.383	0.383	84.436	4.509	5.34	93.271	-9.47	0.124	42.37
0.382	0.382	87.347	4.826	5.53			0.119	42.76
0.382	0.382						0.114	43.45
0.381	0.381						0.108	43.31
0.380	0.380						0.103	43.92
0.380	0.380						0.097	44.28
0.379	0.379						0.092	44.76
0.378	0.378						0.086	45.34
0.378	0.378						0.081	46.12
0.377	0.377						0.075	46.86
0.376	0.376						0.070	47.62
0.376	0.376						0.064	48.03
0.375	0.375						0.059	49.74
0.374	0.374						0.053	50.7
0.373	0.373						0.048	52.52
0.373	0.373						0.042	54.86
0.372	0.372						0.037	58.21
0.371	0.371						0.031	63.46
0.371	0.371						0.026	70.81
0.370	0.370						0.021	74.69
0.369	0.369							
0.369	0.369							
0.368	0.368							
0.367	0.367							
0.367	0.367							
0.366	0.366							
0.365	0.365							
0.365	0.365							
0.364	0.364							
0.363	0.363					95.423		
0.363	0.363					94.207		
0.362	0.362					90.847		
0.361	0.361					84.956		
0.360	0.360					79.275		

Position Data		Ribbed Results (section 5):			Flat Plate Interrupted	
x (m)	x+Zl (m)	h	Uh	Uh/h (%)	h	diff (%)
0.257	0.257	75.69	3.347	4.42	66.139	14.44
0.257	0.257	83.866	3.915	4.67	76.353	9.84
0.256	0.256	97.851	4.9	5.01	95.536	2.42
0.255	0.255	106.637	5.501	5.16		
0.254	0.254					
0.254	0.254					
0.253	0.253					
0.252	0.252					
0.252	0.252					
0.251	0.251					
0.250	0.250					
0.250	0.250					
0.249	0.249					
0.248	0.248					
0.248	0.248					
0.247	0.247					
0.246	0.246					
0.246	0.246					
0.245	0.245					
0.244	0.244					
0.244	0.244					
0.243	0.243					
0.242	0.242					
0.241	0.241					
0.241	0.241					
0.240	0.240					
0.239	0.239					
0.239	0.239					
0.238	0.238					
0.237	0.237					
0.237	0.237					
0.236	0.236					
0.235	0.235					
0.235	0.235				94.493	
0.234	0.234				94.596	
0.233	0.233				86.817	
0.233	0.233				75.746	
0.232	0.232				66.812	
0.231	0.231	(section 4):			68.689	
0.231	0.231				72.254	
0.230	0.230	62.771	2.736	4.36	50.163	25.13
0.229	0.229	58.675	2.481	4.23	46.623	25.85
0.228	0.228	53.993	2.21	4.09	46.182	16.91
0.228	0.228	52.257	2.118	4.05	45.881	13.90
0.227	0.227	51.249	2.064	4.03	46.004	11.40
0.226	0.226	50.63	2.034	4.02	45.962	10.16
0.226	0.226	50.486	2.026	4.01	45.989	9.78
0.225	0.225	50.115	2.008	4.01	46.089	8.74
0.224	0.224	49.995	2.003	4.01	46.167	8.29
0.224	0.224	50.256	2.015	4.01	46.388	8.34

Position Data		Ribbed Results (section 5):			Flat Plate Interrupted	
x (m)	x+Zl (m)	h	Uh	Uh/h (%)	h	diff (%)
0.291	0.291	56.629	2.267	4.00	41.896	35.17
0.291	0.291	52.388	2.042	3.90	41.068	27.56
0.290	0.290	50.309	1.947	3.87	40.894	23.02
0.289	0.289	48.517	1.871	3.86	41.06	18.16
0.289	0.289	47.274	1.814	3.84	41.219	14.69
0.288	0.288	46.399	1.782	3.84	41.119	12.84
0.287	0.287	45.853	1.756	3.83	41.23	11.21
0.287	0.287	45.829	1.752	3.82	41.419	10.65
0.286	0.286	45.792	1.748	3.82	41.478	10.40
0.285	0.285	45.547	1.741	3.82	41.545	9.63
0.285	0.285	45.76	1.749	3.82	41.605	9.99
0.284	0.284	45.728	1.748	3.82	41.959	8.98
0.283	0.283	45.949	1.761	3.83	41.918	9.62
0.283	0.283	46.194	1.77	3.83	42.082	9.77
0.282	0.282	46.555	1.786	3.84	42.229	10.24
0.281	0.281	46.766	1.791	3.83	42.518	9.99
0.280	0.280	47.055	1.808	3.84	42.709	10.18
0.280	0.280	47.359	1.823	3.85	42.898	10.40
0.279	0.279	47.639	1.832	3.85	43.183	10.32
0.278	0.278	47.833	1.842	3.85	43.334	10.38
0.278	0.278	48.129	1.853	3.85	43.544	10.53
0.277	0.277	48.438	1.865	3.85	43.768	10.67
0.276	0.276	48.813	1.88	3.85	44.085	10.72
0.276	0.276	49.193	1.898	3.86	44.322	10.99
0.275	0.275	49.416	1.909	3.86	44.718	10.51
0.274	0.274	49.599	1.916	3.86	44.911	10.44
0.274	0.274	50.015	1.935	3.87	45.019	11.10
0.273	0.273	50.246	1.945	3.87	45.08	11.46
0.272	0.272	50.522	1.955	3.87	45.435	11.20
0.272	0.272	50.852	1.97	3.88	45.736	11.19
0.271	0.271	51.193	1.987	3.88	46.089	11.07
0.270	0.270	51.475	1.998	3.88	46.522	10.65
0.270	0.270	51.835	2.016	3.89	46.714	10.96
0.269	0.269	52.197	2.034	3.90	46.998	11.06
0.268	0.268	52.697	2.06	3.91	47.458	11.04
0.267	0.267	52.94	2.071	3.91	47.691	11.01
0.267	0.267	53.365	2.091	3.92	47.957	11.28
0.266	0.266	54.065	2.128	3.94	48.386	11.74
0.265	0.265	54.93	2.172	3.95	48.915	12.30
0.265	0.265	55.677	2.209	3.97	49.332	12.86
0.264	0.264	56.297	2.243	3.98	49.978	12.64
0.263	0.263	57.438	2.301	4.01	50.819	13.02
0.263	0.263	58.303	2.35	4.03	51.475	13.26
0.262	0.262	59.376	2.401	4.04	52.429	13.25
0.261	0.261	61.058	2.486	4.07	53.868	13.35
0.261	0.261	62.135	2.539	4.09	55.484	11.99
0.260	0.260	63.765	2.627	4.12	56.537	12.78
0.259	0.259	65.508	2.731	4.17	58.053	12.84
0.259	0.259	67.661	2.858	4.22	60.45	11.93
0.258	0.258	70.887	3.049	4.30	62.289	13.80

Position Data		Ribbed Results (section 6):			Flat Plate Interrupted	
x (m)	x+Zl (m)	h	Uh	Uh/h (%)	h	diff (%)
0.326	0.326	58.379	2.342	4.01	50.517	15.56
0.325	0.325	59.983	2.437	4.06	51.836	15.72
0.324	0.324	61.403	2.514	4.09	53.098	15.64
0.324	0.324	63.245	2.612	4.13	54.386	16.29
0.323	0.323	65.154	2.715	4.17	56.321	15.68
0.322	0.322	67.254	2.827	4.20	57.883	16.19
0.321	0.321	69.447	2.947	4.24	59.968	15.81
0.321	0.321	72.75	3.157	4.34	62.492	16.41
0.320	0.320	79.066	3.572	4.52	69.06	14.49
0.319	0.319	95.215	4.67	4.90	94.071	1.22
0.319	0.319	105.86	5.437	5.14		
0.318	0.318					
0.317	0.317					
0.317	0.317					
0.316	0.316					
0.315	0.315					
0.315	0.315					
0.314	0.314					
0.313	0.313					
0.313	0.313					
0.312	0.312					
0.311	0.311					
0.311	0.311					
0.310	0.310					
0.309	0.309					
0.309	0.309					
0.308	0.308					
0.307	0.307					
0.306	0.306					
0.306	0.306					
0.305	0.305					
0.304	0.304					
0.304	0.304					
0.303	0.303					
0.302	0.302					
0.302	0.302					
0.301	0.301					
0.300	0.300					
0.300	0.300					
0.299	0.299				95.348	
0.298	0.298				93.25	
0.298	0.298				87.997	
0.297	0.297				81.063	
0.296	0.296				73.69	
0.296	0.296				67.189	
0.295	0.295				62.759	
0.294	0.294	(section 5):			70.595	
0.293	0.293				70.349	
0.293	0.293	52.051	2.126	4.08	46.547	11.82
0.292	0.292	61.975	2.645	4.27	42.894	44.48

Position Data		Ribbed Results (section 6):			Flat Plate Interrupted	
x (m)	x+Zl (m)	h	Uh	Uh/h (%)	h	diff (%)
0.360	0.360				73.895	
0.359	0.359				67.843	
0.358	0.358				63.305	
0.358	0.358				67.126	
0.357	0.357				71.588	
0.356	0.356	54.143	2.227	4.11	48.694	11.19
0.356	0.356	60.616	2.574	4.25	43.792	38.42
0.355	0.355	52.998	2.081	3.93	41.702	27.09
0.354	0.354	49.987	1.936	3.87	40.825	22.44
0.354	0.354	47.733	1.84	3.85	40.424	18.08
0.353	0.353	45.99	1.762	3.83	40.371	13.92
0.352	0.352	45.057	1.716	3.81	40.418	11.48
0.352	0.352	44.416	1.687	3.80	40.622	9.34
0.351	0.351	44.148	1.684	3.81	40.627	8.67
0.350	0.350	43.952	1.672	3.81	40.619	8.21
0.350	0.350	43.88	1.669	3.80	40.637	7.98
0.349	0.349	44.009	1.673	3.80	41.128	7.00
0.348	0.348	44.212	1.684	3.81	41.266	7.14
0.347	0.347	44.313	1.686	3.80	41.097	7.83
0.347	0.347	44.664	1.701	3.81	41.444	7.77
0.346	0.346	44.851	1.71	3.81	41.723	7.50
0.345	0.345	45.148	1.725	3.82	41.753	8.13
0.345	0.345	45.256	1.728	3.82	41.837	8.17
0.344	0.344	45.581	1.742	3.82	42.053	8.39
0.343	0.343	45.809	1.75	3.82	42.074	8.88
0.343	0.343	46.073	1.765	3.83	42.184	9.22
0.342	0.342	46.333	1.778	3.84	42.429	9.20
0.341	0.341	46.579	1.782	3.83	42.734	9.00
0.341	0.341	46.932	1.797	3.83	42.785	9.69
0.340	0.340	47.188	1.811	3.84	43.078	9.54
0.339	0.339	47.443	1.818	3.83	43.245	9.71
0.339	0.339	47.761	1.836	3.84	43.58	9.59
0.338	0.338	48.015	1.844	3.84	43.969	9.20
0.337	0.337	48.347	1.86	3.85	44.199	9.38
0.337	0.337	48.695	1.875	3.85	44.552	9.30
0.336	0.336	48.871	1.882	3.85	44.588	9.61
0.335	0.335	49.298	1.903	3.86	44.699	10.29
0.334	0.334	49.814	1.924	3.86	45.06	10.55
0.334	0.334	50.159	1.94	3.87	45.391	10.50
0.333	0.333	50.558	1.956	3.87	45.754	10.50
0.332	0.332	50.948	1.973	3.87	45.897	11.01
0.332	0.332	51.195	1.984	3.88	46.273	10.64
0.331	0.331	51.716	2.009	3.88	46.54	11.12
0.330	0.330	52.23	2.034	3.90	46.991	11.15
0.330	0.330	52.696	2.056	3.90	47.278	11.46
0.329	0.329	53.381	2.092	3.92	47.585	12.18
0.328	0.328	54.023	2.127	3.94	48.115	12.28
0.328	0.328	54.755	2.159	3.94	48.662	12.52
0.327	0.327	55.742	2.214	3.97	49.18	13.34
0.326	0.326	57.08	2.28	3.99	49.837	14.53

Position Data		Ribbed Results (section 4):			Flat Plate Interrupted	
x (m)	x+Zl (m)	h	Uh	Uh/h (%)	h	diff (%)
0.223	0.223	50.342	2.018	4.01	46.451	8.38
0.222	0.222	50.373	2.02	4.01	46.477	8.38
0.222	0.222	50.408	2.02	4.01	46.53	8.33
0.221	0.221	50.625	2.031	4.01	46.69	8.43
0.220	0.220	50.836	2.044	4.02	46.673	8.92
0.220	0.220	50.868	2.043	4.02	46.784	8.73
0.219	0.219	51.086	2.055	4.02	46.954	8.80
0.218	0.218	51.415	2.073	4.03	47.141	9.07
0.218	0.218	51.376	2.068	4.03	47.137	8.99
0.217	0.217	51.589	2.079	4.03	47.274	9.13
0.216	0.216	51.749	2.088	4.04	47.46	9.04
0.215	0.215	51.839	2.093	4.04	47.608	8.89
0.215	0.215	52.1	2.105	4.04	47.68	9.27
0.214	0.214	52.304	2.117	4.05	47.77	9.49
0.213	0.213	52.666	2.136	4.06	47.973	9.78
0.213	0.213	52.957	2.15	4.06	48.208	9.85
0.212	0.212	53.13	2.161	4.07	48.417	9.73
0.211	0.211	53.574	2.183	4.08	48.585	10.27
0.211	0.211	53.755	2.193	4.08	48.655	10.48
0.210	0.210	54.001	2.21	4.09	48.931	10.36
0.209	0.209	54.559	2.236	4.10	48.996	11.35
0.209	0.209	55.134	2.268	4.11	49.264	11.92
0.208	0.208	55.593	2.295	4.13	49.747	11.75
0.207	0.207	56.096	2.318	4.13	50.103	11.96
0.207	0.207	56.712	2.352	4.15	50.321	12.70
0.206	0.206	57.372	2.394	4.17	50.586	13.41
0.205	0.205	58.076	2.426	4.18	51.014	13.84
0.205	0.205	59.319	2.496	4.21	51.504	15.17
0.204	0.204	60.086	2.536	4.22	52.307	14.87
0.203	0.203	61.072	2.596	4.25	52.72	15.84
0.202	0.202	61.995	2.643	4.26	53.179	16.58
0.202	0.202	63.126	2.718	4.31	54.026	16.84
0.201	0.201	64.284	2.791	4.34	54.595	17.75
0.200	0.200	65.264	2.844	4.36	55.532	17.53
0.200	0.200	67.324	2.969	4.41	56.408	19.35
0.199	0.199	69.057	3.085	4.47	56.934	21.29
0.198	0.198	70.745	3.172	4.48	57.94	22.10
0.198	0.198	73.464	3.36	4.57	59.188	24.12
0.197	0.197	77.103	3.606	4.68	60.445	27.56
0.196	0.196	81.343	3.905	4.80	61.614	32.02
0.196	0.196	87.468	4.344	4.97	63.502	37.74
0.195	0.195	94.714	4.907	5.18	65.796	43.95
0.194	0.194	102.171	5.514	5.40	69.452	47.11
0.194	0.194	106.547	5.882	5.52	77.327	37.79
0.193	0.193				90.915	
0.192	0.192					
0.192	0.192					
0.191	0.191					
0.190	0.190					
0.189	0.189					

Position Data		Ribbed Results (section 2):			Flat Plate Interrupted	
x (m)	x+Zl (m)	h	Uh	Uh/h (%)	h	diff (%)
0.120	0.120					
0.120	0.120					
0.119	0.119					
0.118	0.118					
0.118	0.118					
0.117	0.117					
0.116	0.116					
0.116	0.116					
0.115	0.115					
0.114	0.114					
0.114	0.114					
0.113	0.113					
0.112	0.112					
0.111	0.111					
0.111	0.111					
0.110	0.110					
0.109	0.109					
0.109	0.109					
0.108	0.108					
0.107	0.107					
0.107	0.107					
0.106	0.106					
0.105	0.105				96.603	
0.105	0.105				89.775	
0.104	0.104				76.093	
0.103	0.103				82.36	
0.103	0.103	53.97	2.107	3.90	73.022	-26.09
0.102	0.102	60.239	2.425	4.03	51.32	17.38
0.101	0.101	56.379	2.228	3.95	48.887	15.33
0.101	0.101	54.138	2.112	3.90	48.667	11.24
0.100	0.100	52.949	2.054	3.88	48.658	8.82
0.099	0.099	52.19	2.017	3.86	48.761	7.03
0.099	0.099	52.049	2.01	3.86	48.665	6.95
0.098	0.098	51.783	1.998	3.86	48.99	5.70
0.097	0.097	51.8	1.999	3.86	49.108	5.48
0.096	0.096	51.845	2.002	3.86	49.52	4.70
0.096	0.096	51.989	2.006	3.86	49.492	5.05
0.095	0.095	52.003	2.008	3.86	49.464	5.13
0.094	0.094	52.09	2.01	3.86	49.705	4.80
0.094	0.094	52.424	2.026	3.86	49.852	5.16
0.093	0.093	52.852	2.049	3.88	50.078	5.54
0.092	0.092	52.867	2.055	3.89	50.459	4.77
0.092	0.092	53.09	2.063	3.89	50.311	5.52
0.091	0.091	53.216	2.067	3.88	50.523	5.33
0.090	0.090	53.504	2.08	3.89	50.664	5.61
0.090	0.090	53.772	2.094	3.89	50.977	5.48
0.089	0.089	54.101	2.109	3.90	51.392	5.27
0.088	0.088	54.397	2.124	3.91	51.705	5.21
0.088	0.088	54.783	2.144	3.91	51.791	5.78
0.087	0.087	55.258	2.173	3.93	51.926	6.42

Position Data		Ribbed Results (section 3):			Flat Plate Interrupted	
x (m)	x+Zl (m)	h	Uh	Uh/h (%)	h	diff (%)
0.155	0.155	51.15	1.93	3.77	47.6	7.46
0.154	0.154	51.327	1.939	3.78	47.677	7.66
0.153	0.153	51.662	1.953	3.78	47.771	8.15
0.153	0.153	51.886	1.963	3.78	47.953	8.20
0.152	0.152	52.098	1.974	3.79	48.233	8.01
0.151	0.151	52.313	1.984	3.79	48.336	8.23
0.150	0.150	52.488	1.992	3.80	48.398	8.45
0.150	0.150	52.637	1.999	3.80	48.555	8.41
0.149	0.149	53.111	2.021	3.81	48.836	8.75
0.148	0.148	53.474	2.036	3.81	48.794	9.59
0.148	0.148	53.896	2.058	3.82	48.984	10.03
0.147	0.147	54.343	2.078	3.82	49.36	10.10
0.146	0.146	54.638	2.094	3.83	49.626	10.10
0.146	0.146	54.942	2.104	3.83	49.714	10.52
0.145	0.145	55.701	2.144	3.85	50.012	11.38
0.144	0.144	56.177	2.169	3.86	50.521	11.20
0.144	0.144	56.365	2.179	3.87	50.566	11.47
0.143	0.143	57.097	2.206	3.86	50.85	12.29
0.142	0.142	57.995	2.258	3.89	51.143	13.40
0.142	0.142	58.788	2.291	3.90	51.951	13.16
0.141	0.141	59.543	2.33	3.91	52.483	13.45
0.140	0.140	60.485	2.373	3.92	52.778	14.60
0.140	0.140	61.54	2.426	3.94	53.565	14.89
0.139	0.139	62.616	2.483	3.97	54.261	15.40
0.138	0.138	63.348	2.513	3.97	54.979	15.22
0.137	0.137	64.893	2.594	4.00	55.939	16.01
0.137	0.137	66.079	2.668	4.04	56.943	16.04
0.136	0.136	67.528	2.738	4.05	57.833	16.76
0.135	0.135	69.229	2.837	4.10	58.821	17.69
0.135	0.135	70.568	2.897	4.11	60.215	17.19
0.134	0.134	72.67	3.013	4.15	61.506	18.15
0.133	0.133	76.312	3.219	4.22	63.095	20.95
0.133	0.133	80.486	3.492	4.34	64.658	24.48
0.132	0.132	86.214	3.83	4.44	66.708	29.24
0.131	0.131	93.839	4.318	4.60	69.867	34.31
0.131	0.131	101.831	4.867	4.78	74.792	36.15
0.130	0.130	106.665	5.215	4.89	84.611	26.07
0.129	0.129				95.582	
0.129	0.129					
0.128	0.128					
0.127	0.127					
0.127	0.127					
0.126	0.126					
0.125	0.125					
0.124	0.124					
0.124	0.124					
0.123	0.123					
0.122	0.122					
0.122	0.122					
0.121	0.121					

Position Data		Ribbed Results (section 3):			Flat Plate Interrupted	
x (m)	x+Zl (m)	h	Uh	Uh/h (%)	h	diff (%)
0.189	0.189					
0.188	0.188					
0.187	0.187					
0.187	0.187					
0.186	0.186					
0.185	0.185					
0.185	0.185					
0.184	0.184					
0.183	0.183					
0.183	0.183					
0.182	0.182					
0.181	0.181					
0.181	0.181					
0.180	0.180					
0.179	0.179					
0.179	0.179					
0.178	0.178					
0.177	0.177					
0.176	0.176					
0.176	0.176					
0.175	0.175					
0.174	0.174					
0.174	0.174					
0.173	0.173					
0.172	0.172					
0.172	0.172					
0.171	0.171					
0.170	0.170					
0.170	0.170				95.517	
0.169	0.169				88.34	
0.168	0.168				76.161	
0.168	0.168				67.519	
0.167	0.167				72.765	
0.166	0.166	58.475	2.284	3.91	71.659	-18.40
0.166	0.166	59.681	2.348	3.93	48.453	23.17
0.165	0.165	54.772	2.102	3.84	47.019	16.49
0.164	0.164	52.837	2.01	3.80	46.497	13.64
0.163	0.163	51.751	1.959	3.79	46.486	11.33
0.163	0.163	51.158	1.932	3.78	46.74	9.45
0.162	0.162	50.687	1.911	3.77	46.712	8.51
0.161	0.161	50.506	1.902	3.77	46.801	7.92
0.161	0.161	50.357	1.896	3.77	47.003	7.14
0.160	0.160	50.378	1.898	3.77	46.917	7.38
0.159	0.159	50.312	1.895	3.77	47.075	6.88
0.159	0.159	50.337	1.895	3.77	47.136	6.79
0.158	0.158	50.425	1.9	3.77	47.301	6.60
0.157	0.157	50.61	1.908	3.77	47.316	6.96
0.157	0.157	50.851	1.918	3.77	47.43	7.21
0.156	0.156	50.817	1.916	3.77	47.647	6.65
0.155	0.155	50.894	1.921	3.78	47.65	6.81

Position Data		Ribbed Results (section 2):			Flat Plate Interrupted	
x (m)	x+Zl (m)	h	Uh	Uh/h (%)	h	diff (%)
0.086	0.086	55.426	2.176	3.93	51.998	6.59
0.086	0.086	55.804	2.191	3.93	52.327	6.64
0.085	0.085	56.404	2.225	3.95	52.873	6.68
0.084	0.084	56.639	2.246	3.97	53.174	6.52
0.083	0.083	57.333	2.273	3.97	53.434	7.30
0.083	0.083	58.04	2.304	3.97	53.928	7.62
0.082	0.082	58.458	2.33	3.99	54.848	6.58
0.081	0.081	58.828	2.35	4.00	54.737	7.47
0.081	0.081	59.563	2.389	4.01	54.784	8.72
0.080	0.080	60.24	2.419	4.02	55.235	9.06
0.079	0.079	61.155	2.475	4.05	55.986	9.23
0.079	0.079	61.607	2.486	4.04	56.64	8.77
0.078	0.078	62.13	2.526	4.07	57.395	8.25
0.077	0.077	63.349	2.584	4.08	58.341	8.58
0.077	0.077	64.43	2.637	4.09	58.892	9.40
0.076	0.076	65.477	2.695	4.12	59.369	10.29
0.075	0.075	66.624	2.78	4.17	60.021	11.00
0.075	0.075	68.001	2.839	4.18	60.832	11.78
0.074	0.074	69.359	2.916	4.20	61.845	12.15
0.073	0.073	70.708	2.992	4.23	62.823	12.55
0.073	0.073	72.79	3.112	4.28	64.102	13.55
0.072	0.072	75.306	3.266	4.34	65.386	15.17
0.071	0.071	78.571	3.464	4.41	66.228	18.64
0.070	0.070	83.186	3.774	4.54	67.136	23.91
0.070	0.070	88.515	4.102	4.64	68.641	28.95
0.069	0.069	95.121	4.555	4.79	70.582	34.77
0.068	0.068	102.573	5.101	4.97	73.204	40.12
0.068	0.068	106.976	5.436	5.08	76.358	40.10
0.067	0.067	108.962	5.6	5.14	82.516	32.05
0.066	0.066				90.086	
0.066	0.066				96.401	
0.065	0.065					
0.064	0.064					
0.064	0.064					
0.063	0.063					
0.062	0.062					
0.062	0.062					
0.061	0.061					
0.060	0.060					
0.060	0.060					
0.059	0.059					
0.058	0.058					
0.057	0.057					
0.057	0.057					
0.056	0.056					
0.055	0.055					
0.055	0.055					
0.054	0.054					
0.053	0.053					
0.053	0.053					

Position Data		Ribbed Results (section 1):			Flat Plate Interrupted	
x (m)	x+Zl (m)	h	Uh	Uh/h (%)	h	diff (%)
0.052	0.052					
0.051	0.051					
0.051	0.051					
0.050	0.050					
0.049	0.049					
0.049	0.049					
0.048	0.048					
0.047	0.047					
0.047	0.047					
0.046	0.046					
0.045	0.045					
0.044	0.044					
0.044	0.044					
0.043	0.043					
0.042	0.042					
0.042	0.042					
0.041	0.041					
0.040	0.040					
0.040	0.040					
0.039	0.039				95.114	
0.038	0.038	58.448	2.821	4.83	73.406	-20.38
0.038	0.038	88.043	4.253	4.83	63.163	39.39
0.037	0.037	68.941	3.283	4.76	60.053	14.80
0.036	0.036	54.279	2.049	3.77	59.927	-9.42
0.036	0.036	53.346	2.002	3.75	60.118	-11.26
0.035	0.035	52.45	1.96	3.74	60.118	-12.75
0.034	0.034	52.117	1.943	3.73	60.654	-14.07
0.034	0.034	52.109	1.944	3.73	61.155	-14.79
0.033	0.033	52.15	1.947	3.73	62.278	-16.26
0.032	0.032	52.611	1.968	3.74	61.644	-14.65
0.031	0.031	52.685	1.971	3.74	61.85	-14.82
0.031	0.031	52.848	1.979	3.75	62.769	-15.81
0.030	0.030	52.881	1.982	3.75	63.472	-16.69
0.029	0.029	53.064	1.987	3.74	63.702	-16.70
0.029	0.029	53.185	1.998	3.76	64.312	-17.30
0.028	0.028	53.34	2.005	3.76	64.87	-17.77
0.027	0.027	53.524	2.013	3.76	64.881	-17.50
0.027	0.027	53.7	2.017	3.76	65.224	-17.67
0.026	0.026	53.838	2.029	3.77	65.745	-18.11
0.025	0.025	54.428	2.05	3.77	66.784	-18.50
0.025	0.025	54.801	2.067	3.77	67.318	-18.59
0.024	0.024	54.855	2.082	3.80	67.764	-19.05
0.023	0.023	55.017	2.085	3.79	68.804	-20.04
0.023	0.023	55.395	2.098	3.79	69.037	-19.76
0.022	0.022	55.636	2.11	3.79	69.115	-19.50
0.021	0.021	56.177	2.132	3.80	69.93	-19.67
0.021	0.021	56.226	2.144	3.81	70.58	-20.34
0.020	0.020	57.113	2.182	3.82	71.363	-19.97
0.019	0.019	57.599	2.197	3.81	73.298	-21.42
0.018	0.018	57.846	2.223	3.84	74.524	-22.38

Position Data		Ribbed Results (section 1):			Flat Plate Interrupted	
x (m)	x+Zl (m)	h	Uh	Uh/h (%)	h	diff (%)
0.018	0.018	58.432	2.265	3.88	75.701	-22.81
0.017	0.017	59.116	2.302	3.89	76.503	-22.73
0.016	0.016	59.968	2.328	3.88	78.25	-23.36
0.016	0.016	60.59	2.359	3.89	79.631	-23.91
0.015	0.015	60.918	2.362	3.88	81.034	-24.82
0.014	0.014	61.785	2.421	3.92	83.842	-26.31
0.014	0.014	62.626	2.455	3.92	85.979	-27.16
0.013	0.013	63.012	2.474	3.93	87.806	-28.24
0.012	0.012	63.624	2.509	3.94	90.461	-29.67
0.012	0.012	64.855	2.569	3.96	92.533	-29.91
0.011	0.011	65.859	2.612	3.97	94.374	-30.21
0.010	0.010	67.348	2.704	4.02	96.18	-29.98
0.010	0.010	68.697	2.776	4.04	97.026	-29.20
0.009	0.009	69.582	2.809	4.04	97.376	-28.54
0.008	0.008	71.397	2.897	4.06	97.312	-26.63
0.008	0.008	73.354	3.024	4.12		
0.007	0.007	76.177	3.183	4.18		
0.006	0.006	78.712	3.332	4.23		
0.005	0.005	83.388	3.617	4.34		
0.005	0.005	89.506	3.993	4.46		
0.004	0.004	96.014	4.413	4.60		
0.003	0.003	103.971	4.921	4.73		
0.003	0.003	108.717	5.201	4.78		
0.002	0.002					
0.001	0.001					
0.001	0.001					

		1557.25		
		381.00	Average	
	Avg Uh/	4.09	Incr. (%)	12.92

APPENDIX L: Equipment Inventory

Power Supply:

      HP 6286A DC Power Supply
      Fluke 45 Dual Display Multimeter
      1.5m X 16 guage power lead wires (2)
      Powerstat 120V AC Variac

Lighting:

      GE Cool White Fluorescent Tube, 20 Watt, T12-0.61 m (2)
      Spectrum 574 UV sleeve filters (2)

Model Fabrication:

      Dow Blue Stryrofoam, ¾" and 1.5" thick (19 mm, 38 mm)
      Elmer's Stix-All cement
      Courtalds Gold Film
      3M Super-77 Spray Adhesive
      Printmasters Speedball Soft Rubber No. 66 Brayer Roller
      MasterFoil Plus Copper Tape, 6.35mm x 33m (1/4" x 36 yds)
      Hallcrest BBG-1 Black Paint
      ProArt Liquid Tempera Paint
      Badger 150M Airbrush
      Hallcrest BM/R30C10W/C17-10 Liquid Crystal

Temperature Acquisition:

      Gateway 2000 P5-90 PC running Labview V4.1
      HP 3455A DVM
      Thermistor

Data Acquisition/Reduction:

      Macbeth ColorChecker
      Sony 3-chip XC-003 CCD camera
      Matrox Meteor RGB Framegrabber
      Micron 166 MHz PC (128 MB RAM)
      Matlab 5.1 with Image Processing Toolbox
      Microsoft Excel

Wind Tunnel:

      Aerolab Educational Wind Tunnel, 12" x 12" test section
      Epic (Wilh. Lambrecht KG Gottingen) Inclined Manometer, 0.834 specific gravity red oil

Miscellaneous:

      X-Acto Knives
      Carpenter's Square
      Breathing Apparatus with charcoal filters
      Black 20 oz. "duck" fabric
      Vanguard Professional Series Camera Tripod

Appendix M: Heat Transfer Picture Gallery Submission

HEAT TRANSFER DISTRIBUTION ON FLAT AND RIBBED SURFACES WITH AN INTERRUPTED THERMAL BOUNDARY CONDITION

J. D. Wolf* and J. W. Baughn
University of California, Davis
Department of Mechanical and Aeronautical Engineering
One Shields Avenue, Davis CA 95616

These photographs show the surface temperature distribution on both flat and ribbed surfaces with interrupted heating. The photographs are of Thermochromic Liquid Crystals (TLC's) on the wall of a wind tunnel. The wall is made of Styrofoam and is covered with a polyester sheet of gold-coated film used for electric heating. The surfaces are airbrushed with a TLC that has a red start temperature of 30°C, with a 10°C range. The liquid crystal images are captured using an RGB camera, and converted into hue, then into temperature distributions. The gold film is electrically heated as shown to produce the interrupted thermal boundary condition. Regions of low temperature represent high heat transfer coefficients, whereas regions of high temperature represent low heat transfer coefficients.

The photos demonstrate the high heat transfer at the leading edge of each heating length and the effect of the cavities on the ribbed surface heat transfer. An example of this type of thermal boundary condition is surface-mounted modules in electronic packaging.

*address after 12/98:
USAF Academy, Department of Aeronautics
2410 Faculty Drive, USAFA, CO 80840

Surface Temperature

36
35
34
33
32
31
30

V=10 m/s

RGB Image

Flat Plate Interrupted Heating
Styrofoam with electrically heated film as shown

25mm

38mm

Surface Temperature

V=10 m/s

RGB Image

36 35 34 33 32 31 30

38mm 25mm **Ribbed Model** 19mm

Styrofoam with electrically heated film on top surface of ribs
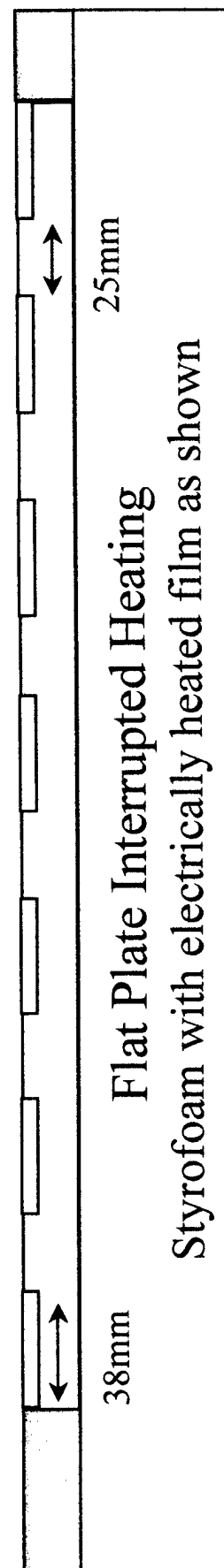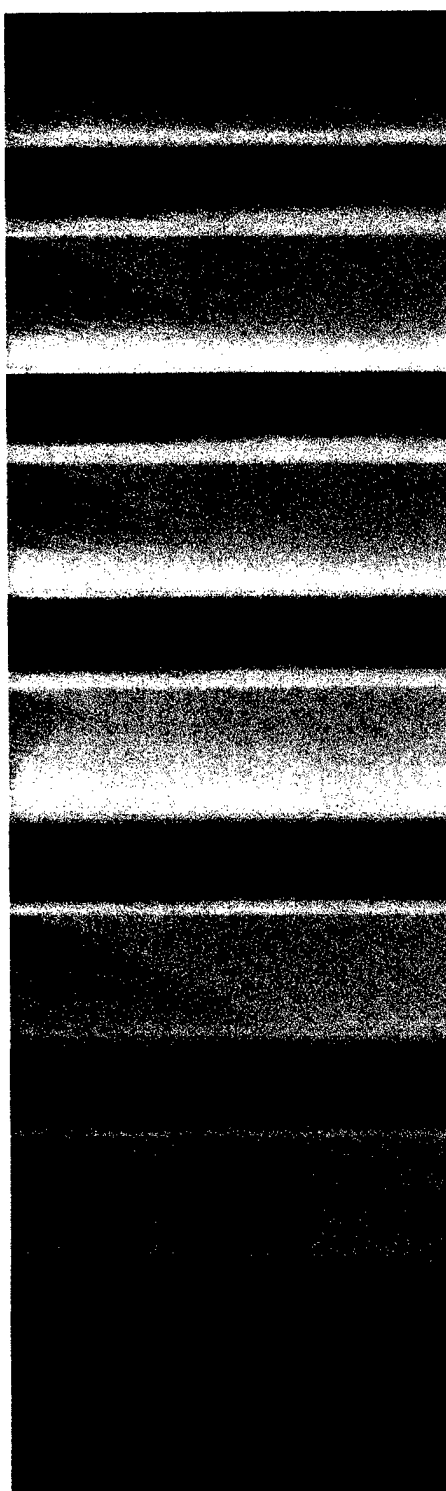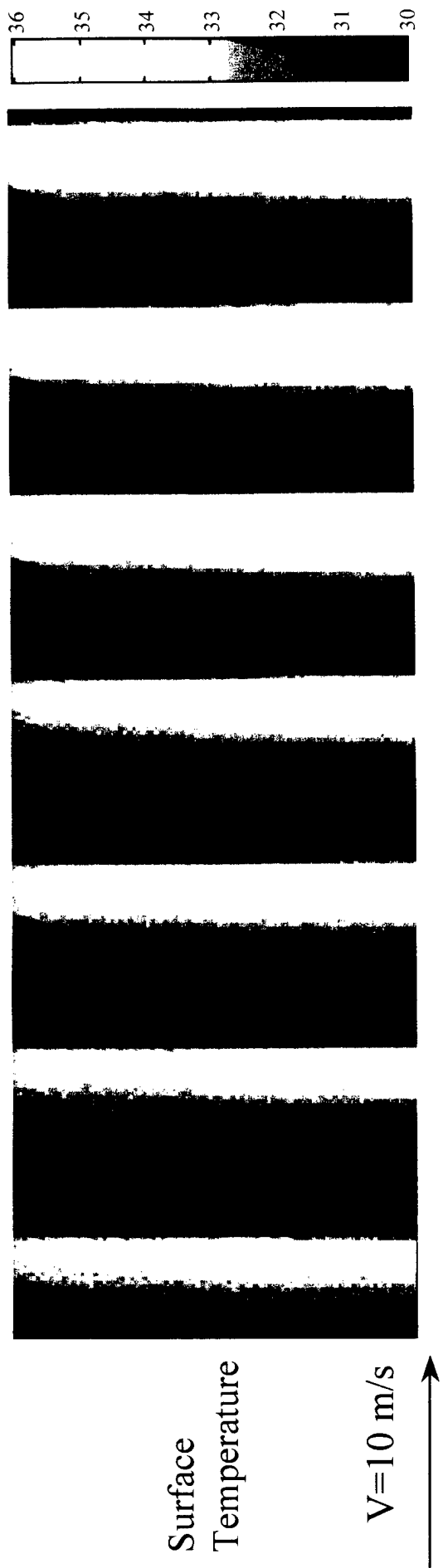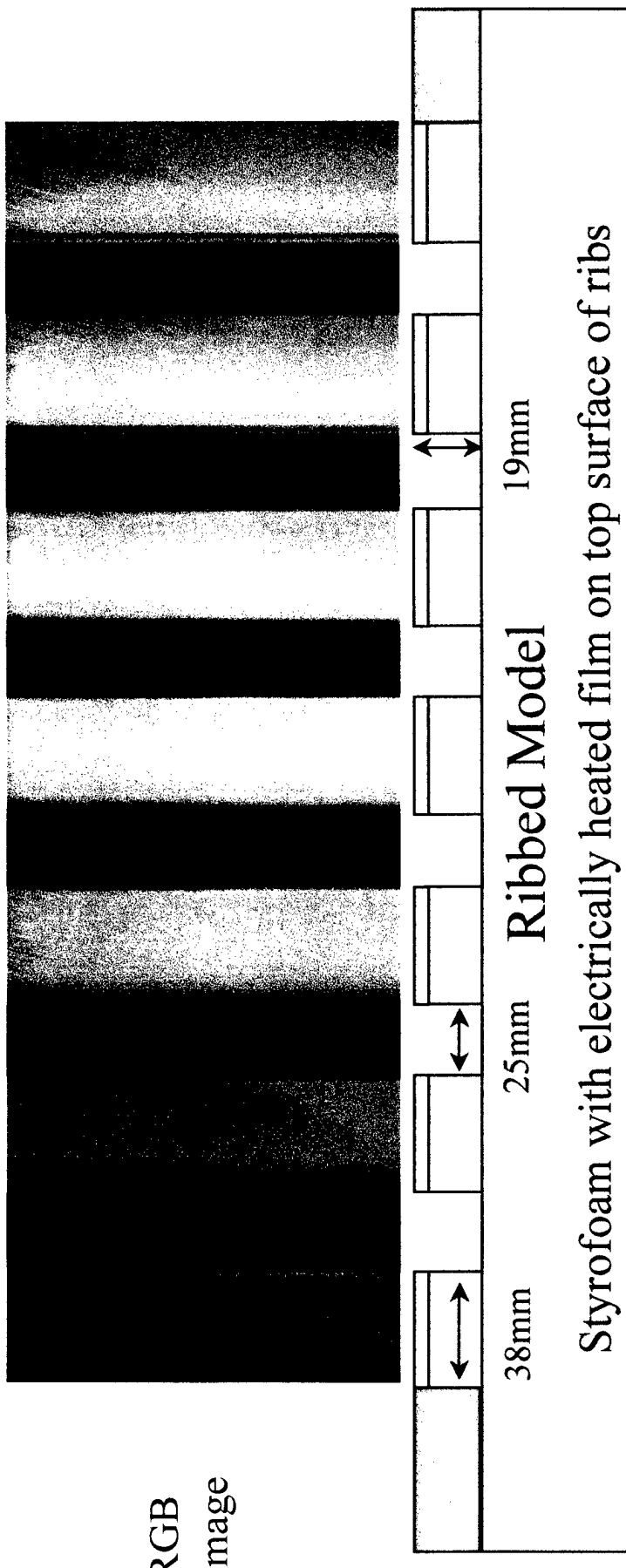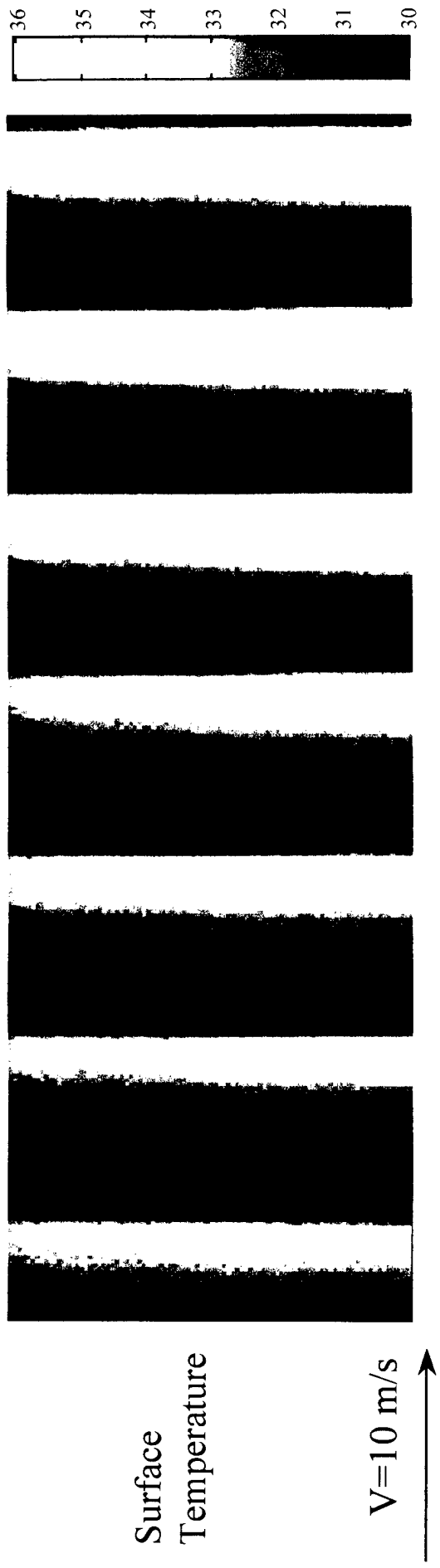
REPRODUCTION QUALITY NOTICE

This document is the best quality available. The copy furnished to DTIC contained pages that may have the following quality problems:

- Pages smaller or larger than normal.

- Pages with background color or light colored printing.

- Pages with small type or poor printing; and or

- Pages with continuous tone material or color photographs.

Due to various output media available these conditions may or may not cause poor legibility in the microfiche or hardcopy output you receive.

☑ If this block is checked, the copy furnished to DTIC contained pages with color printing, that when reproduced in Black and White, may change detail of the original copy.